

**SOLUTE ROTATION AND PHOTOISOMERIZATION
IN COMPLEX FLUIDS**

By

GANGAMALLAIAH VELPULA

CHEM01200904016

Bhabha Atomic Research Centre, Mumbai

*A thesis submitted to the Board of Studies in
Chemical Sciences*

In partial fulfillment of requirements

For the Degree of

DOCTOR OF PHILOSOPHY

OF

HOMI BHABHA NATIONAL INSTITUTE



April, 2014

Homi Bhabha National Institute

Recommendations of the Viva Voce Committee

As members of the Viva Voce Committee, we certify that we have read the dissertation prepared by **Gangamallaiah Velpula** entitled “**Solute Rotation and Photoisomerization in Complex Fluids**” and recommend that it may be accepted as fulfilling the thesis requirement for the award of Degree of Doctor of Philosophy.

Chairman – Dr. D. K. Palit **Date:**

External Examiner – **Date:**

Guide/Convener – Dr. G. B. Dutt **Date:**

External Member – Prof. Anindya Datta **Date:**

Member 1 – Dr. H. Pal **Date:**

Member 2 – Dr. T. K. Ghanty **Date:**

Final approval and acceptance of this thesis is contingent upon the candidate’s submission of the final copies of the thesis to HBNI.

I/We hereby certify that I/we have read this thesis prepared under my/our direction and recommend that it may be accepted as fulfilling the thesis requirement.

Date:

Place:

Dr. G. B. Dutt
(Guide)

STATEMENT BY AUTHOR

This dissertation has been submitted in partial fulfillment of requirements for an advanced degree at Homi Bhabha National Institute (HBNI) and is deposited in the Library to be made available to borrowers under rules of the HBNI.

Brief quotations from this dissertation are allowable without special permission, provided that accurate acknowledgement of source is made. Requests for permission for extended quotation from or reproduction of this manuscript in whole or in part may be granted by the Competent Authority of HBNI when in his or her judgment the proposed use of the material is in the interests of scholarship. In all other instances, however, permission must be obtained from the author.

Gangamallaiiah Velpula

DECLARATION

I, hereby declare that the investigation presented in the thesis has been carried out by me. The work is original and has not been submitted earlier as a whole or in part for a degree/diploma at this or any other Institution / University.

Gangamallaiah Velpula

List of Publications Included in the Thesis

1. Characterizing interfacial friction in AOT reverse micelles from photoisomerization studies of carbocyanine derivatives
Gangamallaiiah, V.; Dutt, G. B. *J. Chem. Phys.* **2011**, *134*, 024706/1–024706/6.
2. Photoisomerization dynamics of 3,3'-diethyloxadicarbocyanine iodide in ionic liquids: Breakdown of hydrodynamic Kramers model
Gangamallaiiah, V.; Dutt, G. B. *J. Chem. Phys.* **2011**, *135*, 174505/1–174505/7.
3. Rotational diffusion of nonpolar and ionic solutes in 1-alkyl-3-methylimidazolium bis(trifluoromethylsulfonyl)imides: Is solute rotation always influenced by the length of the alkyl chain on the imidazolium cation?
Gangamallaiiah, V.; Dutt, G. B. *J. Phys. Chem. B* **2012**, *116*, 12819–12825.
4. Fluorescence anisotropy of a nonpolar solute in 1-alkyl-3-methylimidazolium-based ionic liquids: Does the organized structure of the ionic liquid influence solute rotation?
Gangamallaiiah, V.; Dutt, G. B. *J. Phys. Chem. B* **2013**, *117*, 5050–5057.
5. Influence of the organized structure of 1-alkyl-3-methylimidazolium-based ionic liquids on the rotational diffusion of an ionic solute
Gangamallaiiah, V.; Dutt, G. B. *J. Phys. Chem. B* **2013**, *117*, 9973–9979.
6. Effect of alkyl chain length on the rotational diffusion of nonpolar and ionic solutes in 1-alkyl-3-methylimidazolium bis(trifluoromethylsulfonyl)imides
Gangamallaiiah, V.; Dutt, G. B. *J. Phys. Chem. B* **2013**, *117*, 12261–12267.

Conferences

1. Characterizing interfacial friction in AOT reverse micelles from photoisomerization studies of carbocyanine derivatives

National Symposium on Radiation and Photochemistry 2011, Jodhpur.
2. Photoisomerization dynamics of 3,3'-diethyloxadicarbocyanine iodide in ionic liquids: Is it different in ionic liquids?

Trombay Symposium on Radiation and Photochemistry 2012, Mumbai.

3. Fluorescence anisotropy of a nonpolar solute in 1-alkyl-3-methylimidazolium ionic liquids: Influence of the structure of the ionic liquid on solute rotation?

National Symposium on Radiation and Photochemistry 2013, Shillong.

4. Effect of alkyl chain length on the rotational diffusion of nonpolar and ionic solutes in 1-alkyl-3-methylimidazolium bis(trifluoromethylsulfonyl)imides

Trombay Symposium on Radiation and Photochemistry 2014, Mumbai.

Others

1. Fluorescence anisotropy of a nonpolar solute in 1-alkyl-3-methylimidazolium-based-ionic liquids: Does the structure of the ionic liquid influence solute rotation?

Researchers Scholars Meet 2013, Mumbai

Gangamallaiiah Velpula

Dedicated to.....

My Beloved

Family and Friends

Acknowledgement

This thesis is the end of my journey in obtaining PhD. I have not travelled this journey alone to reach this moment. Coming from small village, it was not so easy to choose academic research instead of job in industry. This occasion has come with the support of numerous people, including my well wishers and friends. I would like to thank all those people who helped me to reach this stage. It is my pleasure to acknowledge all those who contributed in many ways to the success of this study and made it an unforgettable experience for me.

First and foremost, I would like to express my sincere gratitude to my advisor Dr. G. B. Dutt, who will always remain more of a friend than a advisor. I could not have imagined having a better advisor for my PhD. His crystal-clear research ideas, immense knowledge, logical way of thinking and choice of scientific problems have been a great value for me. His advice on both research as well as my career has been priceless. I thank him a lot for being patient with me on many occasions in particular, while reviewing this thesis.

It gives me immense pleasure to thank the members of the doctoral committee Dr. D.K, Palit (Chairman), Dr. H. Pal (Member), Dr. T. K, Ghanty (Member), Prof. Anindya Datta (External member) and Dr. T. Mukherjee (Former Chairman) for their critical review and suggestions during the progress review and pre-synopsis viva-voce.

I also gratefully acknowledge the help rendered by all the members of Molecular Photochemistry Section and Radiation and Photochemistry Division. I would like to thank Board of Research and Nuclear Sciences for their financial support.

I had the pleasure of having discussions with Dr. S. Nath and Dr. Prabhath. Their knowledge in instrumentation helped me during my experiments. Special thanks to Dr. S. K, Sarkar, Dr. D. K, Maity, Dr. P. D. Naik , Dr. Awadesh kumar Dr. S. Adhikari, Dr. R. Ganguly and Dr. Hassan for their constant encouragement and support. I would like to thank to Dr. Alok Samanta for useful discussions.

My sincerest thanks to Chandra Ma'am, Sugosh, Bhawana and Lalita for their moral support and encouragement during all these years.

I also extend many thanks to Chetan, Arun, Sushanth, Apurav, Mhejabeen, Juby, KK, Ridhima, Hari, Abhishek, Mahendra, Ashmita, Mohini, Anand, Kanhu, Pradnya, Farheen, Vishu, Shalini, Chandralekha, Pallavi, Parvathi, Pavithra, Meenakshi, Prachi, Thusar, Partha, Nandita Ma'am and Sumana Ma'am for their support during the period of my doctoral work,

I am very thankful to my roommates, Dilip, Ahmed, Suresh, Venky, Khaiser, Yusuf and Jasna, Vivek and Anju, Satish and Anusha and Naresh and Vani. I always cherish the time spent with all of you during these years. I also extend thanks to my batchmates Avishek, Jerina, Vasundhara, Suman, Monika, Shikha and Debashree.

It gives me immense pleasure to thank Shankar, Ashok, Ramesh and Pavan for their constant and invaluable support during my post graduation. I am also thankful to Chandrashekar, Nagaraju Sir, Gangadhar Sir and Madhu Sagar Sir, for their constant encouragement and help during my graduation.

My Sincere thanks to Sattaiah, Rajendhar, Parandham, Narayana, Vamshi and K, Rajendhar, Mohan, Ganesh, Laxminarsaiah for their support to my family in my absence.

Finally, I would like to thank my family members, for their unconditional support throughout my career. In particular, patience and understanding shown by my mother.

Last but not least, I am thankful to Almighty for all time blessings.

Gangamallaiiah Velpula

(April, 2014)

CONTENTS

	Page No.
SYNOPSIS	xiii
LIST OF FIGURES	xxv
LIST OF TABLES	xxx
Chapter 1: Introduction	1–24
1.1. Introduction	1
1.2. Modern Ionic Liquids	3
1.2.1. Constituent Ions of Ionic Liquids	4
1.2.2. Physicochemical Properties of Imidazolium-Based Ionic Liquids	8
1.2.2.1. Melting Points	9
1.2.2.2. Polarity	10
1.2.2.3. Viscosity	12
1.2.3. Structural Properties of Imidazolium-Based Ionic Liquids	14
1.3. Microheterogeneous Systems	17
1.3.1. Reverse Micelles	19
1.4. Scope of the Thesis	22
Chapter 2: Experimental Techniques	25–50
2.1. Introduction	25
2.2. Steady-State Absorption Measurements	26

2.3. Steady-State and Time-Resolved Emission Measurements	27
2.3.1. Fluorescent Quantum Yield Measurement	28
2.3.2. Fluorescence Lifetime	30
2.3.3. Fluorescence Anisotropy	31
2.3.4. Relation between Steady-State and Time-Resolved Parameters	36
2.3.5. Measurement of Time-Resolved Fluorescence	39
2.3.5.1. Time-Correlated Single-Photon Counting	40
2.3.6. Method of Data Analysis	44
2.3.6.1. Reduced Chi Square Values	46
2.3.6.2. Plot of the Weighted Residuals	46
2.3.7. Measurement of Auxiliary Parameters	47
2.3.7.1. Measurement of Viscosity	47
2.3.7.1.1. Principle	48
2.3.7.2. Measurement of Refractive Index	48
 Chapter 3: Solute Rotation in Imidazolium-Based Ionic Liquids with Strongly Associating Anions	 51–80
3.1. Introduction	51
3.2. Materials and Methods	54
3.3. Results and Discussion	56
3.3.1. The SED Hydrodynamic Theory for Rotational Diffusion	61

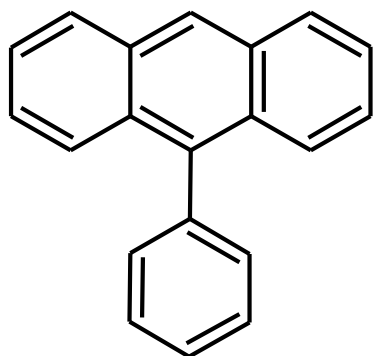
3.3.2. The Gierer-Wirtz Theory	69
3.3.3. The Dote-Kivelson-Schwartz Ttheory	71
3.4. Conclusions	79
Chapter 4: Solute Rotation in Imidazolium-Based Ionic Liquids with Weakly Associating Anions	81–98
4.1. Introduction	81
4.2. Materials and Methods	83
4.3. Results and Discussion	84
4.4. Conclusions	98
Chapter 5: Photoisomerization Dynamics in Ionic Liquids	99–122
5.1. Introduction	99
5.2. Materials and Methods	103
5.3. Results and Discussion	104
5.4. Conclusions	121
Chapter 6: Photoisomerization Dynamics in AOT Reverse Micelles	123–138
6.1. Introduction	123
6.2. Material and Methods	125
6.3. Results and Discussion	127
6.4. Conclusions	137
References	139
List of Publications	159

Synopsis

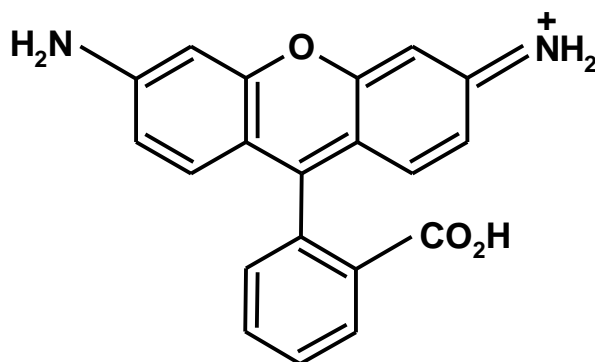
Solute-solvent interactions play an important role in chemical reactions and also on the physicochemical properties of liquids and solutions.¹ Therefore, it is important to comprehend these interactions at the microscopic level. To achieve this objective, numerous photophysical processes have been examined to a large extent in neat liquids with the aid of theoretical and experimental techniques and the outcome of these results have been well-documented in the literature.²⁻⁶ However, understanding these interactions in binary and complex fluids such as ionic liquids and reverse micelles is not trivial compared to neat liquids. These fluids have emerged as alternative reaction media not only in various chemical processes but also in numerous industrial applications.⁷⁻¹² Thus, to get a better appreciation of these interactions and obtain a broad-based understanding of chemical reactivity, various photophysical processes need to be investigated in complex fluids.

Rotational diffusion provides a valuable information about the solute-solvent interactions, while studies involving photoisomerization dynamics of olefins and polyenes enables us to understand role of solute-solvent frictional coupling on unimolecular chemical reactions. Both these processes have been thoroughly investigated in conventional solvents and the ensuing findings shed light on the role of specific interactions, viscous and dielectric frictions on solute rotation and photoisomerization.^{1,13,14} However, understanding of these phenomena in complex fluids especially, ionic liquids and reverse micelles, is at its infancy. Thus, this thesis is an

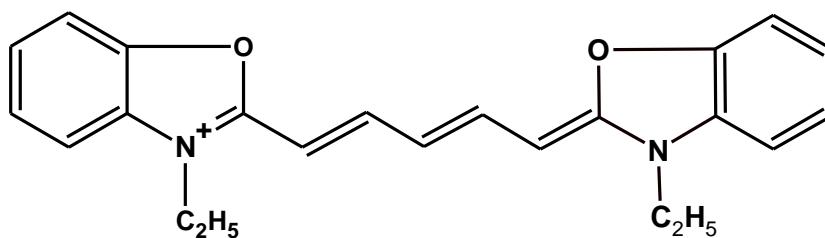
endeavor to comprehend the complex and diverse environments of ionic liquids and reverse micelles. This task has been accomplished with the aid of steady-state and time-



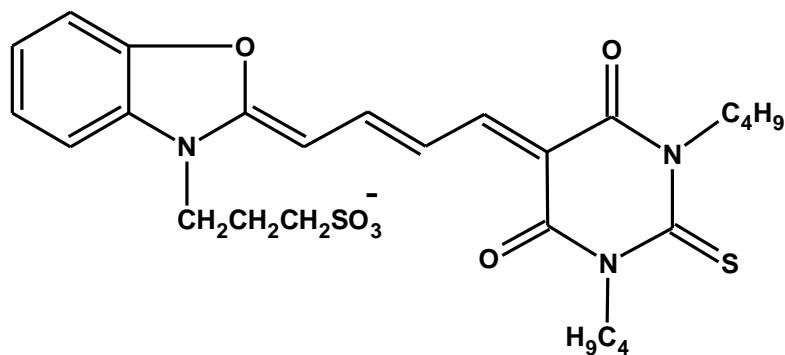
9-phenylanthracene



Rhodamine 110



3,3'-diethyloxadicyanine iodide (DODCI)



Merocyanine 540 (MC 540)

Figure 1 *Molecular structures of the solutes.*

resolved fluorescence spectroscopic techniques. Fluorescence parameters such as quantum yields, lifetimes and reorientation times of suitable fluorescent probes dissolved in select complex fluids have been measured. Figure 1 gives the molecular structures of the fluorescent probes used in this thesis.

1-Alkyl-3-methylimidazolium-based ionic liquids $[\text{Rmim}^+]$ with strongly associating anions such as tetrafluoroborates ($[\text{BF}_4^-]$) and hexafluorophosphates ($[\text{PF}_6^-]$) as well as weakly associating anions bis(trifluoromethylsulfonyl)imides ($[\text{Tf}_2\text{N}^-]$) and tris(pentafluoroethyl)trifluorophosphate ($[\text{FAP}^-]$) have been chosen to investigate the solute rotation. For the purpose of photoisomerization studies, 1-Alkyl-3-methylimidazolium bis(trifluoromethylsulfonyl)imides have been employed. These imidazolium-based ionic liquids are selected because their physicochemical properties have been well-documented in literature.^{7,8,15-17} It has been established that the presence of nonpolar alkyl chains on the imidazolium cation induces van der Waals interactions in addition to Coulombic and hydrogen bonding interactions between the cation and anion leading to the formation of organized structure.¹⁸⁻²⁰ Thus, one of the main objectives of this thesis is to understand the influence of the organized structure of ionic liquids on the dynamical processes. Apart from ionic liquids, photoisomerization studies have been performed in reverse micelles formed with the anionic surfactant bis(2-ethylhexyl) sodium sulfosuccinate (AOT). The structural parameters of AOT reverse micelles have been well-characterized.²¹ Photoisomerization studies have been carried out in this system to identify a parameter that characterizes interfacial friction in reverse micelles.

The results obtained from the investigation of solute rotation and photoisomerization in complex fluids have been presented, analyzed and discussed extensively in this thesis. Based on the theme of the work, the thesis has been divided in to six different chapters. A concise account of each chapter is given below.

Chapter 1

Chapter 1 deals with general introduction to photo-induced fundamental processes and the motivation for investigating them in complex fluids. After presenting a detailed description of the dynamical processes that have been undertaken in the present study, this chapter describes complex fluids and how they are different from molecular solvents. An elaborate account is given on the physicochemical and structural properties of ionic liquids, in particular, how the constituent ions and substituents present on either of the ions influence the formation of organized structure. A brief portrayal of micro-heterogeneous systems has also been presented in this chapter. Towards the end of the chapter, significance of the work presented in this thesis has been depicted.

Chapter 2

Chapter 2 gives an overview of how recent advances in laser Spectroscopy have enabled researchers to investigate photo-induced processes in condensed phase. This chapter essentially deals with steady-state and time-resolved fluorescence spectroscopic techniques that have extensively been employed to carry out the work presented in this thesis. A detailed description of various experimental techniques such as absorption

spectrophotometer, steady-state spectrofluorometer and time-resolved fluorescence spectrometer, which works on the principle of time-correlated single-photon counting (TCSPC),²² has been presented. The principle involved in TCSPC and the experimental set up have been discussed. Apart from these techniques, a brief account of rheometer and refractometer that have been used to measure auxiliary parameters such as viscosities and refractive indices, respectively, of various ionic liquids is also given.

Chapter 3

Chapter 3 deals with studies involving the rotational diffusion of a nonpolar solute 9-phenylanthracene (9-PA) and a cationic solute rhodamine 110 (R110) in 1-alkyl-3-methylimidazolium (alkyl = ethyl, butyl, hexyl and octyl) tetrafluoroborates and hexafluorophosphates. The objective of this work is to understand the influence of organized structure of these ionic liquids on solute rotation. For this purpose, reorientation times (τ_r) of 9-PA and R110 have been measured in [Rmim⁺][BF₄⁻] and [Rmim⁺][PF₆⁻] as a function of viscosity (η) by varying the temperature (T) as well as length of the alkyl chain on the imidazolium cation. The observed results have been analyzed with the aid of Stokes-Einstein-Debye (SED) hydrodynamic theory.^{23,24} It has been observed that for a given η/T , rotation of 9-PA becomes significantly faster with an increase in the length of the alkyl chain from ethyl to octyl on the imidazolium cation, whereas in case of R110, faster rotation of the solute has been observed at higher values of η/T . In other words, two slopes have been obtained in τ_r versus η/T plots of R110 corresponding to lower and higher values of η/T . Despite displaying distinct trends,

rotational diffusion of both 9-PA and R110 in $[\text{Rmim}^+][\text{BF}_4^-]$ and $[\text{Rmim}^+][\text{PF}_6^-]$ deviates significantly from the predictions of SED theory. Even the quasihydrodynamic theories of Gierer-Wirtz (GW) and Dote-Kivelson-Schwartz (DKS), which take into consideration parameters such as solvent size and free volume, fail to explain the observed results. These trends, however, could be rationalized by taking into consideration the organized structure of the ionic liquids. The nonpolar solute 9-PA senses viscosity that is lower than the bulk viscosity due to the presence of organized domains whose size increases upon increasing in the length of the alkyl chain on the imidazolium cation and thus leading to the faster rotation of the solute. In contrast, at higher values of η/T , diminishing hydrogen bonding interactions between the cationic solute R110 and the anions, which transpire as a consequence of the organized structure of the ionic liquids, appears to be responsible for the observed behavior.

Chapter 4

This chapter deals with the rotational diffusion of 9-PA and R110 in 1-alkyl-3-methylimidazolium-based ionic liquids (alkyl = methyl to octadecyl) with a weakly associating anion bis(trifluoromethylsulfonyl)imide ($[\text{Tf}_2\text{N}^-]$). From the results portrayed in the previous chapter it is evident that the presence of strongly associating anions such as $[\text{BF}_4^-]$ and $[\text{PF}_6^-]$ induces the formation of organized structure in ionic liquids even when length of the alkyl chain on the imidazolium cation is short and such an organized structure affects solutes rotation. Thus, the work presented in this chapter is essentially undertaken to find out the role of weakly associating anion and long alkyl chains on

solute rotation as the formation of organized structure governed by these two properties of the ionic liquids.^{25,26} To this effect, reorientation times of 9-PA and R110 have been measured as a function of viscosity by varying the temperature in each member of the solvent series. The observed results have been analyzed using SED hydrodynamic theory, $\tau_r = A(\eta/T)^n$, where A is the ratio of the hydrodynamic volume of the solute to the Boltzmann constant and $n = 1$ as predicted by the SED theory. It has been observed that, for both the solutes, A and n decrease with an increase in the length of the alkyl chain from methyl to octadecyl on the imidazolium cation, especially from the octyl derivative onward indicating the failure of the SED theory. It may be noted that in case of imidazolium-based ionic liquids with weakly associating anions, organized structure forms only in the presence of the longer alkyl chains on the imidazolium cation. The nonpolar solute, 9-PA, resides in the nonpolar regions of the organized structure, whereas the cationic solute R110 is probably located at the interface between the nonpolar domain and ionic region. An increase in the length of the alkyl chain on the imidazolium cation leads to the formation of larger organized structure, which results in the faster rotation of the solutes at a given η/T . In essence, an increase in the length of the alkyl chain on the imidazolium cation facilitates rotation of nonpolar as well as charged solutes despite being located in different regions of the organized structure.

Chapter 5

Chapter 5 describes photoisomerization of a carbocyanine derivative 3,3'-diethyloxadicyanone iodide (DODCI) in 1-alkyl-3-methylimidazolium (alkyl = methyl, ethyl, propyl, butyl and hexyl) bis(trifluoromethylsulfonyl)imides. The present

investigation has been undertaken to find out whether photoisomerization of DODCI in ionic liquids is any different compared to that observed in conventional solvents such as alcohols. For this purpose, nonradiative rate constants (k_{nr}) have been obtained from the measured fluorescence lifetimes and quantum yields. It may be noted that k_{nr} represents rate of photoisomerization for DODCI. The activation energy of the reaction has been calculated from the isoviscosity plots and found to be 22 ± 3 kJ mol⁻¹, which is a factor of two higher compared to that reported in alcohols (11.3 kJ mol⁻¹). The most probable reason for higher activation energy in ionic liquids compared to alcohols is due to the highly organized structure of ionic liquids,²⁷ which inhibits the excited-state twisting process. To understand the reduced isomerization rate constants in terms of solvent friction, Kramers hydrodynamic theory, has been applied. However, Kramers model fails to predict the variation in the reduced isomerization rate constants with viscosity. An empirical power-law relation adequately describes the observed trends. Somewhat similar behavior that has been observed for the DODCI isomerization in alcohols in the ground and excited-states is also discussed.^{28,29} The observed deviation from Kramers hydrodynamic theory could be due to frequency-dependent frictional effect. Therefore, to improve the agreement between the experiment and theory, frequency-dependent friction of the medium needs to be considered. This aspect has been substantiated by the observed nonlinear relationship between the friction and viscosity, especially at lower viscosities.

Chapter 6

Chapter 6 presents photoisomerization of two carbocyanine derivatives, 3,3'-diethyloxadiazocarbocyanine iodide (DODCI) and merocyanine 540 (MC 540) in reverse micelles formed with the anionic surfactant bis(2-ethylhexyl) sodium sulfosuccinate (AOT). Essentially, this study has been performed to identify the parameter that characterizes photoisomerization process in the interfacial region of reverse micelles. For these solutes, nonradiative rate constants (k_{nr}) have been identified as rates of photoisomerization. Thus, nonradiative rate constants of DODCI and MC 540 have been obtained from the measured fluorescence lifetimes and quantum yields as a function of the mole ratio of water to the surfactant (W) in AOT/isooctane/water and AOT/cyclohexane/water reverse micellar systems. It has been established that the solutes DODCI and MC 540 are located in the interfacial region of both the reverse micellar systems at all values of W employed in this study. For DODCI and MC 540 in the two AOT reverse micellar systems, k_{nr} increases upon increasing W , however, this increase is not uniform reaches saturation at higher values of W . If k_{nr} values of DODCI and MC 540 were solely dependent on the water pool radius (R_w), they should have increased linearly with W as these two parameters (W and R_w) have a linear dependence. However, saturation of k_{nr} has been observed at higher values of W for both the solutes in the two AOT reverse micellar systems, which is an indication that R_w is not the sole parameter that governs this process. It is a well-known fact that an increase in W not only increases R_w but also alters other structural parameters such as aggregation number (N_a) and

hydrodynamic radius (R_h) of the reverse micelles. Thus, to explain the observed results, all these structural parameters of the AOT reverse micellar systems have been considered and it may be noted that both N_a and R_h also increase with W .²¹ Such an increase in N_a , R_w and R_h influences the critical packing parameter. It is defined as ν/a_0l_c , where ν , a_0 and l_c are respectively, volume of the hydrophobic tail, effective head group area and effective chain length of the hydrophobic tail. The critical packing parameter has been calculated with the aid of N_a , R_w and R_h using appropriate formulae.³⁰ Critical packing parameter for AOT/isooctane/water and AOT/cyclohexane/water decreases upon increase in W , however, this decrease is not uniform but reaches saturation at higher values of W . Therefore, the steady rise and subsequent saturation observed in k_{nr} has been rationalized with the aid of critical packing parameter. An inverse correlation has been obtained between k_{nr} and ν/a_0l_c , which indicates that the critical packing parameter can be employed to depict interfacial friction in reverse micelles.

References

1. Dutt, G. B. *ChemPhysChem*. **2005**, *6*, 413 and references therein.
2. Horng, M. L.; Gardecki, J. A.; Papazyan, A.; Maroncelli, M. *J. Phys. Chem.* **1995**, *99*, 17311.
3. Weaver, M. J.; McManis, G. E. *Acc. Chem. Res.* **1990** *23*, 294.
4. Strandjord, A. J. G.; Barbara, P. F. *J. Phys. Chem.* **1985**, *89*, 2355.
5. Kurnikova, M. G.; Balbai, N.; Waldeck, D. H.; Coalson, R. D. *J. Am. Chem. Soc.* **1998**, *120*, 6121.
6. Waldeck, D. H. *Chem. Rev.* **1991**, *91*, 415 and references therein.
7. Hallett, J. P.; Welton, T. *Chem. Rev.* **2011**, *111*, 3508.
8. Dupont, J. *Acc. Chem. Res.* **2011**, *44*, 1223.
9. Plechkova, N. V.; Seddon, K. R. *Chem. Soc. Rev.* **2008**, *37*, 123.
10. Weingärtner, H. *Angew. Chem., Int. Ed.* **2008**, *47*, 654.
11. Moulik, S. P.; Paul, B. K. *Adv. Colloid Interface Sci.* **1998**, *78*, 99.
12. Uskokovic, V.; Drogenik, M. *Adv. Colloid Interface Sci.* **2007**, *133*, 23.
13. Fleming, G. R.; Wolynes, P. G. *Phys. Today* **1990**, *36*.
14. Waldeck, D. H. *Conformational Analysis of Molecules in Excited States*, Waluk, J., Ed.; Wiley-VCH: New York, 2000, pp. 113-176. and references therein.
15. Welton, T. A. *Chem. Rev.* **1999**, *99*, 2071.
16. Wasserscheid, W.; Keim, W. *Angew. Chem., Int. Ed.* **2000**, *39*, 3773.
17. Seddon, K. R.; Stark, A.; Torres, M. J. *Pure Appl. Chem.* **2000**, *72*, 12.
18. Pópolo, M. G. D.; Voth, G. A. *J. Phys. Chem. B* **2004**, *108*, 1744.

19. Wang, Y.; Jiang, W.; Yan, T.; Voth, G. A. *Acc. Chem. Res.* **2007**, *40*, 1193.
20. Russina, O.; Triolo, A.; Gontrani, L.; Caminiti, R. *J.Phys. Chem. Lett.* **2012**, *3*, 27.
21. Maitra, A. *J.Phys. Chem.* **1984**, *88*, 5122.
22. O'Connor, D. V.; Phillips, D. *Time-Correlated Single-Photon Counting*, Academic Press: London, 1984.
23. Fleming, G. R. *Chemical Applications of Ultrafast Spectroscopy*; Oxford University Press: New York, 1986.
24. Waldeck, D. H. *The Role of Solute-Solvent Friction in Large-Amplitude Motions. In Conformational Analysis of Molecules in the Excited States*; Waluk, J., Ed.; Wiley-VCH: New York, 2000; pp 113–176.
25. Triolo, A.; Russina, O.; Fazio, B.; Triolo, R.; Cola, E. D. *Chem. Phys. Lett.* **2008**, *457*, 362.
26. Binetti, E.; Panniello, A.; Triggiani, L.; Tommasi, R.; Agostiano, A.; Curii, M. L.; Striccoli, M. *J. Phys.Chem. B.* **2012**, *116*, 3512.
27. Behar, D.; Gonzalez, C.; Neta, P. *J. Phys.Chem. A* **2001**, *105* 7607.
28. Velsko, S P.; Fleming, G. R. *Chem. Phys.* **1982**, *65*, 59.
29. Velsko, S. P.; Waldeck, D. H.; Fleming, G. R. *J. Chem. Phys.* **1983**, *78*, 249.
30. Mitchell, D. J; Ninham, B. W. *J. Chem. Soc. Faraday Trans 2* **1981**, *77*, 601.

List of Figures

	Page No.
Figure 1.1 Constituents of an ionic liquid.	6
Figure 1.2 Structures of conventional salt and modern ionic liquid	10
Figure 1.3 View of two-dimensional model of the polymeric supramolecular structure of 1,3-dialkylimidazolium-based ionic liquids showing hydrogen bonds between the imidazolium cations (C^+) and anions (A^-).	15
Figure 2.1 Creation of ground-state and excited-state anisotropies from isotropic distribution of molecules.	33
Figure 2.2 Schematic diagram describing measurement of fluorescence anisotropy.	34
Figure 2.3 Schematic of a TCSPC setup.	41
Figure 2.4 Schematic diagram describing measurement of refractive index.	49
Figure 3.1 Molecular structures of the solutes.	53
Figure 3.2 Fluorescence anisotropy decays of 9-PA in $[hmim^+][BF_4^-]$, $[moim^+][BF_4^-]$ and $[hmim^+][PF_6^-]$, $[moim^+][PF_6^-]$ at 298 K together with the fitted curves.	64

Figure 3.3 65

Fluorescence anisotropy decays of R110 in [hmim⁺][PF₆⁻] (blue) and [moim⁺][PF₆⁻] (red) at 323 K and 348 K together with the fitted curves.

Figure 3.4 66

Plots of τ_r versus η/T for 9-PA and R110 in [emim⁺][BF₄⁻] (▽), [bmim⁺][BF₄⁻] (□), [hmim⁺][BF₄⁻] (○) and [moim⁺][BF₄⁻] (△), and [emim⁺][PF₆⁻] (▽), [bmim⁺][PF₆⁻] (□), [hmim⁺][PF₆⁻] (○) and [moim⁺][PF₆⁻] (△). The lines passing through data points were obtained by fitting the data to nonlinear η/T relationships that are given below. The black-colored lines are the SED slip and stick lines for 9-PA and R110 solutes.

Figure 4.1 82

Molecular structures of the solutes.

Figure 4.2 84

Fluorescence anisotropy decays of 9-PA and R110 in [mmim⁺][Tf₂N⁻] (blue), [moim⁺][Tf₂N⁻] (red) and [modim⁺][Tf₂N⁻] (olive) at 348 K together with the fitted curves.

Figure 4.3 91

Plots of τ_r versus η/T for 9-PA and R110 in 1-alkyl-3-methylimidazolium bis(trifluoromethylsulfonyl)imides of varying alkyl chain lengths (C₁ to C₁₈). The SED slip and stick lines for the two solutes are also shown in the figure.

Figure 4.4 92

Plots of A and n versus number of carbon atoms present in the alkyl chain on

the imidazolium cation with $[\text{Tf}_2\text{N}^-]$ (olive), $[\text{BF}_4^-]$ (red) and $[\text{PF}_6^-]$ (blue) anions for the solutes 9-PA and R110. The lines passing through the data points are drawn as visual aids and it can be noticed that barring a few exceptions. Data for 9-PA and R110 in $[\text{Rmim}^+][\text{BF}_4^-]$ and $[\text{Rmim}^+][\text{PF}_6^-]$ has been taken from Chapter 3.

Figure 5.1 101

Molecular Structure of DODCI.

Figure 5.2 104

Normalized absorption and emission spectra of DODCI in $[\text{mmim}^+][\text{Tf}_2\text{N}^-]$ (red) and $[\text{hmim}^+][\text{Tf}_2\text{N}^-]$ (olive).

Figure 5.3 105

Fluorescence decays of DODCI in $[\text{mmim}^+][\text{Tf}_2\text{N}^-]$ at different temperatures along with the instrument response function. The fitted decay curves are not shown in the figure for the sake of clarity.

Figure 5.4 106

Plots of n versus T in the 1-alkyl-3-methylimidazolium bis(trifluoromethylsulfonyl)imides. The curves passing through the data points are drawn as a visual aid.

Figure 5.5 109

Isoviscosity plots for DODCI in the 1-alkyl-3-methylimidazolium bis(trifluoromethylsulfonyl)imides. The lines passing through the points are obtained by linear-least squares fit.

Figure 5.6	111
Plots of $\ln(k_{nr})$ versus $1/T$ in $[\text{emim}^+][\text{Tf}_2\text{N}^-]$ (blue) and $[\text{hmim}^+][\text{Tf}_2\text{N}^-]$ (red). The lines passing through the data points are obtained by linear-least squares fit.	
Figure 5.7	115
Plot of the reduced isomerization rate constant versus viscosity for DODCI in 1-alkyl-3-methylimidazolium bis(trifluoromethylsulfonyl)imides. The green, orange and purple colored curves represent fits to the Kramers model after considering the entire data, low viscosity data (8–20 mPa s) and high viscosity data (25–63 mPa s), respectively. The blue curve is a fit to the power law equation.	
Figure 5.8	118
Plot of friction versus viscosity for DODCI isomerization in 1-alkyl-3-methylimidazolium bis(trifluoromethylsulfonyl)imides. The curve passing through the data points is drawn as a visual aid. The straight line is obtained from the linear least-squares fit of the data from 40 mPa s to show the transition from nonlinear to linear dependence of friction on η .	
Figure 6.1	125
Molecular structures of the solutes.	
Figure 6.2	127
Normalized absorption and emission spectra of DODCI and MC 540 in AOT/isooctane/water reverse micelles at $W = 4$ (olive) and $W = 30$ (red) (top) and in AOT/cyclohexane/water reverse micelles at $W = 1$ (olive) and $W = 15$	

(red) (bottom). The spectra of the solutes in water (blue) are also shown.

Figure 6.3

129

Fluorescence decays of DODCI and MC 540 in AOT/cyclohexane/water reverse micelles at $W = 1$ (red) and $W = 15$ (blue) along with the fitted curves (black lines). The instrument response function (olive) is also shown in the figure.

Figure 6.4

130

Plots of k_{nr} versus W for DODCI (red) and MC 540 (blue) in AOT/isooctane/water and AOT/cyclohexane/water reverse micelles. The curves passing through the data points are used to highlight the observed trends.

Figure 6.5

135

Plots of k_{nr} versus v/a_0l_c for DODCI and MC 540 in AOT/isooctane/water (red) and AOT/cyclohexane/water (blue) reverse micellar systems. The lines passing through the data points are obtained by linear least-squares fits.

List of Tables

	Page No.
Table 1.1 Shapes of the surfactant self-assembly for different values of the packing parameter.	19
Table 3.1 Reorientation times of 9-PA and R110 in [emim ⁺][BF ₄ ⁻] as a function of temperature along with solvent viscosity.	57
Table 3.2 Reorientation times of 9-PA and R110 in [bmim ⁺][BF ₄ ⁻] as a function of temperature along with solvent viscosity.	57
Table 3.3 Reorientation times of 9-PA and R110 in [hmim ⁺][BF ₄ ⁻] as a function of temperature along with solvent viscosity.	58
Table 3.4 Reorientation times of 9-PA and R110 in [moim ⁺][BF ₄ ⁻] as a function of temperature along with solvent viscosity.	58
Table 3.5 Reorientation times of 9-PA and R110 in [emim ⁺][PF ₆ ⁻] as a function of temperature along with solvent viscosity.	59
Table 3.6 Reorientation times of 9-PA and R110 in [bmim ⁺][PF ₆ ⁻] as a function of temperature along with solvent viscosity.	59

Table 3.7	60
Reorientation times of 9-PA and R110 in [hmim ⁺][PF ₆ ⁻] as a function of temperature along with solvent viscosity.	
Table 3.8	60
Reorientation times of 9-PA and R110 in [moim ⁺][PF ₆ ⁻] as a function of temperature along with solvent viscosity.	
Table 3.9	63
Solute dimensions and van der Waals volumes together with shape factors and boundary condition parameters calculated using the SED hydrodynamic theory.	
Table 3.10	67
Values of A and n obtained for 9-PA and in [Rmim ⁺][BF ₄ ⁻] from linear Least-Squares Fits of τ_r versus η/T Plots.	
Table 3.11	67
Values of A and n obtained for 9-PA and R110 in [Rmim ⁺][PF ₆ ⁻] from linear least-squares fits of τ_r versus η/T plots.	
Table 3.12	68
Values of A and n obtained for R110 in [Rmim ⁺][BF ₄ ⁻] from linear least-squares fits of τ_r versus η/T plots at low and high values of η/T .	
Table 3.13	68
Values of A and n obtained for R110 in [Rmim ⁺][PF ₆ ⁻] from linear least-squares fits of τ_r versus η/T plots at low and high values of η/T .	

Table 4.1	85
Reorientation times of 9-PA and R110 in [mmim ⁺][Tf ₂ N ⁻] as a function of temperature along with solvent viscosity.	
Table 4.2	86
Reorientation times of 9-PA and R110 in [emim ⁺][Tf ₂ N ⁻] as a function of temperature along with solvent viscosity.	
Table 4.3	86
Reorientation times of 9-PA and R110 in [mpim ⁺][Tf ₂ N ⁻] as a function of temperature along with solvent viscosity.	
Table 4.4	87
Reorientation times of 9-PA and R110 in [bmim ⁺][Tf ₂ N ⁻] as a function of temperature along with solvent viscosity.	
Table 4.5	87
Reorientation times of 9-PA and R110 in [hmim ⁺][Tf ₂ N ⁻] as a function of temperature along with solvent viscosity.	
Table 4.6	88
Reorientation times of 9-PA and R110 in [moim ⁺][Tf ₂ N ⁻] as a function of temperature along with solvent viscosity.	
Table 4.7	88
Reorientation times of 9-PA and R110 in [dmim ⁺][Tf ₂ N ⁻] as a function of temperature along with solvent viscosity.	
Table 4.8	89
Reorientation times of 9-PA and R110 in [ddmim ⁺][Tf ₂ N ⁻] as a function	

of temperature along with solvent viscosity.

Table 4.9 89

Reorientation times of 9-PA and R110 in [mtdim⁺][Tf₂N⁻] as a function of temperature along with solvent viscosity.

Table 4.10 90

Reorientation times of 9-PA and R110 in [hdmim⁺][Tf₂N⁻] as a function of temperature along with solvent viscosity.

Table 4.11 90

Reorientation times of 9-PA and R110 in [modim⁺][Tf₂N⁻] as a function of temperature along with solvent viscosity.

Table 5.1 107

Viscosities of 1-alkyl-3-methylimidazolium bis(trifluoromethylsulfonyl)imides, quantum yields, fluorescence lifetimes, radiative and nonradiative rate constants of DODCI in 1-alkyl-3-methylimidazolium bis(trifluoromethylsulfonyl)imides at 298 K.

Table 5.2 110

Pre-exponential factors and activation energies for the isomerization of DODCI obtained from isoviscosity plots.

Table 5.3 112

Activation energies for the isomerization of DODCI and for viscous flow obtained from Arrhenius plots.

Table 6.1 130

Variation of fluorescence lifetimes and nonradiative rate constants of DODCI and MC 540 in AOT/isooctane/water reverse micelles as a

function of W at 298 K.

Table 6.2

131

Variation of fluorescence lifetimes and nonradiative rate constants of DODCI and MC 540 in AOT/cyclohexane/water reverse micelles as a function of W at 298 K.

Chapter 1

Introduction

1.1. Introduction

Solvent, a major constituent of solutions, has a profound influence on chemical reactions. To find out how the solvent affects chemical reactivity, intermolecular interactions between the solutes and the solvents have to be understood at the microscopic level. Furthermore, these intermolecular interactions also control the physicochemical properties of solutions.¹ Therefore, it is essential to comprehend these interactions in detail, a challenging task to the physical chemist. To achieve this objective, numerous photophysical processes such as solvent relaxation, electron transfer, proton transfer, photoisomerization and rotational diffusion have been examined with the aid of theoretical and experimental techniques in neat liquids.²⁻⁶ However, understanding these solute-solvent interactions in binary and complex fluids is not trivial compared to neat liquids. Thus, to get a better appreciation of these interactions and obtain a broad-based understanding of chemical reactivity, the above-mentioned processes need to be investigated in complex fluids.

Complex fluids are binary mixtures that have coexistence between two phases. These are made up of atoms and molecules at the very smallest scales. However, these atoms and molecules organize to form larger structures, which in turn make up complex

fluids such as polymers, micelles, reverse micelles and ionic liquids.^{7,8} Although ionic liquids do not strictly adhere to the above-mentioned definition, the complexity arises as a consequence of numerous intermolecular interactions such as Coulombic, hydrogen bonding and dispersive interactions prevailing between the cations and anions of the ionic liquids.⁹⁻¹¹ Since complex fluids are heterogeneous at the microscopic level, their microscopic properties such as microviscosity and micropolarity are vastly different compared to the bulk properties. Therefore, to understand these microscopic properties, various photo-induced processes have to be investigated. For this purpose, suitable experimental techniques are required, which can monitor these events transpiring on rapid time scales. Recent advances in laser spectroscopy and the subsequent development of numerous experimental techniques have enabled researchers to examine fast and ultrafast features of solution phase reaction dynamics.¹² Among the photo-induced processes, rotational diffusion studies provide valuable information about the solute-solvent interactions, while photoisomerization dynamics of olefins and polyenes enables us to understand role of solute-solvent frictional coupling on unimolecular chemical reactions. Both these processes have been thoroughly investigated in conventional solvents and the ensuing findings shed light on the role of specific interactions, viscous and dielectric frictions on solute rotation and photoisomerization.^{1,13,14} However, understanding of these phenomena in complex fluids especially, ionic liquids and reverse micelles, is at its infancy. In recent times, room temperature ionic liquids have emerged as “green” alternatives to volatile organic solvents not only in catalysis and synthesis but also in many other fields of science and technology.^{9,15,16-18} Reverse micelles, on the other hand,

can be considered as compartmentalized organized systems, wherein chemical reactions can be performed in an organic phase, but hosting the reactive species in the water pool.^{19,20} Therefore, it is imperative to understand the microscopic properties of these complex fluids by examining dynamical processes such as solute rotation and photoisomerization. Thus, this thesis is an endeavor to comprehend the complex and diverse environments of ionic liquids and reverse micelles by exploring the above-mentioned processes. This task has been accomplished with the aid of steady-state and time-resolved fluorescence spectroscopic techniques. Fluorescence parameters such as quantum yields, lifetimes and reorientation times of suitable fluorescent probes dissolved in select complex fluids have been measured. This chapter gives a detailed account of various aspects of complex fluids such as ionic liquids and reverse micelles.

1.2 Modern Ionic Liquids

Ionic liquids are a special group of molten salts and the widely accepted definition is *the substance that is entirely composed of ions and has melting point below 373 K*. However, most of the modern ionic liquids are liquids at room temperature and hence, known as *room temperature ionic liquids* (RTIL). Similarly, these liquids are sometimes also referred to as *fused salts, molten salts, ionic melts, liquid organic salts* and all of these terms are considered to be entirely valid. The first ionic liquid, ethanolanmonium nitrate with a melting point in the range of 325-328 K, was synthesized by S. Gabriel and J. Weiner in 1888.²² Although, it adheres to the above-mentioned definition, the true room temperature ionic liquid ethylammonium nitrate ($[\text{EtNH}_3^+][\text{NO}_3^-]$) with a melting

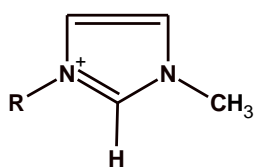
point of 285 K was synthesized by Paul Walden²³ in 1914. For the next forty years there was no activity in this field. But, in 1960s copper (I) chloride and alkyl ammonium chloride formed a liquid at room temperature when they were mixed together.²⁴ In 1978, various alkylpyridinium chlorides were mixed with aluminium chlorides to form colorless liquids. Physicochemical properties of these liquids were measured and reported in the literature.²⁵ However, hygroscopic nature of these ionic liquids made the researchers to seek air and moisture stable ionic liquids. In view of this, 1-alkyl-3-methylimidazolium-based ionic liquids with various fluorinated anions that have a wide range of applications and more stable towards hydrolysis^{26,27} were synthesized.

1.2.1 Constituent Ions of Ionic Liquids

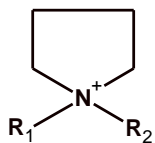
According to the definition, ionic liquids are entirely composed of ions, mostly organic cations and inorganic or organic anions. These ions are held together by various interactions such as Coulombic, hydrogen bonding and dispersive interactions.^{9-11,18,28,29} The major difference between modern ionic liquids and conventional molten salts is that, ionic liquids generally consist of bulky sized and low symmetric organic rather than inorganic cations. Besides, the charge is delocalized over the many atoms in the cation of the ionic liquids. In designing ionic liquids, the cations are used in combination with various anions. There are two different types of anions,³⁰ the first category, also known as first generation anions, includes non-fluorous anions such as aluminium halides (e.g., AlCl_4^-). However, ionic liquids with aluminium halides are difficult to handle due to their highly hygroscopic and air-sensitive nature. The latter ones, also referred to as second

generation anions, comprise fluorous anions such as tetrafluoroborate ($[\text{BF}_4^-]$), hexafluorophosphate ($[\text{PF}_6^-]$), trifluoromethanesulfonate ($[\text{CF}_3\text{SO}_3^-]$), bis(trifluoromethylsulfonyl)imide ($[(\text{CF}_3\text{SO}_2)_2\text{N}^-]$) and tris(pentafluoroethyl)trifluorophosphate ($[\text{P}(\text{C}_2\text{F}_5)_3\text{F}_3^-]$). Among these, the most widely used anions are $[\text{BF}_4^-]$ and $[\text{PF}_6^-]$. Especially, $[\text{PF}_6^-]$ is the prominent anion in the ionic liquid research due its unusual hydrophobicity. In spite of various utilitarian aspects of $[\text{BF}_4^-]$ and $[\text{PF}_6^-]$ anions in ionic liquid chemistry, they have a major disadvantage in the sense that these two anions decompose in the presence of water and liberate the toxic product hydrofluoric acid (HF).^{8,30,31} To prevent the evolution of HF, researchers have altered the bonding style of anion and they have developed some other fluorous anions, which are very stable towards hydrolysis. In other words, the fluorine of the anion bonded to carbon atom and C-F bond becomes inert to hydrolysis. In this way anions such as $[\text{CF}_3\text{SO}_3^-]$ and $[(\text{CF}_3\text{SO}_2)_2\text{N}^-]$ are produced.^{8,32,33} Since fluorous anions are tend to be expensive, halogen-free anions such as dicyanamides and tosylate, or alkyl sulfates have been introduced.^{8,34} Thus, various cations in conjunction with different anions generate a large number of ionic liquids. In recent years, the number of possible cation and anion combinations has increased significantly such that researchers believe that there are billions of different structures that may form ionic liquids. By combining different kinds of cation and anion structures, about 10^{18} ionic liquids can be designed.^{35,36} Amongst these most commonly used ionic liquids are those based on *N,N'*-dialkylimidazolium salts although other cations such as *N*-alkylpyrrolidinium, *N*-alkylpiperidinium, *N*-alkylpyridinium, tetraalkylammounium, tetraalkylphosphonium and trialkylsulfonium are also used. Figure 1.1 shows the different

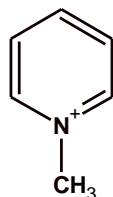
Most Commonly Used Cations



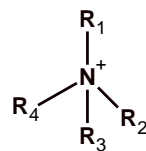
Imidazolium



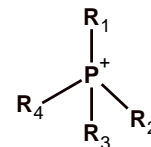
Pyrrolidinium



Pyridinium

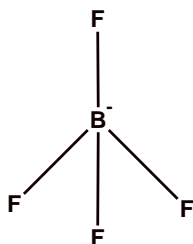


Ammonium

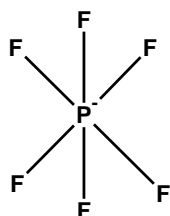


Phosphonium

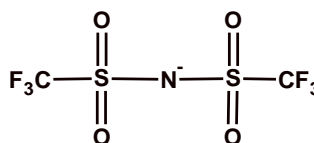
Fluorous Anions



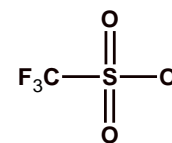
Tetrafluoroborate



Hexafluorophosphate

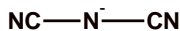


bis(trifluoromethanesulfonyl)imide

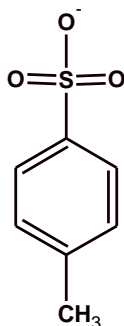


Trifluoromethanesulfonate

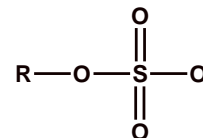
Halogen-Free Anions



Dicyanamide



Tosylate



Alkyl Sulfate

Figure 1.1 *Constituents of an ionic liquid.*

cations and anions that constitute the ionic liquids. In addition to above-mentioned cations, the presence of specific functional groups on the cations give “functionalized”

cations and these are most favorable for a given application. Such cations in combination with anions are known as task specific ionic liquids.⁸ Physicochemical properties and structural properties of these ionic liquids have been explored by carrying out theoretical as well as experimental investigations.³⁷⁻⁵⁰ Moreover, properties of these ionic liquids can be tailored by varying the constituent ions as well as substituents present on either the cation or the anion of the ionic liquids. Hence, these liquids are also known as “designer” solvents. As solvents, ionic liquids possess many advantages over the conventional organic solvents, which make them attractive reaction media in catalysis and synthesis. Some of their physicochemical properties and other features are given below.

1. Ionic liquids are well-known as “green solvents” because of their low or non-measurable vapor pressure under ambient conditions. In view of negligible vapor pressures use of ionic liquids in place of conventional volatile organic solvents effectively reduces the loss of solvent caused by evaporation. Therefore, these liquids can be used as recyclable and reusable media for various catalytic and synthetic processes.⁵¹ Besides, their non-volatile nature prevents the environmental damage. The only drawback of these liquids is that conventional volatile solvents are still required to synthesize ionic liquids and hence these may not be necessarily green.⁵² However, it is possible to design ionic liquids by appropriate structural modifications and also using natural resources.⁵³
2. They possess high thermal and electrochemical stability.^{34,54-56} In fact, research on ionic liquids began with their applications as electrolytes in batteries.^{57,58}
3. They have high liquidus range, in some cases it extends up to 673 K.⁵⁹

4. They dissolve numerous substances such as organic, inorganic, metal salts, and are able to electrodeposit metals, which are impossible to reduce in aqueous solutions.⁶⁰ Furthermore, ionic liquids have been used as reaction media in the synthesis of nanoparticles⁶¹ and have widespread applications in various branches of analytical chemistry.⁶²⁻⁶⁷
5. They are non-aqueous polar alternatives for phase transfer processes.¹⁵
6. They are composed of poorly coordinating ions and therefore have the potential to be highly polar yet non-coordinating solvents.¹⁵
7. The properties of these liquids can be tuned for a specific application by varying the constituent ions of ionic liquids.¹⁶

Apart from the above-mentioned simple physicochemical properties, various other important properties have also been investigated and are utilized in academic as well as numerous industrial applications. A number of articles, specialized reviews and books are available, which deal with the step-wise advancement of synthesis of ionic liquids, unique physicochemical and structural properties and their applications in catalysis, synthesis, separation processes and many other fields of science and technology.^{15-18,68-92}

1.2.2 Physicochemical Properties of Imidazolium-Based Ionic Liquids

To get a better appreciation of the utilitarian aspects of 1-alkyl-3-methylimidazolium ([Rmim⁺]) ionic liquids in a variety of processes, a comprehensive understanding of their physicochemical properties is needed. Moreover, as mentioned earlier, these properties can be fine-tuned for a specific need by altering the constituent

ions and substituents present on either of these ions. Some of the important properties of imidazolium-based ionic liquids have been discussed in the following section.

1.2.2.1 Melting Points

Modern ionic liquids and conventional molten salts, both are entirely composed of ions however, there is a large difference in their melting points. For example, sodium chloride (NaCl), melts at 1074 K, whereas modern ionic liquids have melting points below 373 K. One can question, although both are composed of ions, why there is a large difference in their melting temperatures? What are the factors that control the melting points of these ionic substances? In case of conventional molten salts, the ions are symmetrical and small in size and are held together by strong electrostatic interactions as a result they can pack close to each other. This leads to high lattice energies and thus, they melt at higher temperatures. Usually, the strength of electrostatic attraction depends on the amount of charge on the ions and distance between them. Therefore, to reduce the strength of electrostatic attraction, either charge on the ions has to be lowered or distance between the ions needs to be increased. In other words, choosing an ion that has bulky size and low molecular symmetry preferentially diminishes the strength of electrostatic attraction. As mentioned earlier, ionic liquids are composed of bulky-sized and low symmetric organic cations, which prevent close packing and hence lead to low lattice energy, consequently melt at lower temperatures. Similarly, small-sized anions replace with bulkier ones and these can have a significant influence on melting temperatures. In addition to these factors, if charge on either the cation or the anion is delocalized over

many atoms, it leads to a further decrease in the melting point. All the above-mentioned factors contribute towards weakening of the interactions between the ions, which results in low lattice energy and hence ions remain in the liquid state.

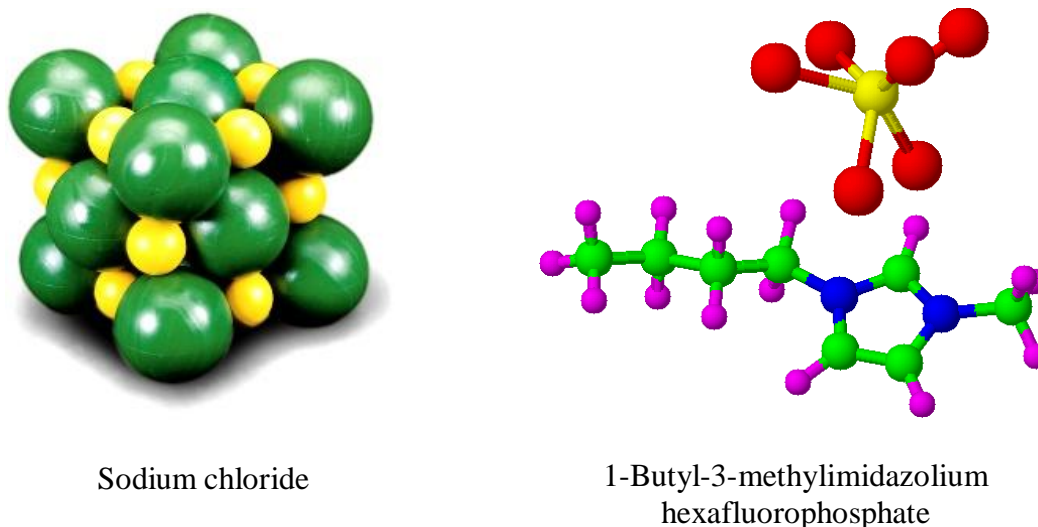


Figure 1.2 Structures of conventional molten salt and modern ionic liquid.

1.2.2.2 Polarity

As mentioned earlier, solvents have a dramatic affect on chemical reactions⁹³ and these are generally classified based on one of their most important properties, which is the polarity. Polarity may be defined as the sum of all possible (specific and nonspecific) intermolecular interactions between the solvent and any potential solute, excluding those interactions leading to definitive chemical changes of the solute.^{94,95} There are many experimental methods, to characterize the solvent polarity and each scale highlights different aspects of these interactions. Among them, dielectric constant, the most widely used polarity scale for a large number of molecular liquids. The experimental methods to

determine polarities have been extended to ionic liquids and are extensively reviewed by Hallet and Welton.¹⁶ According to them, polarities of these liquids are similar to alcohols having short to medium alkyl chain length. In ionic liquids numerous interactions prevail between cations and anions. Since polarity arises due to all the possible interactions between solvent and solute it is not possible to describe the polarity of ionic liquids with single parameter such as dielectric constant. Therefore, multi-parameter scales such as Kamlet-Taft and Abraham model that are available in the literature^{16,96} have been considered. These scales describe polarity, hydrogen bond acidity and hydrogen bond basicity of ionic liquids.^{97,98} It may be noted that the Kamlet-Taft method employs solvatochromic comparisons of UV-vis spectra data of closely related dyes, whereas Abraham model uses gas chromatography experiments. In these experiments ionic liquids are used as stationary phases for gas chromatography and the retention times of various probe molecules are analyzed with the aid of solvation parameter model. Both the models predict qualitatively similar trends for hydrogen bond basicities of the ionic liquids and it mainly depends on the nature of the anion. In contrast, the trends predicted by the two scales for the hydrogen bond acidities are in conflict with each other. Welton and co-workers,^{99,100} rationalized this discrepancy by taking into consideration the presence and absence of charge on the solute molecules used in both the methodologies. On the basis of their work, it has been suggested that phenomena dominated by Coulombic interactions are better modeled using polarity scales based upon charged solutes, whereas those for which Coulombic interactions are not significant, polarity scales based upon neutral solutes need to be considered.¹⁰⁰ Hydrogen bond acidity and basicity have been widely

used to describe the specific interactions between solutes and constituent ions of ionic liquids.^{101,102}

1.2.2.3 Viscosity

Viscosity is an internal property of liquids, which describes the resistance for flow. This is an important property of the solvents and plays a significant role on the rates of chemical reactions. Viscosities of ionic liquids are higher than most molecular solvents and this is a limitation for large-scale applications. Higher viscosities of ionic liquids arise due to Coulombic, hydrogen bonding and van der Waals interactions that prevail between the constituent ions. Therefore, viscosities of these liquids can be varied by altering the interaction strength, which in turn depends on the nature of the ions present in the ionic liquid. Besides, viscosities of these liquids also vary notably with chemical structure, composition, temperature and the presence of impurities. In this thesis, temperature-dependent viscosities of 1-alkyl-3-methylimidazolium ([Rmim⁺]) based ionic liquids with various anions such as tetrafluoroborate ([BF₄⁻]), hexafluorophosphate ([PF₆⁻]), bis(trifluoromethylsulfonyl)imide ([Tf₂N⁻]) and tris(pentafluoroethyl)trifluorophosphate ([FAP⁻]) have been measured by varying the length of the alkyl chain on the imidazolium cation. It has been observed that, viscosities of [Rmim⁺][Tf₂N⁻] ionic liquids are, in general, lower than those found for [Rmim⁺][PF₆⁻] as a result of delocalization of the charge over the large [Tf₂N⁻] anion. For a instance, at 298 K, viscosity of 1-butyl-3-methylimidazolium ([bmim⁺]) with [Tf₂N⁻] is, 50.2 mPa s, much lower than the viscosity of [bmim⁺][PF₆⁻], which is 267 mPa s. This observation indicates that there is a dramatic

influence of the nature of the anion on the viscosity of ionic liquids. Furthermore, with an increase in temperature the strength of the interactions diminishes between the cations and anions of the ionic liquid resulting in lower the viscosities. An increase in viscosity has been observed with an increase in the length of the alkyl chain on the imidazolium cation for all the anions employed in this study. For example, at 298 K, the viscosity of 1-ethyl-3-methylimidazolium tetrafluoroborate is 37.4 mPa s and this number increases to 328 mPa s for the octyl derivative at the same temperature. In the Chapters 3 and 4, temperature-dependent as well as alkyl chain length-dependent viscosities will be given for all the ionic liquids used in the present study.

Apart from the above-mentioned factors, addition of cosolvent to ionic liquids remarkably influences the viscosity without alteration of cation or anion of the ionic liquids. The addition of cosolvents diminishes the Coulombic interactions between the cations and anions of the ionic liquid leading to lowering of the viscosities.^{89,101,104} However, the extent of reduction largely depends on nature of cosolvent added to the ionic liquids. Therefore, at present, research on the binary mixtures has received considerable attention due to their unusual affect not only on the viscosity but also on various structural and physicochemical properties of ionic liquids.¹⁰⁵⁻¹⁰⁸

1.2.3 Structural Properties of Imidazolium-Based Ionic Liquids

The structural properties of imidazolium-based ionic liquids have been explored by theoretical as well as experimental investigations.³⁷⁻⁵⁰ The observed results indicate

that the structure of the ionic liquids plays a significant role on their physicochemical properties, which in turn depends on the constituent ions and substituents present on either of the ions. It may be noted that the overall properties of ionic liquids result from the collective properties of the cationic and anionic structures. For example, anion controls water miscibility and hydrogen bond basicities, while cation has a significant influence on hydrophobicity and hydrogen bond donating ability.¹⁰⁹ Therefore, investigation of structural aspects of an ionic liquid is a preliminary step towards understanding its physicochemical properties.

Early studies dealing with the structural aspects of ionic liquids emphasized the role of hydrogen bonding interactions between the imidazolium cation and the anions by nuclear magnetic resonance (NMR) studies.¹¹⁰⁻¹¹⁴ Furthermore, X-ray studies on 1,3-dialkylimidazolium-based ionic liquids have also been carried out and the observed results indicate that, they form an extended network of cations and anions connected together by hydrogen bonds. The monomeric unit of imidazolium cation is surrounded by at least three anions and in turn each anion by a minimum of three imidazolium cations.¹⁷ Figure 1.3 gives a schematic of supramolecular structure of imidazolium-based ionic liquids. However, the number of anions surrounding the imidazolium cation (and *vice versa*) can vary depending on size of the anion and type of *N*-alkylimidazolium cation. The presence of hydrogen bonds in the imidazolium-based ionic liquids can be identified by substituting a methyl (-CH₃) group in place of the protons on the imidazolium cation, which results in the complete disappearance of the spectral bands associated with hydrogen bonds. Ludwig and his group¹¹⁵⁻¹¹⁷ have extensively used various spectroscopic

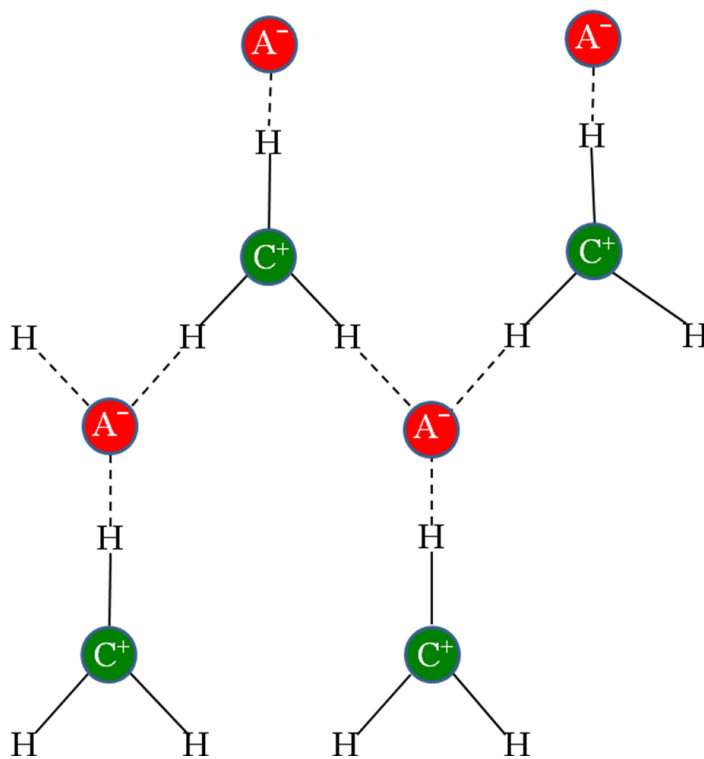


Figure 1.3 View of two-dimensional model of the polymeric supramolecular structure of 1,3-dialkylimidazolium-based ionic liquids showing hydrogen bonds between the imidazolium cations (C^+) and anions (A^-).

techniques to identify the presence of hydrogen bonds in various dialkylimidazolium-based ionic liquids with bis(trifluoromethylsulfonyl)imide and they have observed that the spectral bands related to hydrogen bonds disappeared when protons of the imidazolium cation were replaced by the methyl groups.

Apart from the above-mentioned hydrogen bonding interactions, strong Coulombic interactions prevailing between constituent ions as well as van der Waals interactions between the nonpolar alkyl chains present on one of the ions play a significant role in the structure and properties of ionic liquids.^{28,118} As a consequence of these interactions, supramolecular organized structures arise on various length

scales.^{37,39,119-127} The possible formation of organized structure in ionic liquids has been predicted by molecular dynamics simulation studies and the organized structure can be considered as a three-dimensional network comprising aggregation of alkyl chains in nonpolar domains and ionic channels formed by the anions and cations.^{37,119-121,127,128} The predicted structure has also been confirmed by X-ray diffraction,^{129,130} diffusion measurements,^{131,132} neutron diffraction,⁴⁵ ultrafast excited dynamics¹³³⁻¹³⁷ and low-frequency Raman spectroscopy.¹²² Besides, new experimental evidence supporting the organized structure of ionic liquids has also been discussed to a large extent by Russina and Triolo¹³⁸ with the aid of the small-wide angle X-ray scattering technique. The observed results indicate that the structure and properties of ionic liquids are influenced by the nature of the ions and substituents such as the nonpolar alkyl chains attached to the constituent ions of the ionic liquids. The alkyl chains on the imidazolium cation undergo aggregation, and this behavior, in particular, depends on the length of the alkyl chain and also on the nature of the anion present in ionic liquids.⁴⁶⁻⁵⁰ Thus, as mentioned above, the aggregation behavior of alkyl chains and numerous interactions prevailing between the constituent ions lead to a complex organized structure of the ionic liquids. The complex structure of these ionic liquids results in novel physicochemical properties, which are vastly different compared to the conventional solvents. Therefore, to get a better appreciation of the influence of organized structure on the chemical reactivity, various chemical processes need to be carried out in different classes of ionic liquids.

In the present thesis, rotational diffusion of various organic solutes has been investigated in 1-alkyl-3-methylimidazolium-based ionic liquids with strongly associating

anions $[\text{BF}_4^-]$ and $[\text{PF}_6^-]$ as well as weakly associating anions $[\text{Tf}_2\text{N}^-]$ and $[\text{FAP}^-]$. Photoisomerization dynamics of a carbocyanine derivative has also been examined in 1-alkyl-3-methylimidazolium bis(trifluoromethylsulfonyl)imides. These ionic liquids have been chosen because their physicochemical and structural properties have been well-documented.^{15-18,37-50} Influence of these properties on solute rotation will be extensively discussed in the Chapters 3 and 4, while Chapter 5 describes photoisomerization of a carbocyanine derivative in ionic liquids and how it is different compared to that observed in conventional solvents such as alcohols.

1.3 Microheterogeneous Systems

An amphiphilic molecule essentially consists of two parts with each having the propensity to get solubilized in polar and nonpolar solvents. One is a head group, which is made up of an ionic or a polar nonionic group, while the other is a tail group having hydrocarbon chains of varying length.¹³⁹⁻¹⁴² In polar solvents, such as water, amphiphiles have a tendency to arrange themselves at the air-water interface in such a way that the hydrophobic groups point away from water. The driving force for amphiphilic aggregation is the hydrophobic interactions, which are arising from the water molecules to reduce contact with the hydrocarbon chain of the amphiphilic molecule. Above certain concentration, known as critical aggregation concentration, the amphiphilic molecules undergo self-aggregation so that the energetically unfavorable hydrocarbon-water interactions are diminished.¹³⁹⁻¹⁴³ The self-aggregation of amphiphilic molecules to form definitive structures, such as micelles, vesicles and reverse micelles, are controlled by a

balanced hydrophobic attractive forces at the hydrocarbon-water interface and electrostatic or steric repulsions of the head groups. Thus, a balance is achieved at certain interfacial area, a_0 , per molecule exposed to the aqueous phase, termed as effective head group area. Once the volume of the hydrophobic alkyl chain v and its effective chain length l_c are known, the type of structure can be predicted by the geometrical packing considerations. It depends on the critical packing parameter P , which can be defined as v/a_0l_c .¹⁴⁴⁻¹⁴⁶ The critical packing parameter concept is extremely useful, especially, to predict changes in the shapes of the organized assemblies induced by variations in the

Table 1.1: Shapes of the Surfactant Self-assembly for Different Values of the Packing Parameter

Critical packing parameter	Shape of self-assembly
$< 1/3$	<i>Spherical micelles</i>
$1/3 < P < 1/2$	<i>Cylindrical micelles</i>
$1/2 < P < 1$	<i>Vesicles or Flexible bilayers</i>
$P = 1$	<i>Planar bilayers</i>
$P > 1$	<i>Reverse micelles</i>

experimental conditions. Table 1.1 gives the shapes of various types of organized assemblies that are formed for different values of the critical packing parameter. Among

these organized assemblies, reverse micelles have received a considerable attention because they have emerged as model systems for investigating the behavior of the molecules in restrictive geometries. In addition to these aspects, reverse micellar media are extensively employed in various industrial applications such as detergency, food products, cosmetics, separation technology and material synthesis.¹⁴⁷⁻¹⁴⁹

1.3.1 Reverse Micelles

The aggregation of surfactant molecules to form organized assemblies not only takes place in aqueous solutions but also occurs in a variety of nonpolar solvents. Organized assemblies such as reverse micelles are aggregates of surfactants formed in nonpolar solvents with the polar head groups of the surfactants pointing inwards and the hydrocarbon chains pointing towards the nonpolar bulk phase.¹⁵⁰⁻¹⁵² The simplest reverse micellar systems to be considered are those consisting of three or four component systems with surfactant, hydrocarbon and water, which may or may not contain a co-surfactant. The physicochemical properties of these reverse micelles are markedly different compared to normal micelles, in particular, their ability to solubilize large amounts of water in the inner polar core. Furthermore, the size of the water pool can be controlled by adjusting the mole ratio of water to the surfactant, W . The nature of the water present in the core, especially water bound to the head group region, is different compared to bulk water. These are some of the unique features of the reverse micelles. Therefore, a good number of studies dealing with reverse micelles are devoted to carrying out various types

of chemical reactions in these water pools. The properties of water pool largely depend on nature and type of surfactant employed in the formation of reverse micelles.¹⁵³

Reverse micelles formed by the anionic surfactant, Aerosol OT [sodium bis(2-ethylhexyl)sulfosuccinate] (AOT) in nonpolar solvents is one of the widely studied and well-characterized systems.¹⁵⁴⁻¹⁷⁴ In particular, AOT is of special interest due to its ability to solubilize relatively large amounts of water in a wide variety of nonpolar solvents. Besides, the presence of branched alkyl chains enables AOT surfactant molecules to attain the requisite critical packing parameter easily.^{175,176} In contrast, surfactants having single alkyl chain such as sodium dodecyl sulfate (SDS) and cetyltrimethylammoniumbromide (CTAB) also form reverse micelles under ambient conditions but only in the presence of a co-surfactant.¹⁷⁷⁻¹⁸¹ The structural aspects of AOT reverse micelles have been well-characterized as a function of W .^{151,161} Many researchers have carried out investigations dealing with AOT reverse micelles to understand the water pool properties such as size, polarity, microviscosity and reactivity of the solutes dissolved in them.¹⁵⁴⁻¹⁷³ The observed results indicate that the water pool properties change as a function of W especially, at lower values. At higher water content, water molecules inside AOT reverse micelles attain the characteristics of bulk water. Apart from the water pool, interfacial region of AOT reverse micelles is another interesting aspect that has been extensively studied.¹⁸²⁻¹⁹⁰ Dynamics of water molecules located at the interface^{180,191,192} and other properties such as polarity, viscosity and hydrogen bonding ability of the water molecules in the vicinity of the interface have also been investigated for different values of W .^{150,151,193-195} Even though, most of these studies

devoted to characterization of the interface, there is no quantitative relation that describes the friction experienced by the solute molecules at the interface. Thus, the present thesis aimed at finding out a quantitative parameter that describes the interfacial friction.

Investigation of dynamical processes such as solute rotation and photoisomerization of medium-size solute molecules in reverse micelles provides important information pertinent to molecular motions in restricted geometries. These processes, especially, rotational diffusion of various organic solutes has been extensively investigated in reverse micelles and the observed results have been rationalized in terms of water droplet size and micellar packing.^{185,188-190,196-200} Photoisomerization of carbocyanine derivatives in AOT reverse micelles were also carried out at low and high values of W and the observed results have been explained on the basis of the size of the water pool.^{201,202} It is a well-known fact that an increase in W alters not only the water pool size but also other structural parameters such as aggregation number and hydrodynamic radius of the reverse micelles. Therefore, it is not clear whether the size of the water pool alone is sufficient to explain the isomerization process in reverse micelles. Thus, the Chapter 6 of the thesis will present a systematic description of photoisomerization of carbocyanine derivatives in AOT reverse micelles to characterize the interfacial friction.

1.4 Scope of the Thesis

Studies involving rotational diffusion and photoisomerization provide a useful handle to probe the local environment in complex fluids. In simple liquids these processes

have been examined to a large extent and the observed results indicate that the rates of dynamical processes are essentially governed by the macroscopic properties of the medium. In contrast, solute dynamics in complex fluids is usually dictated by the microenvironment. Therefore, it is imperative to comprehend the microenvironment of the complex fluids to get a better appreciation of chemical reactivity in these media. Thus, this thesis is directed towards understanding the dynamics of solute molecules in complex fluids such as ionic liquids and reverse micelles. The outline of the work to be discussed in the thesis is given below.

Ionic liquids have emerged as promising alternatives to conventional solvents due to their novel structural and physicochemical properties. In the recent past, theoretical and experimental methods have been employed to unravel structure and properties of ionic liquids.³⁷⁻⁵⁰ The observed results indicate that the nature of the ions and the presence of alkyl chains on either of the ions significantly influence structural and physicochemical properties. Moreover, the long alkyl chains attached to one of the ions undergo aggregation, which in turn leads to the formation of organized structure. Although, the presence of organized structure in ionic liquids has been well-documented in literature, little information is available pertinent to its influence on the dynamical processes. Therefore, understanding the affect of organized structure on solute rotation is one of the main goals of the present thesis. For this purpose, rotational diffusion of two structurally similar nonpolar and ionic solutes has been examined in 1-alkyl-3-methylimidazolium-based ionic liquids using time-resolved fluorescence spectroscopy. The results were analyzed with the aid of Stokes-Einstein-Debye (SED) hydrodynamic theory and the

observed deviations have been explained by taking into consideration the organized structure of these ionic liquids. Furthermore, the thesis also addresses the influence of strongly and weakly associating anions of the ionic liquids on solute rotation as the nature of the anion has a profound bearing on their organized structure. Besides rotational diffusion studies, photoisomerization investigations have also been carried out in ionic liquids to find out how the photoisomerization of a carbocyanine derivative is influenced by the organized structure of the ionic liquids. Apart from ionic liquids, photoisomerization studies of carbocyanine derivatives have also been performed in AOT reverse micelles to understand how the interfacial packing affects isomerization rates and whether the observed rates can be correlated with micellar structural parameters.

In summary, this thesis essentially provides a comprehensive understanding of the role of organized structure of ionic liquids on solute dynamics. It also deals with photoisomerization process in reverse micelles to characterize interfacial friction in these systems. The references given at the end of the thesis will provide a glimpse of the work that has been carried out in ionic liquids and reverse micelles.

Chapter 2

Experimental Techniques

2.1. Introduction

Recent advances in laser spectroscopy have enabled chemists to examine various physical, chemical and biological processes at the molecular level. These techniques facilitate exploration of many of the elementary processes in condensed media that take place on rapid time scales, which pave way for the formation of intermediate species. However, it was not possible to study such fast processes till a few decades ago. The availability of laser sources that are capable of delivering extremely short pulses has allowed physical chemists to initiate and monitor these fast processes. As a consequence of these technological strides it is now possible to elucidate detailed mechanisms of numerous biological and chemical processes.²⁰³ The present doctoral work deals with investigation of dynamical processes such as solute rotation and photoisomerization in complex fluids and these processes take place on time scales of tens of picoseconds to a few nanoseconds. This endeavor is made possible by the latest technological advances in laser spectroscopy.

To explore the above-mentioned dynamical processes, the main experimental techniques used in the present thesis are steady-state and time-resolved fluorescence spectroscopy. Quantum yield measurements were carried out using steady-state

absorbance and fluorescence techniques, whereas time-resolved fluorescence and anisotropy measurements were performed using time-correlated single-photon counting technique. Auxiliary parameters such as viscosity and refractive index were measured using rheometer and refractometer, respectively. This Chapter gives a brief account of various experimental techniques that have been used to carry out the research work described in this thesis.

2.2. Steady-State Absorption Measurements

Optical absorption (Ultraviolet visible; UV-Vis) spectroscopy is a simple yet a powerful tool to obtain the information about the ground-state absorption characteristics of the chemical systems in terms of wavelengths of the absorption bands and extinction coefficients at different wavelengths. UV-Vis absorption spectroscopy, being dependent on electronic structure and environment of the chromophore, allows the characterization or identification of the various chromophoric systems and their microenvironments.²⁰⁴⁻²⁰⁶

Optical absorption spectroscopy has innumerable applications such as structure elucidation, quantitative and qualitative evaluation of chemical species.²⁰⁷⁻²⁰⁹

Furthermore, a small change in the polarity of the solvent can induce a significant shift in the absorption spectra hence, this photochemical technique gives preliminary information about a chromophore in the ground-state and the environment surrounding it. Measurement of optical absorption spectra is essential to get the knowledge about absorbance of an experimental solution containing the chromophore at a given wavelength, which in turn is useful for adjusting its concentration. In this work,

absorbance measurements have mostly been used to make solutions with a desired concentration of the chromophore for the purpose of quantum yield estimates and also during time-resolved experiments.

The absorbance (A_λ) of a species in a solution is directly proportional to its concentration (C) and molar extinction coefficient (ϵ_λ) at the wavelength (λ) of measurement, which is given by equation 2.1.

$$A_\lambda = \log\left(\frac{I_0}{I}\right) = \epsilon_\lambda Cl \quad (2.1)$$

In the above equation, I_0 and I are the intensities of the incident and transmitted light, respectively, and l is the path length of the light beam passing through the sample. For the purpose of absorbance measurements, the sample is usually kept in a quartz cuvette of 1 cm path length.

2.3. Steady-State and Time-Resolved Emission Measurements

Fluorescence spectroscopy is a simple but extremely useful technique for investigating various photochemical processes that take place in the first excited state (S_1) of chromophore molecules. Intensity of the fluorescence, fluorescence maximum (emission maximum) and shapes of fluorescence spectra are in general very sensitive to environmental effects. In this work, steady-state fluorescence measurements were carried out using a Hitachi F-4500 spectrofluorometer. This fluorometer employs a 150 W continuous powered high pressure xenon lamp as the excitation source and R-928F (Hamamatsu) photomultiplier tube as the photodetector. Sample is usually kept in 1 cm²

quartz cuvette, which is illuminated at the centre and fluorescence emission is collected perpendicular to the direction of the excitation beam. The wavelength range covered in the present instrument is from 220 to 800 nm. In this thesis, the important parameter that was measured using steady-state fluorescence technique is quantum yield and the following section describes the procedure involved in the measurement of quantum yields.

2.3.1. Fluorescence Quantum Yield Measurement

Fluorescence quantum yield is an intrinsic property of fluorophore and is important for the characterization of novel fluorescent probes. Quantum yield of fluorescence is defined as the ratio of the number of fluorescence photons emitted to the total number of photons absorbed.

$$\phi_{fluorescence} = \frac{\text{Number of Photons Emitted}}{\text{Number of Photons Absorbed}} \quad (2.2)$$

Since, the determination of absolute number of photons absorbed and emitted by the sample is difficult, fluorescence quantum yield of an unknown sample is usually obtained by a comparative method. Solutes dissolved in ethanol were used as standards for the studies described in this thesis. Absorbance of the sample and standard were matched up to third decimal and it was ensured that the value did not exceed 0.1 at the wavelength of excitation to avoid the inner filter effects. Samples containing the fluorophores were excited at suitable wavelengths and corrected emission spectra were recorded. Quinine sulfate was used as quantum counter to record the corrected emission spectra. The

integrated areas in the corresponding wavelength regions were calculated and compared to that of a standard. Fluorescence quantum yield (ϕ_{sample}) of sample has been determined with respect to the quantum yield of a standard ($\phi_{standard}$) using the following equation.²⁰⁶

$$\phi_{sample} = \phi_{standard} \times \frac{I_{sample}}{I_{standard}} \times \frac{A_{standard}}{A_{sample}} \times \frac{n_{sample}^2}{n_{standard}^2} \quad (2.3)$$

In the above equation, I_{sample} and $I_{standard}$ are the integrated areas under the corrected emission spectra of the sample and the standard, respectively, while A_{sample} and $A_{standard}$ are the corresponding absorbance values. n_{sample} and $n_{standard}$ are refractive indices of the sample and the standard, respectively. In this expression it is assumed that the sample and the standard are excited at the same wavelength so that it is not necessary to correct for the different excitation intensities at different wavelengths. In the present thesis, experimentally measured quantum yields in combination with the fluorescence lifetimes have been used to obtain the radiative and nonradiative rate constants.

Steady-state fluorescence technique, however, cannot provide information pertinent to the dynamics of the fluorophore, which can be obtained with the aid of time-resolved techniques. The dynamical parameters that have been measured during the course of the doctoral work are lifetimes from time-resolved fluorescence decays and reorientation times from anisotropy decays. A detailed account of these parameters and the measurement methods have been described in the following sections.

2.3.2. Fluorescence Lifetime

Prior to the discussion concerning the measurement of lifetimes, it is essential to know the meaning of the term lifetime or decay time (τ_f). Excitation of the sample containing fluorophores with a very short pulse of light results in an initial population of n_0 in the excited-state. The excited-state population decays due to a combination of radiative and nonradiative rate processes, which is given by the following equation.²⁰⁶

$$\frac{dn(t)}{dt} = -(k_r + k_{nr})n(t) \quad (2.4)$$

In the above equation, $n(t)$ is the number of molecules in the excited-state at time t following the excitation, k_r is the radiative rate constant and k_{nr} is the nonradiative rate constant. Emission from the excited state is a random event, and each excited fluorophore has the same probability of emitting a photon in a given period of time. This results in an exponential decay of the excited state population as a function of time. However, in an actual fluorescence experiment, it is often difficult to observe number of excited molecules and it is a well-known fact that fluorescence intensity is directly proportional to the number of excited molecules present in the solution. Therefore, equation 2.4 can be simply expressed in terms of the time-dependent intensity $I(t)$ and integration of equation 2.4 gives the following expression.

$$I(t) = I_0 \exp(-t/\tau_f) \quad (2.5)$$

In the above equation, I_0 is the intensity at time zero. The lifetime of the sample is the inverse of the total decay rate constant ($k_r + k_{nr}$) and is given by

$$\tau_f = \frac{1}{k_r + k_{nr}} \quad (2.6)$$

If the width of the excitation pulse is unusually short (δ -pulse) and the response time of the detection system is very fast compared to the fluorescence lifetime of the sample then fluorescence lifetime can be obtained from the observed fluorescence decay by following two procedures. In the first method, τ_f can be obtained simply by noting the time at which the fluorescence intensity decreases to $1/e$ of its initial value. In the other method, the lifetime can be determined from the slope of the plot of $\log I(t)$ versus t .²⁰⁶ In a scenario where fluorescence lifetime of the sample is quite short such that the excitation pulse width and/or the response time of the detection system distorts the observed decay, it is not possible to apply the above-mentioned procedures to obtain the fluorescence lifetime of the sample. Under such circumstances, the observed fluorescence decays are analyzed using a deconvolution procedure, which will be discussed in due course.

2.3.3. Fluorescence Anisotropy

In a homogeneous solution, ground-state fluorophores are all randomly oriented. When such an isotropic ensemble of chromophores is excited with polarized light, an anisotropic distribution is created due to preferential excitation of the suitably oriented fluorophores in the solution and this phenomenon is commonly known as photoselection.

Therefore, observation and measurement of fluorescence anisotropy is based on photoselective excitation of fluorophores, which can be understood by considering the orientation of absorption and emission transition dipoles. Each fluorophore has, within its molecular framework, a set of fixed absorption and emission transition dipoles, which have a definite orientation with respect to the molecular axis and separated from each other by an angle β . Fluorophores, preferentially, absorb those photons whose electric field vector aligned parallel to their absorption transition dipole moment of the polarized excitation light. The probability of absorption is proportional to $\cos^2 \theta$, where θ is an angle the transition dipole of the molecule makes with the electric field vector of the polarized light. Thus, the absorption is maximum when $\theta = 0^\circ$ and becomes negligible when θ approaches 90° . Therefore, the excited state population is not randomly oriented. Instead, there will be anisotropic distribution of excited molecules that have their absorption transition dipole moment aligned to the polarization of the excitation light. The preferential excitation of molecules creates anisotropy in excited electronic state and a mirror image of this anisotropy in the ground-state, which is schematically shown in the Figure 2.1. In dilute solution, where depolarization via energy transfer is insignificant, the ground-state anisotropy decays due to rotational relaxation and electronic relaxation, while the excited-state anisotropy decays solely due to rotational relaxation. The anisotropy measurements reveal the average angular displacement of the fluorophore that occurs between the absorption and the subsequent emission of a photon. This angular displacement is dependent upon the rate and extent of rotational diffusion during the lifetime of the excited state. The rotational diffusion of a molecule, in turn,

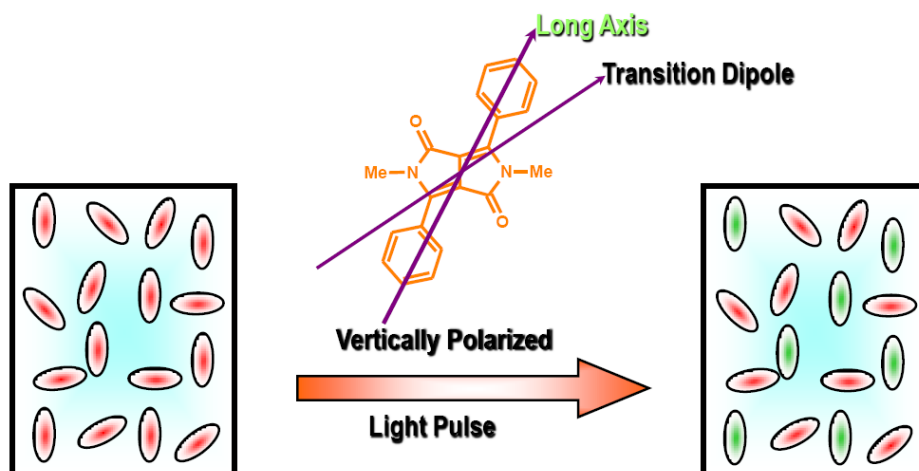


Figure 2.1 *Creation of ground-state and excited-state anisotropies from isotropic distribution of molecules.*

depends on its size and shape and also on the viscosity of the surrounding medium. Thus, studies dealing with fluorescence anisotropy of various organic solutes have extensively been used to explore solute-solvent interactions as well as the local environment.²⁰⁶

Fluorescence anisotropy can be measured using steady-state as well as time-resolved methods. Steady-state measurements are those performed under constant illumination and observation. In the steady-state measurement, the sample is illuminated with a continuous beam of light, and the intensity or the emission spectrum is recorded. When the sample is first exposed to light, steady-state is reached almost instantaneously. The sample is excited with vertically polarized light, and fluorescence spectra are recorded for both parallel and perpendicular polarizations of the emitted light with respect to the excitation polarization. The general measurement procedure of the fluorescence anisotropy is illustrated in the Figure 2.2.

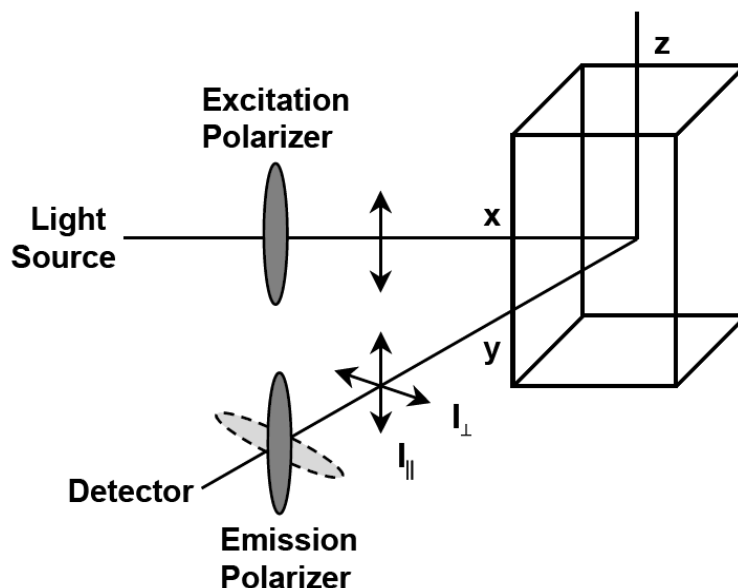


Figure 2.2 Schematic diagram describing measurement of fluorescence anisotropy.

The sample is excited with vertically polarized light, in other words, the electric vector of the excitation light oriented along the z-axis. The emission from the sample measured through the polarizer either parallel (\parallel) or perpendicular (\perp) with respect to the excitation polarization. When the emission polarizer is oriented parallel to the excitation polarization, the observed intensity is labeled as I_{\parallel} . On the other hand, when the emission polarizer is oriented perpendicular to the excitation polarization, the observed intensity is designated as I_{\perp} . Since, the response of the emission monochromator is not same for the parallel and perpendicularly polarized light, the measured perpendicular component, I_{\perp} , is corrected by an appropriate correction factor, known as *G*-factor, which depends upon the emission wavelength, and to some extent the

bandpass of the monochromator. Thus, from the measured I_{\parallel} and I_{\perp} values, steady-state anisotropy ($\langle r \rangle$) can be calculated by the following equation.

$$\langle r \rangle = \frac{I_{\parallel} - GI_{\perp}}{I_{\parallel} + 2GI_{\perp}} \quad (2.7)$$

In the above equation, G is the correction factor, which is obtained independently by keeping the excitation polarization horizontal and measuring the fluorescence intensities with the emission polarizers oriented vertical (I_{HV}) and horizontal (I_{HH}). The intensity ratio I_{HV}/I_{HH} gives the measure of the G -factor. Fluorescence anisotropy, as indicated in the equation 2.7, is a dimensionless quantity. Furthermore, it can be noted that the measured anisotropy is independent of the total intensity of the sample. This is because the difference ($I_{\parallel} - GI_{\perp}$) is normalized with total intensity, which is given by $I_T = (I_{\parallel} + 2GI_{\perp})$.

The second type of measurement, time-resolved method, has been extensively used in the present work for measuring the anisotropy decays. In these measurements, the sample is excited by a pulse of light whose the pulse width is typically shorter than the decay time of the sample. The intensity decay is recorded with a high-speed detection system that permits the intensity or anisotropy to be measured on the nanosecond to picosecond time scale. Time-resolved anisotropy measurements are carried out by measuring polarized fluorescence decays $I_{\parallel}(t)$ and $I_{\perp}(t)$ with respect to the polarization

of the excitation light. The time-resolved anisotropy, $r(t)$ is given by the following equation.

$$r(t) = \frac{I_{\parallel}(t) - GI_{\perp}(t)}{I_{\parallel}(t) + 2GI_{\perp}(t)} \quad (2.8)$$

The decay of anisotropy usually follows exponential function of the form given by equation 2.9.

$$r(t) = r_0 \exp(-t/\tau_r) \quad (2.9)$$

In the above equation, r_0 is the anisotropy at time $t=0$, immediately following the δ -pulse excitation pulse. It essentially describes the inherent depolarization for a given molecule; in other words, its value depends on the angle between absorption and emission transition dipoles, which is β . The time constant of the anisotropy decay, τ_r is known as the reorientation time.

2.3.4. Relation between Steady-State and Time-Resolved Parameters

There exists a rather simple relation between steady-state and time-resolved parameters. A steady-state observation is simply an average of the time-resolved phenomena over the intensity decay of the sample. The steady-state intensity $\langle I \rangle$ is related to the decay time of the sample by following expression.

$$\langle I \rangle = \int_0^{\infty} I_0 \exp(-t/\tau_f) dt = I_0 \tau_f \quad (2.10)$$

The value of I_0 depends on the fluorophore concentration and a number of instrumental parameters. Therefore, in molecular terms the steady-state intensity is proportional to the lifetime.

Similarly, the steady-state anisotropy is simply an average of time-resolved anisotropy weighted by the intensity decay of the sample. The steady-state anisotropy $\langle r \rangle$ is given by the average of $r(t)$ weighted by $I(t)$.²⁰⁶

$$\langle r \rangle = \frac{\int_0^{\infty} r(t) I(t) dt}{\int_0^{\infty} I(t) dt} \quad (2.11)$$

Substituting the functional forms of $r(t)$ and $I(t)$ from equations 2.5 and 2.9, respectively, in equation 2.11 and upon integration, the equation for $\langle r \rangle$ can be obtained in terms of r_0 , τ_r and τ_f , which is given below.

$$\langle r \rangle = r_0 \left(\frac{\tau_r}{\tau_r + \tau_f} \right) \quad (2.12)$$

However, this expression is valid only if the intensity and anisotropy decays follow single exponential functions. In most cases, however, intensity and anisotropy decays are more complex and do not obey the relations given by equations 2.5 and 2.9. The intensity decay of a fluorophore can follow a biexponential decay law when it is present in different environments (e.g. micelle bound and free dye) and is given by,

$$I(t) = a_1 \exp(-t/\tau_{f1}) + a_2 \exp(-t/\tau_{f2}) \quad (2.13)$$

where τ_{f1} and τ_{f2} are the two lifetimes associated with the decay of fluorescence, while a_1 and a_2 are the pre-exponential factors. The decay of a fluorophore residing in two different environments usually contains two time constants. Thus, for the same fluorophore in different environments, the pre-exponential values represent the fraction of the fluorophore in different environments. Similarly, in case of anisotropy decay, a biexponential functional form is given by

$$r(t) = r_0 [\beta_1 \exp(-t/\tau_{r1}) + \beta_2 \exp(-t/\tau_{r2})] \quad (2.14)$$

In the above expression, τ_{r1} and τ_{r2} are the two time constants associated with decay of the anisotropy and β_1 and β_2 are represent the contributions of τ_{r1} and τ_{r2} to the anisotropy decay. Biexponential anisotropy decays usually arise when the fluorophore undergoes different kinds of motion as a consequence of its shape or being in a complex environment. More complex intensity and anisotropy decays are also possible and they are usually expressed as the sums of exponentials, which are indicated below.

$$I(t) = \sum_i a_i \exp(-t/\tau_{fi}) \quad (2.15)$$

$$r(t) = r_0 \left[\sum_i \beta_i \exp(-t/\tau_{ri}) \right] \quad (2.16)$$

2.3.5. Measurement of Time-Resolved Fluorescence

Two widely used techniques for the measurement of time-resolved fluorescence are the frequency-domain and time-domain method. In frequency-domain or phase-modulation method, the sample is excited with intensity-modulated light, typically, sine wave modulation is employed. The intensity of the incident light is varied at a high frequency thus, its reciprocal frequency is comparable to the reciprocal of the decay time, τ_f . When a fluorescent sample is excited in this manner, the emission is forced to respond at the same modulation frequency. Because of the finite lifetime of the excited state, the modulated emission is delayed in phase by an angle that depends on the lifetime. This delay is measured as a phase shift, which can be used to calculate the decay time.

However, the work presented in this thesis was carried out using time-domain method. Among the different techniques that are available for measuring fluorescence decays, time-correlated single-photon counting (TCSPC) is the most widely used experimental method.⁸ In the early days, the time-resolution was somewhat limited due to flash lamp excitation and conventional photomultiplier detection. However, recent advances in laser technology and microchannel plate (MCP) photomultiplier tubes (PMTs) have led to a significant improvement in the time-resolution of the TCSPC method.²¹¹⁻²¹⁷ As a consequence TCSPC has become the most widely used method for time-resolved fluorescence measurements. In the present study, a TCSPC spectrometer

from Horiba Jobin Yvon IBH, UK (model Data Station Hub) has been used to measure the fluorescence decays and the important aspects of TCSPC are described below.

2.3.5.1. Time-Correlated Single-Photon Counting (TCSPC)

TCSPC is a digital technique of counting photons, which are time-correlated with respect to the excitation pulse. The principle of TCSPC measurement relies on the concept that the probability distribution for the emission of a single photon after an excitation event yields the actual intensity against the time-distribution of all the photons emitted as a result of excitation. By sampling the single photon emission following a large number of excitation pulses, the experiment constructs this probability distribution. The essential prerequisite for this measurement is that only one photon is observed for a large number of excitation pulses. In other words, an extremely low count rate must be maintained such that the system operates in single photon counting mode. In such a situation, the statistics follows the Poisson distribution and true time-resolved emission profile is obtained.^{206,210} A schematic of TCSPC setup, which has been used to measure the time-resolved fluorescence decays, is represented in Figure 2.3. An excitation pulse either from laser or light emitting diode (LED) is split into two parts, one part is used to excite the sample kept in the sample chamber and the other part is used to generate a start pulse from the start PMT or high-speed photodiode. The optical signal from the start PMT generates an electrical START pulse, which is then routed through a constant fraction discriminator (CFD) to START the input of the time to amplitude converter (TAC) to initialize the charging operation. The part of the optical pulse, which excites the

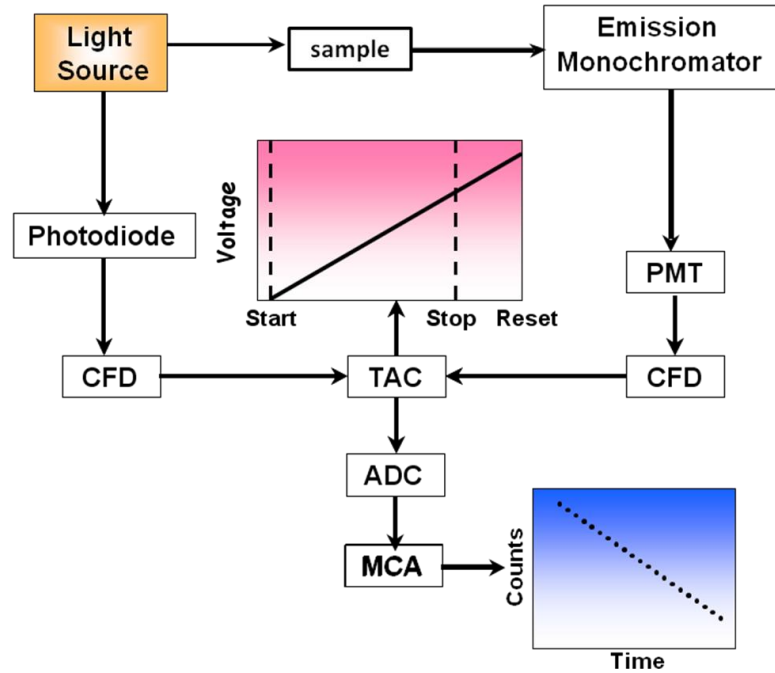


Figure 2.3 Schematic of a TCSPC setup.

sample effectively, gives rise to emission of photons. These photons are then detected by STOP PMT (at the right angle to the direction of excitation) to generate an electrical STOP pulse. The STOP pulse is also routed to the TAC after passing through another CFD and a variable delay line. On receiving the STOP signal, TAC stops its charging operation and generates an electrical output, having amplitude proportional to the time difference between the START and STOP pulses reaching the TAC. The TAC output pulse is then fed to the input of multi channel analyzer (MCA) through an analogue to digital converter (ADC). The ADC generates a numerical value corresponding to the TAC output pulse and thus selects an appropriate channel of the MCA and the count is stored in the channel. The above cycle (from excitation to data storage) is repeated a large number of times and as a result, a histogram of the counts against the channel number of

MCA is generated. It represents the true emission decay, when the collection rate of emission photons by the STOP pulse is very low (2% or less) compared to the repetition rate of the excitation pulses.

If the optical pulses that excite the sample were infinitely sharp (δ -pulse) and if the response of the detection system was infinitely fast, the observed decay curve would represent the true fluorescence decay of the sample. However, the excitation pulse has a finite pulse width and the detection system also has a finite response time. As a consequence, the observed decay $F(t)$ is a convolution of the true decay curve $I(t)$ and the instrument response function $R(t)$. Hence, the emission decay thus observed has to be deconvoluted with the instrument response to get the actual lifetime and the deconvolution procedure is described extensively in the next section. The instrument response function also referred to as the lamp function sometimes is the response of the instrument to a zero lifetime sample. This curve is typically collected using a scattering solution placed in place of the sample and it represents the shortest time profile that can be measured by the instrument. The full-width at half-maximum (FWHM) of the instrument response function depends on the excitation source and detection systems used. The instrument response function is usually measured using a very dilute scattering solution made up titanium dioxide (TiO_2) suspension in water. The lifetime measurements were performed by keeping the emission polarizer at the magic angle (54.7°) with respect to the excitation polarizer. The fluorescence collected at the magic angle with respect to the excitation polarizer is free of anisotropy components and represents the fluorescence decay. The decay of the anisotropy was monitored by measuring the fluorescence decays

parallel $I_{\parallel}(t)$ and perpendicular $I_{\perp}(t)$ with respect to the polarization of the excitation source. When the counts in the decay channel reach a certain precision (usually a decay curve with its peak channel having about five to ten thousand counts is considered to have suitable precision), the number of counts in each channel follows Poisson distribution. For the investigations presented in this thesis, 10000 peak counts were collected for the fluorescence lifetime measurements. Anisotropy decay measurements were carried out by collecting parallel and perpendicular decay components with respect to the polarization of the excitation laser. The two decay components were acquired for at least 900 s each such that a good signal to noise ratio was obtained. Typically more than 20000 counts were collected in the peak channel and the perpendicular component of the decay was corrected for the G -factor of the spectrometer. For anisotropy measurements more number of counts were collected compared to the fluorescence lifetime measurements so that a better precision in the reorientation times is obtained as they are extracted from the simultaneous analysis of the $I_{\parallel}(t)$ and $I_{\perp}(t)$ decay curves.^{218,219} The decays were collected in 4096 channels with a time increment of 13.8 ps/channel.

As mentioned earlier, the TCSPC spectrometer used in the present study is from Horiba Jobin Yvon IBH, UK model Data Station Hub. Different pulsed-laser diodes (LDs) and pulsed light-emitting diodes (LEDs) were used to carry out the work described in this thesis. The use of laser diodes and LEDs results in FWHM of about 100 ps and 1.3 ns, respectively. To carry out part of the work described in this thesis 374 and 445 nm laser diodes have been employed as excitation sources. The IRF for the TCSPC spectrometer used in these studies is about 150 ps. When 560 nm LED was used to excite

the carbocyanine derivatives, the FWHM of the IRF has been found to be 1.3 ns. The temperature of the sample was controlled with the aid of a thermoelectric controller (model DS) from IBH.

2.3.6. Method of Data Analysis

As mentioned in the earlier section, the experimentally measured fluorescence decay $F(t)$ is the convolution of the instrument response function $R(t)$ and the actual fluorescence decay $I(t)$.

$$F(t) = \int_0^t R(t-s)I(s)ds \quad (2.17)$$

Knowing $F(t)$ and $R(t)$, one obtains $I(t)$ by deconvolution of $F(t)$.^{210,220,221} A variety of methods^{206,210} have been proposed for estimation of the impulse response function $I(t)$ from the measured decay curve and the instrument response function $R(t)$. The least-squares method seems to provide the most reliable results.²²²

The nonlinear least-squares method is the most commonly used deconvolution technique for single-photon counting data. The basis of this method is to convolute the integration in equation 2.17 iteratively by adjusting the free parameters in an assumed decay function $I(t)$. The calculated curve $I_c(t)$ is compared with the measured one $I(t)$. The iteration is continued until convergence is attained in the $I_c(t)$ and $I(t)$

values. In the least-squares formulation, the optimum description of a set of data points is one that minimizes the weighted sum of the squares of the deviations of the experimental points $I(t_i)$ from the calculated fitting function $I_c(t_i)$. That is, the quantity

$$\chi^2 = \sum_{i=1}^n W_i [I(t_i) - I_c(t_i)]^2 \quad (2.18)$$

is minimized. In this equation W_i is weighting factor for the i^{th} data point and n is the total number of data points. In the application to SPC data, W_i is the reciprocal of the expected value for $I_c(t_i)$, which, until the fit is completed, is unknown. Usually W_i is approximated by the reciprocal of the measured value $I(t_i)$.²¹⁰ The computer algorithm used for the data analysis is based on Marquardt algorithm²¹ for adjusting the free parameters in successive iterations. In the case of mono- or multi-exponential decay equation for $I(t)$, it is possible to find a recursion relation,²²³ which simplifies the calculation of the convolution integral and the partial derivatives, saving considerable computer time. Various statistical tests are applied to eliminate bias in the analysis of the data. The goodness of the fit of the reconvoluted data with the experimental data is generally tested by a number of statistical tests such as reduced χ^2 being close to unity and random distribution of weighted residuals. These tests are described in detail below.

2.3.6.1. Reduced Chi Square (χ_R^2) Values

It is not convenient to interpret the values of χ^2 because it depends on the number of data points. For this reason it is customary to use the value of reduced χ_R^2 given by equation 2.19.

$$\chi_R^2 = \frac{\chi^2}{n_2 - n_1 + 1 - P} \quad (2.19)$$

Where χ^2 is as defined in equation 2.18, n_1 and n_2 are the first and the last channels of the region chosen for analysis and P is the number of variable parameters in the fitting function. χ_R^2 should be close to 1 for Poisson distributed data.²²³ Values much less than 1 (0.75) are usually a symptom of data in which the number of counts is not large enough.²¹⁰ In case of a good fit, χ_R^2 values range from 0.8 to 1.2. Higher values may have to be accepted in some instances and acceptable values of χ_R^2 may be obtained even for poor fits.

2.3.6.2. Plot of the Weighted Residuals

The weighted residuals are nothing but deviations between the measured and the calculated data weighted by the standard deviations of the measurements. The weighted residuals in channel i are calculated by equation 2.20.

$$r_i(t) = \sqrt{W_i} [I(t_i) - I_c(t_i)] \quad (2.20)$$

These residuals from successful fits when plotted against channel number should be randomly distributed about zero indicating that the only source of difference is the random error in the data.

In the present work, analyses of fluorescence and anisotropy decays were performed using the software supplied by IBH. The anisotropy decays were analyzed using impulse reconvolution method as well as tail fit of the anisotropy data (without reconvolution). Both the methods of analysis yielded identical numbers for the anisotropy decay constants when the time constants measured are more than 450 ps, which is 3 times longer than the FWHM of the IRF.

2.3.7. Measurement of Auxiliary Parameters

This section deals with the measurement of auxiliary parameters such as viscosity and refractive index of the ionic liquids with the aid of rheometer and refractometer, respectively, and a detailed measurement procedure is given below.

2.3.7.1. Measurement of Viscosity (η)

The viscosity of a liquid arises from the internal friction of the fluid, and it manifests itself externally as the resistance of the fluid to flow. In the present study, various ionic liquids were used, and these ionic liquids are usually more viscous than the most common molecular solvents. For the purpose of rotational diffusion and photoisomerization studies, temperature dependent viscosities, of all the ionic liquids

employed in the doctoral work, were measured using a Physica MCR 101 rheometer. Rheometer is a laboratory device used to examine study of flow and deformation of materials under applied force.²²⁴

A. Principle

The liquid is placed within the annulus of one cylinder inside another and one of the cylinders rotates at a set speed. This determines the shear rate inside the annulus. The liquid tends to drag the other cylinder round, and the force it exerts on that cylinder (torque) is measured, which can be converted into shear stress and from the shear stress, viscosity can be calculated by the formula given below.

$$\text{Viscosity} = \frac{\text{Shear Stress}}{\text{Shear Rate}} \quad (2.21)$$

2.3.7.2. Measurement of Refractive Index (n)

Refractive index of the medium is defined as the ratio of speed of light in vacuum (C) to that in the medium (V).

$$n = \frac{C}{V} \quad (2.22)$$

Temperature dependent refractive indices of ionic liquids such as 1-alkyl-3-methylimidazolium bis(trifluoromethylsulfonyl)imides were measured for the purpose of quantum yield measurements with the aid of ATAGO RX-5000 α refractometer. The

principle involved in the refractometer can be understood in the following manner. When light crosses a boundary from one medium into another its direction of travel also changes, that means it is refracted (see Figure 2.4).

The relationship between light's speed in the medium A (V_A) and medium B (V_B), the angles of incidence in the medium A (θ_A) and medium B (θ_B), and the corresponding refractive indices, respectively, n_A and n_B is given below.

$$\frac{V_A}{V_B} = \frac{\sin \theta_A}{\sin \theta_B} = \frac{n_B}{n_A} \quad (2.23)$$

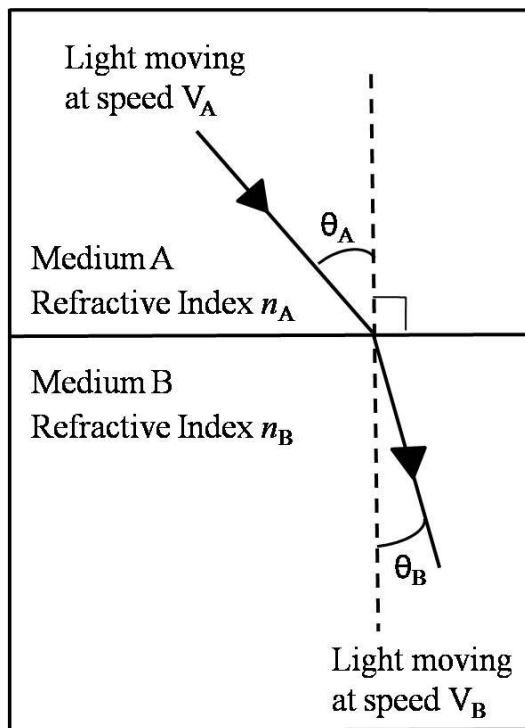


Figure 2.4 Schematic diagram describing measurement of refractive index.

Thus, it is not necessary to measure the speed of light in a sample in order to determine its index of refraction. Instead, by measuring the angle of refraction, and knowing the index of refraction of the layer that is in contact with the sample, it is possible to determine the refractive index of the sample quite accurately.

Chapter 3

Solute Rotation in Imidazolium-Based Ionic Liquids with Strongly Associating Anions

3.1. Introduction

Rotational diffusion studies in ionic liquids are a convenient means to probe solute-solvent interactions and also glean information about the local environment offered by them. A comprehensive understanding of these features will enable us to get a better appreciation of chemical reactivity in ionic liquids. Numerous studies carried out in literature indicate that the structure of the ionic liquids is vastly different compared to molecular solvents, which arises as a consequence of a multitude of interactions prevailing between the cations and the anions, and also hydrophobic interactions between the nonpolar alkyl chains on either the cation or the anion of the ionic liquid. Thus, the prevalence of Coulombic, hydrogen bonding and van der Waals interactions leads to the formation of a complex organized structure of ionic liquids. Such an organized structure is known to cause dynamic heterogeneity in fast processes, which can be defined as the distribution of relaxation rates due to molecules residing in distinct environments of the ionic liquids.^{127,225,226}

Solute rotation is one of the fast processes that has been extensively investigated in ionic liquids.^{101,102,226-242} From recent studies it has become evident that length of the

alkyl chain attached to one of the constituents of the ionic liquid significantly affects solute rotation.^{235,238,239} However, exceptions to this trend have also been reported.²²⁹ These results assume importance since the presence of long alkyl chains on one of the ions of the ionic liquid facilitate the formation of organized structures. In other words, these studies can be used to gauge how the organized structure of the ionic liquids influences dynamical processes. Recently, Khara and Samanta²³⁸ have carried out fluorescence anisotropy measurements of a dipolar solute coumarin 153 (C153) in a series of *N*-alkyl-*N*-methylmorpholinium bis(trifluoromethylsulfonyl)imides and found that for a given viscosity at constant temperature (η/T), the solute rotation becomes faster from ethyl to octyl derivatives. The observed result has been rationalized on the basis of the organized domain structure of these ionic liquids, which offers lower microviscosity to the rotating solute molecule. Based on excitation wavelength and temperature-dependent studies it was also concluded that *N*-alkyl-*N*-methylmorpholinium ionic liquids are more structured and heterogeneous compared to imidazolium-based ionic liquids. Similar studies have been performed by Fruchey and Fayer,²³⁵ using a nonpolar solute perylene in a series of 1-alkyl-3-methylimidazolium bis(trifluoromethylsulfonyl)imides and it has been noticed that for a given η/T , the solute rotation becomes faster from ethyl to octyl derivatives. However, this result has been explained on the basis of perylene molecule experiencing alkane-like environment with an increase in the length of the alkyl chain. For a given η/T , faster rotation of the solute has been noticed upon the variation of the length of the alkyl chain from ethyl to octyl on the anion of the ionic liquids as well.²³⁹ It

may be noted that the examples discussed here are merely illustrative and by no means exhaustive.

From the results portrayed in the preceding paragraph, however, it is not conclusive whether the organized structure of the ionic liquid or the increasingly nonpolar environment that is responsible for the observed behavior. Thus, to address this issue, the present study has been undertaken, wherein temperature-dependent fluorescence anisotropies of a nonpolar solute 9-phenylanthracene (9-PA) and an ionic hydrogen bond donating, solute rhodamine 110 (R110) (Figure 3.1 gives their molecular structures) have been measured in 1-alkyl-3-methylimidazolium $[Rmim^+]$ based ionic liquids with strongly associating anions such as tetrafluoroborate ($[BF_4^-]$) and hexafluorophosphate ($[PF_6^-]$). From Figure 3.1 it can be noticed that the solutes used in the present study are

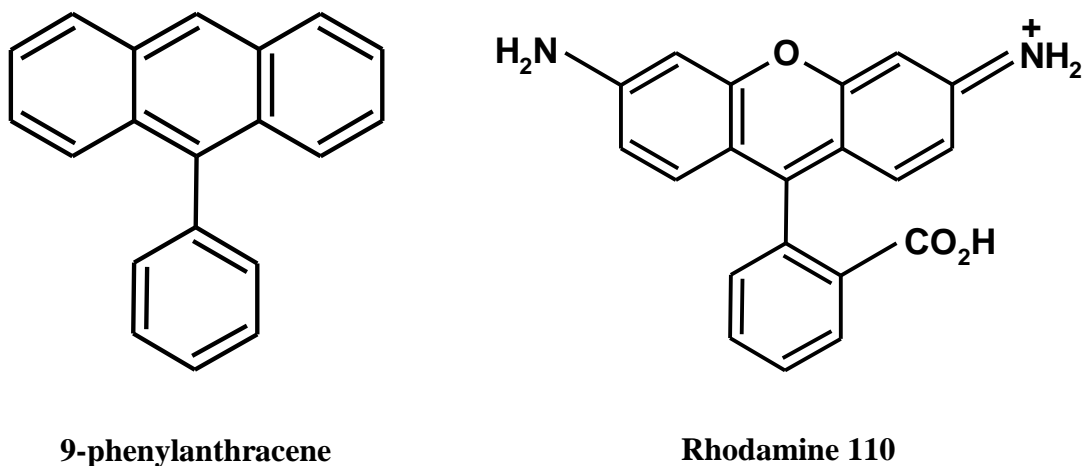


Figure 3.1 *Molecular structures of the solutes.*

structurally similar but chemically distinct. In other words, cationic R110 comprises two terminal NH_2 groups and a carboxylic acid moiety. Thus, R110 essentially forms hydrogen bonds with the anions of the ionic liquids and the strengths of these specific interactions are governed by the hydrogen bond basicities of the anions.¹⁰¹ The ionic liquids used in this work have the cations 1-ethyl-3-methylimidazolium ($[\text{emim}^+]$), 1-butyl-3-methylimidazolium ($[\text{bmim}^+]$), 1-hexyl-3-methylimidazolium ($[\text{hmim}^+]$) and 1-methyl-3-octylimidazolium ($[\text{moim}^+]$) in combination with $[\text{BF}_4^-]$ and $[\text{PF}_6^-]$ anions.

3.2. Materials and Methods

1-Alkyl-3-methylimidazolium ionic liquids with $[\text{BF}_4^-]$ and $[\text{PF}_6^-]$ anions were purchased from io-li-tec. The stated purity of the ionic liquids is >99% with <100 ppm water content and <100 ppm halide ion concentration. Water content of the ionic liquids was estimated by Karl Fischer titration with the aid of Metrohm 831 KF Coulometer and found to be within limits specified by the manufacturer. The fluorophores 9-PA and R110 were obtained from Aldrich and Exciton, respectively. The ionic liquids and fluorophores are of the highest available purity and were used without further purification. Concentrations of 9-PA and R110 in ionic liquids were chosen such that the absorbance is in the range of 0.1–0.2 at the wavelength of excitation. Viscosities of the ionic liquids were measured as a function of temperature using a Physica MCR 101 rheometer and the procedure has been explained in the Chapter 2. The uncertainties on the measured numbers are about 5%.

Time-resolved fluorescence measurements were carried out with a setup that works on the principle of time-correlated single-photon counting.²¹⁰ The setup used in the present study was purchased from IBH, UK and employs a diode laser as the excitation source. The instrumental details have been described in the Chapter 2. Samples containing the probe 9-PA were excited with a 374 nm diode laser and the emission from the samples was collected at 420 nm. On the other hand, samples with the probe R110 were excited with a 445 nm diode laser and the emission was monitored at 550 nm. The decays were collected in 4096 channels with a time increment of 13.8 ps/channel. The instrument response function of the setup was measured by collecting the scattered light from a TiO₂ suspension in water and the full-width at half-maximum was found to be around 150 ps. For lifetime measurements, decays were collected by keeping the emission polarizer at magic angle (54.7°) with respect to the polarization of the excitation laser to ensure the complete depolarization of the fluorescence. Anisotropy decay measurements were carried out by collecting parallel and perpendicular decay components with respect to the polarization of the excitation laser. The two decay components were acquired for at least 900 s each such that a good signal to noise ratio was obtained. To account for the discrepancies in transmission efficiency of the monochromator, the perpendicular component was corrected for the *G*-factor of the spectrometer. All the anisotropy measurements were carried out over the temperature range 298–348 K, only in case of [emim⁺][PF₆⁻] the decays were measured in the range of 338–358 K as its melts around 333 K. The temperature of the sample was controlled with the aid of a thermoelectric controller (model DS) from IBH. Each measurement was repeated 2–3 times and the

average values are reported. The analyses of fluorescence and anisotropy decays were performed using the software supplied by IBH.

3.3. Results and Discussion

The reorientation times (τ_r) of 9-PA and R110 in all the ionic liquids employed in this work have been obtained by fitting the measured anisotropy decays to single exponential function of the form described by the following equation.

$$r(t) = r_0 \exp(-t/\tau_r) \quad (3.1)$$

where r_0 is the limiting anisotropy, whose magnitude is determined by the angle between absorption and emission transition dipoles of the solute molecule. The limiting values of r_0 were found to be in the range of 0.33-0.37. The limiting anisotropy is always less than the fundamental anisotropy (0.4) because, the absorption and emission dipoles are may not be perfectly collinear. Apart from that, the presence of ultrafast component can also lower the r_0 , which cannot be resolved by the finite response time of the instrument. The reorientation times of 9-PA and R110 in [Rmim⁺][BF₄⁻] (from methyl to octyl) along with solvent viscosities at different temperatures are listed in Tables 3.1 to 3.4 and the corresponding parameters in [Rmim⁺][PF₆⁻] are given in Tables 3.5 to 3.8. The uncertainties on the reorientation times are in the range of 5–10%. Stokes–Einstein–Debye (SED) hydrodynamic theory^{14,203} has been employed to analyze the experimental results. The following section provides a detailed description of the SED theory.

Table 3.1: Reorientation Times of 9-PA and R110 in [emim⁺][BF₄⁻] as a Function of Temperature Along with Solvent Viscosity

<i>T</i> / K	η / mPa s	τ_r / ns	
		9-PA	R110
298	37.4	1.23	4.59
303	31.5	1.02	3.82
308	26.6	0.89	3.20
313	22.8	0.80	2.69
318	19.7	0.73	2.26
323	17.1	0.68	1.98
328	15.1	0.60	1.73
338	11.8	0.43	1.33
348	9.53	0.37	0.87

Table 3.2: Reorientation Times of 9-PA and R110 in [bmim⁺][BF₄⁻] as a Function of Temperature Along with Solvent Viscosity

<i>T</i> / K	η / mPa s	τ_r / ns	
		9-PA	R110
298	106.0	2.51	9.83
303	83.0	1.93	8.34
308	66.4	1.58	7.05
313	53.2	1.27	5.75
318	42.7	1.05	4.78
323	35.2	0.88	3.98
328	29.8	0.73	3.34
338	21.3	0.55	2.41
348	16.0	0.41	1.77

Table 3.3: Reorientation Times of 9-PA and R110 in [hmim⁺][BF₄⁻] as a Function of Temperature Along with Solvent Viscosity

<i>T</i> / K	η / mPa s	τ_r / ns	
		9-PA	R110
298	206.0	3.59	12.68
303	157.0	2.75	10.81
308	120.0	2.14	9.79
313	93.8	1.68	8.86
318	74.7	1.37	7.45
323	60.6	1.12	6.46
328	49.4	0.93	5.60
338	33.8	0.62	4.05
348	24.2	0.45	3.00

Table 3.4: Reorientation Times of 9-PA and R110 in [moin⁺][BF₄⁻] as a Function of Temperature Along with Solvent Viscosity

<i>T</i> / K	η / mPa s	τ_r / ns	
		9-PA	R110
298	328.0	3.77	12.99
303	247.0	2.95	12.03
308	185.0	2.48	10.82
313	143.0	1.95	10.00
318	112.0	1.62	9.20
323	88.8	1.34	7.96
328	71.6	1.08	6.99
338	48.2	0.80	5.21
348	33.6	0.60	3.87

Table 3.5: Reorientation Times of 9-PA and R110 in [emim⁺][PF₆⁻] as a Function of Temperature Along with Solvent Viscosity

T / K	$\eta / \text{mPa s}$	τ_r / ns	
		9-PA	R110
338	27.1	0.65	2.13
348	20.3	0.53	1.52
358	15.8	0.39	1.14

Table 3.6: Reorientation Times of 9-PA and R110 in [bmim⁺][PF₆⁻] as a Function of Temperature Along with Solvent Viscosity

T / K	$\eta / \text{mPa s}$	τ_r / ns	
		9-PA	R110
298	267.0	4.62	14.43
303	202.0	3.48	13.84
308	154.0	2.68	12.04
313	120.0	2.20	9.34
318	94.0	1.75	7.64
323	75.0	1.42	6.59
328	61.0	1.17	5.25
338	41.2	0.79	3.57
348	29.1	0.60	2.42

Table 3.7: Reorientation Times of 9-PA and R110 in [hmim⁺][PF₆⁻] as a Function of Temperature Along with Solvent Viscosity

T / K	$\eta / \text{mPa s}$	τ_r / ns	
		9-PA	R110
298	484.0	5.48	-----
303	354.0	4.43	-----
308	261.0	3.46	16.31
313	199.0	2.75	14.53
318	153.0	2.23	12.63
323	118.0	1.76	10.39
328	93.7	1.44	8.56
338	61.5	1.06	5.97
348	41.8	0.75	4.08

Table 3.8: Reorientation Times of 9-PA and R110 in [moin⁺][PF₆⁻] as a Function of Temperature Along with Solvent Viscosity

T / K	$\eta / \text{mPa s}$	τ_r / ns	
		9-PA	R110
298	701.0	5.53	-----
303	498.0	4.46	14.31
308	358.0	3.54	13.59
313	263.0	2.85	12.72
318	199.0	2.19	11.62
323	153.0	1.76	10.37
328	120.0	1.43	9.52
338	76.3	1.05	7.07
348	51.8	0.72	5.31

3.3.1 The SED Hydrodynamic Theory for Rotational Diffusion

According to SED hydrodynamic theory, the rotation of a solute molecule dissolved in a solvent continuum takes place by small-step diffusion and its reorientation time is proportional to the viscosity (η) of the fluid at a given temperature, T . The solute properties that govern the rotation are its size and shape, which are expressed in terms of van der Waals volume, V and shape factor, f , which accounts for the nonspherical nature of the solute. These parameters are incorporated into the SED model by treating the solute as a symmetric or an asymmetric ellipsoid.²⁴³ In addition to the above-mentioned parameters, the coupling between the solute and the solvent also plays an important role in controlling the rotational diffusion of a solute molecule. In the SED model, the magnitude of the solute-solvent coupling parameter or the boundary condition parameter, which is usually denoted by C , depends on the axial ratio of the solute molecule and the two limiting cases are, the hydrodynamic stick and slip.²⁴⁴ The stick boundary condition assumes that the tangential velocity of the fluid relative to the body vanishes on the surface of the body. In other words, there is a perfect coherence between the motion of the body and the neighboring fluid. The slip boundary condition assumes that the fluid can exert no tangential stress on the rotating object. Stick boundary condition is appropriate for rotating bodies that are considerably larger than the surrounding fluid molecules. On the other hand, slip boundary condition is valid when the rotating body is smaller than the fluid molecules or of comparable size. Thus, the expression for τ_r is given by

$$\tau_r = \frac{VfC}{k} \left(\frac{\eta}{T} \right) \quad (3.2)$$

where k is the Boltzmann constant. According to SED theory, τ_r for a given solute molecule is proportional to η/T . To apply the SED theory, the solute molecules used in the present study, 9-PA and R110 have been treated as asymmetric ellipsoids and van der Waals volumes were obtained using Edward's increment method²⁴⁵. For the purpose of modeling, 9-PA and R110 as ellipsoids, the axial radii of the solutes were measured with the aid of Corey–Pauling–Koltun (CPK) space filling models. The best ellipsoid dimensions for the two solute molecules were arrived at in the following manner. The largest dimension, the distance between the two farthest atoms, of the solute molecule was taken as the long axis ($2a$), the largest dimension perpendicular to it was considered as the short-in-plane axis ($2b$) and the thickness of the aromatic ring is considered as out-of-plane axis ($2c$). Since the phenyl ring in both the solutes is oriented orthogonal to the anthracene moiety, it is difficult to get a precise estimate of c . To circumvent this problem, the out-of-plane radius c was calculated from the relation $V = (4\pi/3)abc$ and was found to be 1.8 Å for both 9-PA and rhodamine 110. Since the value of c obtained in this manner is identical for both the solutes, this method of estimation appears to be reasonable. The friction coefficients ζ_i s along the three principal axes of rotation with stick and slip boundary conditions were obtained from the interpolation of numerical tabulations available in the literature^{246,247} and the diffusion coefficients D_i s were calculated from the friction coefficients using Einstein relation,²⁴⁸ which is given below.

$$D_i = \frac{kT}{\zeta_i} \quad (3.3)$$

Reorientation times were computed from the diffusion coefficients along the three principal axes of rotation (D_a , D_b and D_c) using equation 3.4, which is valid if the transition dipole is along the long axis of the molecule²⁴⁸ and for 9-PA and R110, it is assumed that this condition is fulfilled. From the calculated reorientation times with stick

$$\tau_r = \frac{1}{12} \left[\frac{4D_a + D_b + D_c}{D_a D_b + D_b D_c + D_c D_a} \right] \quad (3.4)$$

and slip boundary conditions, the parameters f and C_{slip} have been obtained. Solute dimensions, van der Waals volumes, shape factors and boundary condition parameters (C_{slip}) for the two solutes that have been calculated in this manner are listed in Table 3.9. It is evident from the table that the solutes 9-PA and R110 have similar dimensions and volumes, and as a consequence their shape factors and the boundary condition parameters are almost identical. In other words, the SED hydrodynamic theory predicts that the reorientation times of the two solute molecules should be similar.

Table 3.9: Solute Dimensions and van der Waals Volumes together with Shape Factors and Boundary Condition Parameters Calculated Using the SED Hydrodynamic Theory

Solute	Axial radii/Å ³	V/Å ³	f	C_{slip}
9-PA	5.7x5.5x1.8	236	1.73	0.12
R110	6.7x5.5x1.8	275	2.02	0.15

As mentioned before, the SED hydrodynamic theory predicts that τ_r should be proportional to η/T . To find out if the SED theory is indeed applicable to the systems under investigation, anisotropy decays of 9-PA in $[\text{hmim}^+][\text{BF}_4^-]$ and $[\text{moim}^+][\text{BF}_4^-]$, and also in $[\text{hmim}^+][\text{PF}_6^-]$ and $[\text{moim}^+][\text{PF}_6^-]$ at 298 K are displayed in Figure 3.2. It can be noticed from the figure that the anisotropy decays of 9-PA in $[\text{hmim}^+][\text{BF}_4^-]$ and

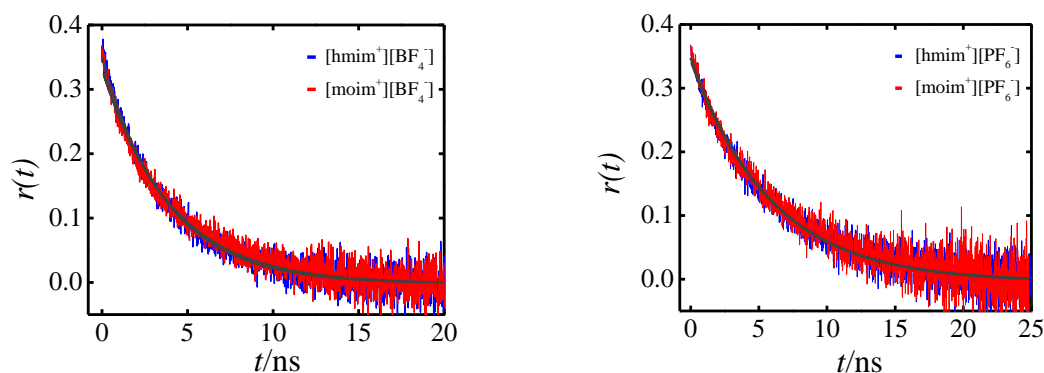


Figure 3.2 Fluorescence Anisotropy decays of 9-PA in $[\text{hmim}^+][\text{BF}_4^-]$, $[\text{moim}^+][\text{BF}_4^-]$ and $[\text{hmim}^+][\text{PF}_6^-]$, $[\text{moim}^+][\text{PF}_6^-]$ at 298 K together with the fitted curves.

$[\text{moim}^+][\text{BF}_4^-]$ are identical despite the octyl derivative having significantly higher viscosity compared to the hexyl derivative and a similar result has been obtained in case of ionic liquids with $[\text{PF}_6^-]$ anion. Thus, these results are in conflict with the predictions of the SED theory. Furthermore, to find out whether the SED hydrodynamic theory is applicable in case of the cationic solute over the entire temperature range, characteristic anisotropy decays of R110 in $[\text{hmim}^+][\text{PF}_6^-]$ and $[\text{moim}^+][\text{PF}_6^-]$ at 323 K and also at 348 K are shown in the Figure 3.3. It may be noted that at 323 K, the viscosity of

$[\text{moim}^+][\text{PF}_6^-]$ is 30% higher compared to $[\text{hmim}^+][\text{PF}_6^-]$. However, inspection of the Figure 3.3 reveals that the anisotropy decays of R110 in the two solvents are almost identical at 323 K, which is an indication that the predictions of the SED hydrodynamic theory do not hold. In contrast at 348 K, the trends in the anisotropy decays comply with the respective viscosities of the solvents. Thus, from these figures (Figures 3.2 and 3.3) it is evident that the SED hydrodynamic theory fails to explain the observed trends for 9-PA

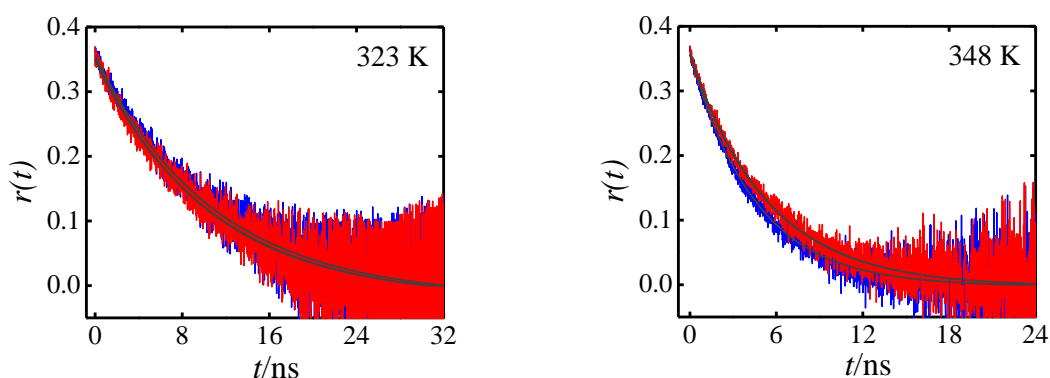


Figure 3.3 Fluorescence anisotropy decays of R110 in $[\text{hmim}^+][\text{PF}_6^-]$ (blue) and $[\text{moim}^+][\text{PF}_6^-]$ (red) at 323 K and 348 K together with the fitted curves.

in $[\text{hmim}^+][\text{BF}_4^-]$ and $[\text{moim}^+][\text{BF}_4^-]$, and also in $[\text{hmim}^+][\text{PF}_6^-]$ and $[\text{moim}^+][\text{PF}_6^-]$ over the entire temperature range studied, whereas for R110 SED predictions fail at lower temperatures. To understand these results in totality, reorientation times of 9-PA and R110 are plotted as a function of η/T in Figure 3.4 for ionic liquids with $[\text{BF}_4^-]$ and $[\text{PF}_6^-]$ anions. The SED slip and stick lines are also shown in the figures. It is evident from these figures, the rotational diffusion of 9-PA is closer to the predictions of slip hydrodynamics, whereas reorientation times of R110 obey stick boundary condition due

to specific interactions prevailing between R110 and the $[\text{BF}_4^-]$ as well as $[\text{PF}_6^-]$ anions. A close scrutiny of Figure 3.4 indicates that for a given η/T , the rotation of 9-PA becomes progressively faster from ethyl to octyl derivatives of $[\text{Rmim}^+][\text{BF}_4^-]$ and $[\text{Rmim}^+][\text{PF}_6^-]$. On the other hand, in case of R110, two slopes have been obtained for

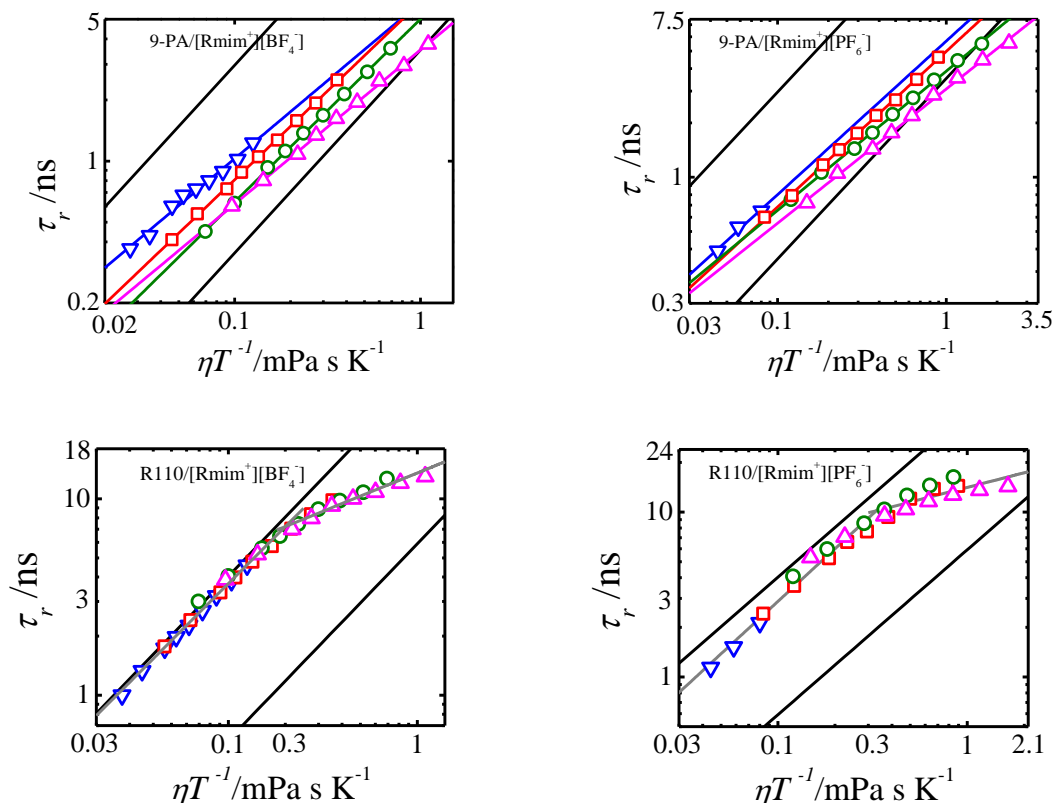


Figure 3.4 Plots of τ_r versus η/T for 9-PA and R110 in $[\text{emim}^+][\text{BF}_4^-]$ (∇), $[\text{bmim}^+][\text{BF}_4^-]$ (\square), $[\text{hmim}^+][\text{BF}_4^-]$ (\odot) and $[\text{moim}^+][\text{BF}_4^-]$ (\triangle), and $[\text{emim}^+][\text{PF}_6^-]$ (∇), $[\text{bmim}^+][\text{PF}_6^-]$ (\square), $[\text{hmim}^+][\text{PF}_6^-]$ (\odot) and $[\text{moim}^+][\text{PF}_6^-]$ (\triangle). The lines passing through data points were obtained by fitting the data to nonlinear η/T relationships that are given below. The black-colored lines are the SED slip and stick lines for 9-PA and R110 solutes.

each plot, corresponding to lower and higher values of η/T . For the ionic liquid $[\text{Rmim}^+][\text{BF}_4^-]$, the transition occurs around 0.2 mPa s K^{-1} , whereas in case of $[\text{Rmim}^+][\text{PF}_6^-]$, it is around 0.3 mPa s K^{-1} . However, it must be noted that these transitions are not sharp but somewhat gradual. Linear least-squares fits of log–log plots indicate that variation of τ_r with η/T follows the relation, $\tau_r = A(\eta/T)^n$. The values of

Table 3.10: Values of A and n Obtained for 9-PA in $[\text{Rmim}^+][\text{BF}_4^-]$ from Linear Least-Squares Fits of τ_r versus η/T Plots

Ionic liquids	9-PA	
	$A/\text{ns K (m Pa s)}^{-1}$	n
$[\text{emim}^+][\text{BF}_4^-]$	6.0 ± 0.6	0.77 ± 0.03
$[\text{bmim}^+][\text{BF}_4^-]$	6.1 ± 0.1	0.87 ± 0.01
$[\text{hmim}^+][\text{BF}_4^-]$	5.0 ± 0.1	0.90 ± 0.01
$[\text{moim}^+][\text{BF}_4^-]$	3.5 ± 0.1	0.76 ± 0.01

Table 3.11: Values of A and n Obtained for 9-PA in $[\text{Rmim}^+][\text{PF}_6^-]$ from Linear Least-Squares Fits of τ_r versus η/T Plots

Ionic liquids	9-PA	
	$A/\text{ns K (m Pa s)}^{-1}$	n
$[\text{emim}^+][\text{PF}_6^-]$	5.7 ± 0.5	0.85 ± 0.03
$[\text{bmim}^+][\text{PF}_6^-]$	5.0 ± 0.1	0.86 ± 0.01
$[\text{hmim}^+][\text{PF}_6^-]$	3.9 ± 0.1	0.77 ± 0.01
$[\text{moim}^+][\text{PF}_6^-]$	3.1 ± 0.1	0.74 ± 0.01

A and n for 9-PA in $[\text{Rmim}^+][\text{BF}_4^-]$ and $[\text{Rmim}^+][\text{PF}_6^-]$ are given Tables 3.10 and 3.11, respectively. It can be noticed from these tables that A decreases with an increase in the length of the alkyl chain on the imidazolium cation, while the variation in n is not

Table 3.12: Values of A and n Obtained for R110 in $[\text{Rmim}^+][\text{BF}_4^-]$ from Linear Least-Squares Fits of τ_r versus η/T Plots at Low and High Values of η/T

System	$A/\text{ns K (m Pa s)}^{-1}$	n
For $\eta/T < 0.2$ R110/ $[\text{Rmim}^+][\text{BF}_4^-]$	34.0 ± 2.00	0.96 ± 0.02
For $\eta/T > 0.2$ R110/ $[\text{Rmim}^+][\text{BF}_4^-]$	13.5 ± 0.7	0.39 ± 0.03

Table 3.13: Values of A and n Obtained for R110 in $[\text{Rmim}^+][\text{PF}_6^-]$ from Linear Least-Squares Fits of τ_r versus η/T Plots at Low and High Values of η/T

System	$A/\text{ns K (m Pa s)}^{-1}$	n
For $\eta/T < 0.3$ R110/ $[\text{Rmim}^+][\text{PF}_6^-]$	33.0 ± 3.00	1.06 ± 0.05
For $\eta/T > 0.3$ R110/ $[\text{Rmim}^+][\text{PF}_6^-]$	14.1 ± 0.6	0.29 ± 0.07

systematic. These parameters for R110 in [Rmim⁺][BF₄⁻] and [Rmim⁺][PF₆⁻] are given in Tables 3.12 and 3.13, respectively. It can be noticed that in case of R110, at low η/T , the values of n are close to unity indicating that its rotational diffusion in [Rmim⁺][BF₄⁻] and [Rmim⁺][PF₆⁻] follows SED hydrodynamic theory with stick boundary condition. However, at high η/T , the values of n are much less than unity. Apart from the values of n being much less than one, it can also be noticed that the slopes of τ_r versus η/T plots are considerably smaller compared to the ones observed at low η/T (see Figure 3.4). In essence, the analysis carried out in this manner suggests that the rotational diffusion of 9-PA as well as R110 (at high η/T) deviates significantly from the predictions of the SED theory and the reasons for the observed behavior are discussed below.

In case of 9-PA, as mentioned earlier, A decrease with an increase in the length of the alkyl chain on the imidazolium cation. In other words, for a given η/T , the rotation of 9-PA becomes faster from ethyl to octyl derivatives of [Rmim⁺][BF₄⁻] and [Rmim⁺][PF₆⁻]. These results are an indication that the boundary condition parameter C is not uniform but varies in each solvent. Thus, to understand these results quasihydrodynamic theories of Gierer-Wirtz (GW)²⁴⁹ and Dote-Kivelson-Schwartz (DKS)²⁵⁰ have been applied to systems under investigation and these theories take into consideration the relative sizes of the solute and solvent while calculating the boundary condition parameter. These theories have been successful in explaining the influence of solvent size on solute rotation in case of conventional solvents qualitatively.²⁵¹⁻²⁵⁶ The following section provides a detailed discussion of GW and DKS theories.

3.3.2. The Gierer-Wirtz Theory

This is a relatively old theory proposed by Gierer and Wirtz²⁵¹ in 1953, which takes into account both the size of the solute as well as that of the solvent while calculating the boundary condition parameter. According to Gierer–Wirtz quasihydrodynamic theory, the solvent is made up of concentric shells of spherical particles surrounding the spherical solute molecule at the center. The boundary condition parameter C_{GW} is calculated by considering how the angular velocity of the solvent molecules in successive shells surrounding the solute decreases as a function of distance away from it. The expression for C_{GW} is given by the following equation.

$$C_{GW} = \sigma C_0 \quad (3.5)$$

where the parameters σ and C_0 are given by eqs 3.6 and 3.7, respectively.

$$\sigma = \left[1 + 6(V_s/V_p)^{1/3} C_0 \right]^{-1} \quad (3.6)$$

$$C_0 = \left\{ \frac{6(V_s/V_p)^{1/3}}{\left[1 + 2(V_s/V_p)^{1/3} \right]^4} + \frac{1}{\left[1 + 4(V_s/V_p)^{1/3} \right]^3} \right\}^{-1} \quad (3.7)$$

In these equations, V_s and V_p are the volumes of the solvent and solute, respectively.

When the ratio V_s/V_p is very small, the solvent becomes continuous and C_{GW} approaches unity, which is the SED equation with stick boundary condition.

It may be noted that an increase in the length of the alkyl chain on the imidazolium cation leads to an enhancement in the van der Waals volume of the ionic liquid. The van der Waals volumes of ionic liquids were obtained by the addition of the volumes of the individual cations and anions. The procedure adopted here to calculate the van der Waals volumes of the ionic liquids is not rigorous since the distribution of cations and anions about a medium sized organic solute is not random.²⁵⁷ Moreover, because of the significant degree of order present in these systems due to ion-ion interactions, the applicability of concepts such as solvation shell, and the utility of continuum models for the solvent are somewhat suspect. Nonetheless, in the absence of an alternative treatment, the methodology employed here is reasonably satisfactory. The van der Waals volume (V_s) increases by 50% in $[\text{Rmim}^+][\text{BF}_4^-]$ and $[\text{Rmim}^+][\text{PF}_6^-]$ ionic liquids with an increase in the length of the alkyl chain from ethyl to octyl on the imidazolium cation. The C_{GW} values of 9-PA have been calculated using eqs 3.5–3.7 and for the systems used in this work they decrease by about 15% and 13% from ethyl to octyl derivatives of $[\text{Rmim}^+][\text{BF}_4^-]$ and $[\text{Rmim}^+][\text{PF}_6^-]$, respectively. Thus, the GW theory fails to account for the observed faster rotation of 9-PA at a given η/T with an increase in the length of the alkyl chain from ethyl to octyl on the imidazolium cation of $[\text{Rmim}^+][\text{BF}_4^-]$ and $[\text{Rmim}^+][\text{PF}_6^-]$.

In an attempt to find out if the experimentally observed trends can at least be mimicked in qualitative manner, Dote-Kivelson-Schwartz quasihydrodynamic theory has also been applied.

3.3.3 The Dote-Kivelson-Schwartz theory

The second quasihydrodynamic theory, which is relatively new, was proposed by Dote, Kivelson and Schwartz (DKS)²⁵² in 1981. The DKS theory, on the other hand, not only considers the solvent size but also incorporates the cavities or free spaces created by the solvent around the probe molecule while calculating the boundary condition. The boundary condition parameter is assumed to depend on the ratio of the solute volume to the total volume available for solute rotation. According to this theory, the boundary condition parameter C_{DKS} has been calculated using the following equations.

$$C_{DKS} = (1 + \gamma / \phi)^{-1} \quad (3.8)$$

where γ / ϕ is a measure of the ratio of the free volume of the solvent to the effective size of the solute molecule, with

$$\gamma = \frac{\Delta V}{V_p} \left[4 \left(\frac{V_p}{V_s} \right)^{2/3} + 1 \right] \quad (3.9)$$

and ϕ is the ratio of the rotation time predicted by slip hydrodynamics to the stick prediction for the sphere of the same volume or essentially ϕ is a product of $f C_{slip}$. ΔV is the smallest volume of free space per solvent molecule and is empirically related to viscosity, the Hilderbrand-Batschinski parameter B and also the isothermal compressibility k_T of the solvent by the following expression.

$$\Delta V = Bk_T \eta kT \quad (3.10)$$

However, Anderton and Kauffman²⁵⁸ suggested that the Frenkel hole theory and the Hilderbrand treatment of solvent viscosity were developed for simple liquids. Thus, eq 3.10 is not a valid measure of the free space per solvent molecule for highly associative solvents such as the ionic liquids used in the present study. For associative liquids, ΔV can be calculated by the following expression.²⁵⁸

$$\Delta V = V_m - V_s \quad (3.11)$$

where V_m is the ratio of solvent molar volume and the Avogadro number. It may be noted that C_{DKS} is a temperature-dependent parameter since molar volume depends on density, which in turn decreases with temperature. C_{DKS} values of 9-PA have been calculated using eq 3.8 and they decrease by about 10% over the temperature range 298–348 K and from ethyl to octyl derivatives these numbers decrease by 44 and 50%, respectively, in [Rmim⁺][BF₄⁻] and [Rmim⁺][PF₆⁻]. Thus, the large decrease obtained in the C_{DKS} values from ethyl to octyl derivatives of [Rmim⁺][BF₄⁻] and [Rmim⁺][PF₆⁻] indicates that the DKS theory mimics the experimental trends in a superior manner compared to the GW model. However, even the DKS theory fails to account for the significantly faster rotation of 9-PA with an increase in the length of the alkyl chain on the imidazolium cation in 1-alkyl-3-methylimidazolium tetrafluoroborates and hexafluorophosphates.

From the discussion presented so far, it is evident that neither the hydrodynamic nor the quasihydrodynamic theories are able to explain the rotational diffusion of 9-PA in

1-alkyl-3-methylimidazolium tetrafluoroborates and hexafluorophosphates. In other words, as mentioned earlier, rotation of 9-PA becomes progressively faster at a given η/T upon increasing the length of the alkyl chain on the imidazolium cation having $[\text{BF}_4^-]$ and $[\text{PF}_6^-]$ anions. What is the reason for the observed behavior? As mentioned in the Introduction, ionic liquids are known to form organized structures and the solute molecule 9-PA is experiencing an environment that cannot be characterized by the bulk viscosity of the ionic liquid. In other words, the friction sensed by 9-PA decreases with an increase in the length of the alkyl chain on the imidazolium cation, which is predominantly due to the organized domains formed by the ionic liquids. High charge to size ratio of $[\text{BF}_4^-]$ and $[\text{PF}_6^-]$ ions facilitates stronger association with the cation of the ionic liquid and thus leads to the formation of organized domain structure. When organized domains are formed as in the case of ionic liquids with $[\text{BF}_4^-]$ and $[\text{PF}_6^-]$ ions, solute rotation is no longer governed by the bulk viscosity of the medium. Instead the domain size and the packing of the polar and nonpolar groups in these organized structures are probably responsible for the friction experienced by the solute molecule. It is likely that the domain sizes increase with an increase in the length of the alkyl chain on the imidazolium cation and as a consequence the solute 9-PA, which resides in these nonpolar domains, experiences lower friction leading to the faster rotation.

The rotational diffusion of R110 in $[\text{Rmim}^+][\text{BF}_4^-]$ and $[\text{Rmim}^+][\text{PF}_6^-]$ is somewhat different compared to that observed for 9-PA. In other words, as mentioned before, rotation of 9-PA becomes progressively faster at a given η/T upon increasing the

length of the alkyl chain on the imidazolium cation. However, two slopes corresponding to lower and higher values of η/T have been noticed in τ_r versus η/T plots for R110 in $[\text{Rmim}^+][\text{BF}_4^-]$ and $[\text{Rmim}^+][\text{PF}_6^-]$. What could be the reason for this contrasting behavior? As mentioned earlier, R110 is a hydrogen bond donating cationic solute and hence it is more likely to be surrounded by $[\text{BF}_4^-]$ and $[\text{PF}_6^-]$ ions of the ionic liquids. In other words, R110 will probably be located at the boundary between nonpolar and polar domains. Thus, the two slopes obtained in the τ_r versus η/T plots and the observed nonlinear relationships between τ_r and η/T at higher η/T is somewhat intriguing. It may be noted that the deviations from the SED relation are a norm in case of supercooled liquids and polymer glasses especially at higher η/T and such a behavior has been attributed to decoupling of rotational diffusion from the viscosity of the medium.^{259,260} It has been demonstrated that introduction of ~ 2 nm structural inhomogeneities into a homogeneous liquid leads to a decoupling of diffusion from viscosity similar to that observed in supercooled liquids.²⁶¹ Thus, the structural heterogeneity present in ionic liquids can lead to decoupling of rotational diffusion from the viscosity of the medium. Recently, a similar hypothesis has been used to explain the rotational diffusion of a dipolar solute in ionic liquids.²⁴² To find out if the observed behavior of R110 is unique to the ionic liquids used in the present study or a similar behavior can be found in ionic liquids of comparable viscosities, rotational diffusion of R110 in *N*-(2-methoxyethyl)-*N*-methylmorpholinium tris(pentafluoroethyl)trifluorophosphate ($[\text{Moemmo}^+][\text{FAP}^-]$)²⁶²

has been considered. The following relationship has been obtained between τ_r and η/T for R110 in [Moemmo⁺][FAP⁻].

$$\text{R110/[Moemmo}^+][\text{FAP}^-] \quad \tau_r = (12.5 \pm 0.6)(\eta/T)^{0.93 \pm 0.04} \quad (N = 7, R = 0.995)$$

It can be noticed that the relationship between τ_r and η/T is almost linear and thus the exercise carried out in this manner rules out the possibility that the nonlinear τ_r versus η/T relationships obtained for R110 in [Rmim⁺][BF₄⁻] and [Rmim⁺][PF₆⁻] at higher η/T are due to decoupling of rotational diffusion from the viscosity of the medium. Another possibility for the observed behavior could be the microviscosity experienced by the solute molecules at higher η/T . To test this hypothesis quasihydrodynamic theories of Gierer-Wirtz (GW)²⁴⁹ and Dote-Kivelson-Schwartz (DKS)²⁵⁰ have been employed. C_{GW} values of R110 have been calculated using eqs 3.5–3.7 for the systems used in this work and they decrease by about 15% from ethyl to octyl derivatives of [Rmim⁺][BF₄⁻] and [Rmim⁺][PF₆⁻]. Since the calculated C_{GW} does not vary with η/T , the GW theory is unable to mimic the two slopes observed in τ_r versus η/T plots. In an attempt to find out if the experimentally observed trends can at least be mimicked in qualitative manner, Dote-Kivelson-Schwartz quasihydrodynamic theory has also been applied. C_{DKS} values of R110 in [Rmim⁺][BF₄⁻] and [Rmim⁺][PF₆⁻] calculated with the aid of eq 3.8 decrease by 30% from ethyl to octyl derivatives. Over the temperature range 298–348 K, these numbers decrease by about 10% since the densities of the ionic liquids decrease with an

increase in temperature. Despite these minor variations in C_{DKS} values, the DKS theory fails to replicate the trends noticed in τ_r versus η/T plots.

The analysis carried out so far indicates that the observed faster rotation of R110 in $[\text{Rmim}^+][\text{BF}_4^-]$ and $[\text{Rmim}^+][\text{PF}_6^-]$ at higher values of η/T could not be explained using hydrodynamic and quasihydrodynamic theories. As mentioned earlier, this result is somewhat different from the one obtained for the nonpolar solute 9-PA, where a faster rotation of the solute has been noticed at a given η/T upon increasing the length of the alkyl chain on the imidazolium cation. In the case of R110, however, two slopes corresponding to lower and higher values of η/T have been noticed in τ_r versus η/T plots for R110 in $[\text{Rmim}^+][\text{BF}_4^-]$ and $[\text{Rmim}^+][\text{PF}_6^-]$. The presence of two slopes in the Figure 3.4 reveals that the strengths of specific interactions between R110 and constituent ions of the ionic liquids are not the same at lower and higher values of η/T . As mentioned before, at lower values of η/T , the reorientation times of R110 in $[\text{Rmim}^+][\text{BF}_4^-]$ and $[\text{Rmim}^+][\text{PF}_6^-]$ follow the stick hydrodynamics, which indicates that R110 experiences stronger specific interactions with the respective anions of the ionic liquids. In contrast, deviations from the stick hydrodynamics at higher values of η/T suggest that the strengths of the specific interactions between R110 and the respective anions of the ionic liquids are different at lower and higher values of η/T . If R110 were to experience specific interactions with identical strengths over the entire range of η/T then its rotational diffusion would have been similar at lower as well as higher values of

η/T . In other words, τ_r versus η/T plot would have contained a single slope instead of two. However, at higher η/T , the scenario appears to be different. What could be the probable reason for the unusual behavior at higher values of η/T ? It is plausible that at ambient temperatures, (higher η/T), these ionic liquids are more structured and hence do not facilitate stronger specific interactions between R110 and $[\text{BF}_4^-]$ and $[\text{PF}_6^-]$ anions. Molecular dynamics simulations using multiscale coarse-graining models carried out on imidazolium-based ionic liquids confirm that at ambient temperature with enough attractive interactions between the nonpolar groups on the cationic side chain, the tail groups form relatively stable spatially heterogeneous tail domains. However, at high enough temperatures, the tail groups are expected to have sufficient thermal energy so that they no longer aggregate.¹²⁸ Thus, at ambient temperatures (higher η/T) it is likely that $[\text{BF}_4^-]$ and $[\text{PF}_6^-]$ anions are not readily accessible to the solute R110 as a result of the organized structure of the ionic liquids, which leads to diminishing hydrogen bonding interactions between them and ensuing the faster rotation of the solute. Although the method employed in this work essentially probes solute-solvent interactions, the heterogeneous nature of the medium has a bearing on the microenvironment experienced by the solute molecule.

Thus, the rotational diffusion of R110 in conjunction with the results of 9-PA in $[\text{Rmim}^+][\text{BF}_4^-]$ and $[\text{Rmim}^+][\text{PF}_6^-]$ indicate that rotational diffusion of both charged and nonpolar solutes is affected by the organized structure of 1-alkyl-3-methylimidazolium-based ionic liquids with $[\text{BF}_4^-]$ and $[\text{PF}_6^-]$ anions, albeit in a contrasting manner. As

mentioned earlier, the rotational diffusion of the nonpolar solute 9-PA at a given η/T becomes faster from ethyl to octyl derivatives of $[\text{Rmim}^+][\text{BF}_4^-]$ and $[\text{Rmim}^+][\text{PF}_6^-]$. In contrast, for the charged solute R110, the variation of τ_r with η/T is not uniform but displays different slopes at lower and higher values of η/T . Such a contrasting behavior arises as a consequence of the two solute molecules residing in distinct environments of the ionic liquids and experiencing different types of interactions. Another point that needs to be addressed here is the lack of systematic variation in the reorientation times of R110 upon increasing the length of the alkyl chain at higher η/T . It is evident from molecular dynamics simulations that aggregation of alkyl chains is more pronounced in case of ionic liquids having longer alkyl chains¹²⁸ and the results obtained for the nonpolar solute 9-PA comply with this premise. It may be recalled that in case of 9-PA, a systematic decrease in τ_r has been noticed with an increase in the length of the alkyl chain at a given η/T . However, the cationic solute does not reside in these organized nonpolar domains of the ionic liquids, instead it experiences specific interactions with the anions of the ionic liquids and hence it is probable that systematic alkyl chain length dependence is not observed on the rotational diffusion of R110.

3.4 Conclusions

As a consequence of their highly associative nature, ionic liquids are known to form organized structures, which in turn can have a profound influence on rates of dynamical processes. In an attempt to find out whether the organized structure of an ionic

liquid affects rotational diffusion of nonpolar and ionic solutes, the present study has been undertaken and the important findings are summarized in this section. For the nonpolar solute 9-PA, significantly faster rotation has been observed in octyl derivatives of 1-alkyl-3-methylimidazolium tetrafluoroborates and hexafluorophosphates compared to their ethyl counterparts at given η/T , while for R110, two slopes have been noticed in τ_r versus η/T plots. These results could not be rationalized using the hydrodynamic and quasihydrodynamic theories. The observed behavior of 9-PA and R110 could only be explained by taking into consideration the organized structure of the ionic liquids. 9-PA experiences less friction due to increase in the nonpolar domain size upon increasing the length of the alkyl chain on imidazolium cation with $[\text{BF}_4^-]$ and $[\text{PF}_6^-]$ anions, whereas in case of R110, the organized structure of the ionic liquids precludes stronger hydrogen bonding interactions between the solute and the anions $[\text{BF}_4^-]$ and $[\text{PF}_6^-]$ leading to a faster rotation than predicted by the stick hydrodynamics.

Chapter 4

Solute Rotation in Imidazolium-Based Ionic Liquids with Weakly Associating Anions

4.1. Introduction

The previous Chapter describes rotational diffusion of nonpolar and ionic solutes in 1-alkyl-3-methylimidazolium-based ionic liquids with strongly associating anions such as tetrafluoroborate ($[\text{BF}_4^-]$) and hexafluorophosphate ($[\text{PF}_6^-]$). The outcome of the study indicates that the organized structure, which results as a consequence of highly associative nature of the anions of the ionic liquids, significantly affects the solute rotation. Furthermore, the structure and physicochemical properties of imidazolium-based ionic liquids are influenced by the constituent ions and substituents such as nonpolar alkyl chains attached to either of the ions. Thus, to get a complete perspective of the role of organized structure of the ionic liquids on solute rotation, these studies need to be extended to various classes of ionic liquids by varying the constituent ions as well as substituents present on either of the ions.

As mentioned earlier, a significant influence of organized structure on solute rotation has been observed in the case of ionic liquids having strongly associating anions $[\text{BF}_4^-]$ and $[\text{PF}_6^-]$. As a subsequent stride, it would be interesting to find out how the organized structure arising due to the presence of a weakly associating anion such as

bis(trifluoromethylsulfonyl)imide in combination with 1-alkyl-3-methylimidazolium cations with varying alkyl chain length affects solute rotation. Thus, to achieve this goal the present study has been undertaken wherein rotational diffusion of the nonpolar solute 9-PA and the cationic solute R110 (see Figure 4.1 for the molecular structures of the solutes) has been examined in a series of 1-alkyl-3-methylimidazolium bis(trifluoromethylsulfonyl)imides. In these studies, length of the alkyl chain has been varied from methyl to octadecyl.

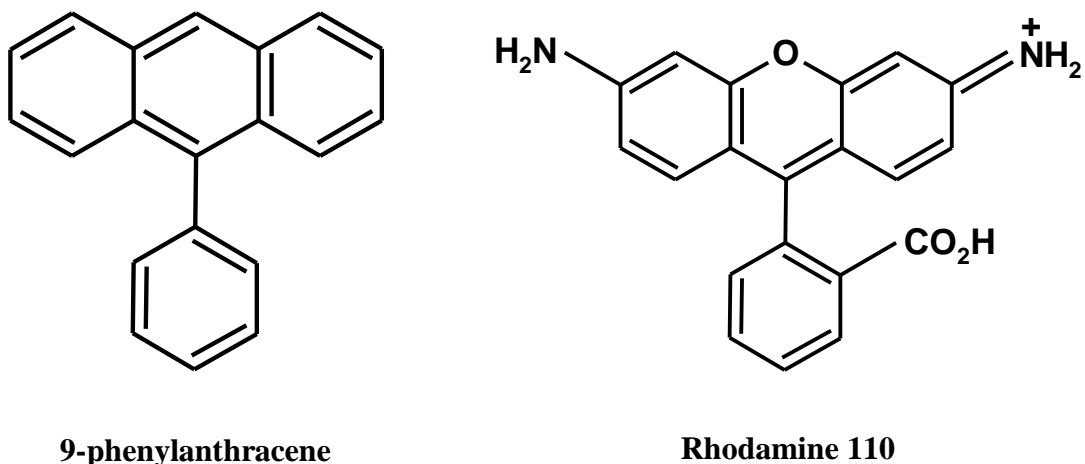


Figure 4.1 *Molecular structures of the solutes.*

The ionic liquids having the alkyl chains on the imidazolium cation such as such as 1,3-dimethylimidazolium ([mmim⁺]), 1-ethyl-3-methylimidazolium ([emim⁺]), 1-methyl-3-propylimidazolium ([mpim⁺]), 1-butyl-3-methylimidazolium ([bmim⁺]), 1-hexyl-3-methylimidazolium ([hmim⁺]), 1-methyl-3-octylimidazolium ([moim⁺]), 1-decyl-3-methylimidazolium ([dmim⁺]), 1-dodecyl-3-methylimidazolium ([ddmim⁺]), 1-methyl-3-tetradecylimidazolium ([mtdim⁺]), 1-hexadecyl-3-methylimidazolium ([hdmim⁺]) and

1-methyl-3-octadecylimidazolium ([modim⁺]) in combination with [Tf₂N⁻] anion have been employed for this purpose. We hope that the results obtained in this study will provide a conclusive understanding regarding the influence of the length of the alkyl chain on solute rotation in case of 1-alkyl-3-methylimidazolium bis(trifluoromethylsulfonyl)imides.

4.2. Materials and Methods

All the ionic liquids used in this study were purchased from io-li-tec and the stated purity of the ionic liquids is >99% with <100 ppm water content and <100 ppm halide ion concentration. Water content of the ionic liquids was estimated by Karl Fischer titration with the aid of Metrohm 831 KF Coulometer and found to be within limits specified by the manufacturer. All the ionic liquids are of the highest available purity and were used without further purification. Concentrations of the fluorophores in ionic liquids were chosen such that the absorbance is in the range of 0.1–0.2 at the wavelength of excitation. Viscosities of the ionic liquids were measured as a function of temperature using a Physica MCR 101 rheometer and the uncertainties on the measured numbers are about 5%.

Time-resolved fluorescence anisotropy measurements were carried out by exciting the samples containing the probes 9-PA and R110 at 374 nm and 445 nm, respectively. The emission from the samples was monitored at 420 nm and 550 nm for 9-PA and R110, respectively. The anisotropy measurements were carried out over the temperature range

298–348 K in case of [mmim⁺][Tf₂N⁻], [emim⁺][Tf₂N⁻], [mpim⁺][Tf₂N⁻], [bmim⁺][Tf₂N⁻], [hmim⁺][Tf₂N⁻], [moim⁺][Tf₂N⁻], [[dmim⁺][Tf₂N⁻] and [ddmim⁺][Tf₂N⁻]. However, for [mtdim⁺][Tf₂N⁻], [hdmim⁺][Tf₂N⁻] and [modim⁺][Tf₂N⁻], the measurements were performed over the temperature ranges 308–348 K, 323–358 K and 338–358 K, respectively, as these are solids at ambient temperatures.

4.3. Results and Discussion

The experimentally measured anisotropy decays of 9-PA and R110 in 1-alkyl-3-methylimidazolium bis(trifluoromethylsulfonyl)imides can be fit with a single-exponential function over the temperature range employed in this study. Typical anisotropy decays of the two solutes in [mmim⁺][Tf₂N⁻], [moim⁺][Tf₂N⁻] and [modim⁺][Tf₂N⁻] measured at 348 K along with the fitted curves are shown in the

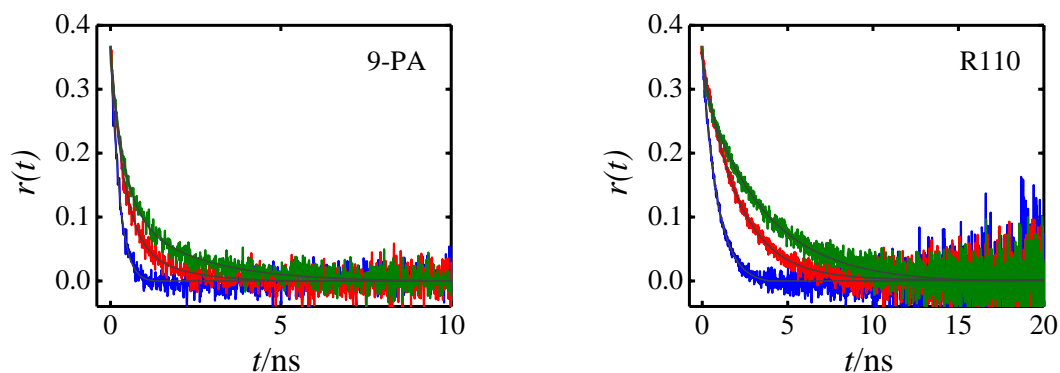


Figure 4.2 Fluorescence Anisotropy decays of 9-PA and R110 in [mmim⁺][Tf₂N⁻] (blue), [moim⁺][Tf₂N⁻] (red) and [modim⁺][Tf₂N⁻] (olive) at 348 K together with the fitted curves.

Figure 4.2. It can be noticed from the figure that the decays of both the solutes become progressively slower from methyl to octadecyl derivatives as a consequence of increase in the viscosity upon increasing in the length of the alkyl chain on the imidazolium cation. The measured reorientation times of 9-PA and R110 in [Rmim⁺][Tf₂N⁻] (from methyl to octadecyl) along with the solvent viscosities at different temperatures are listed in Tables 4.1 to 4.11. The uncertainties on the τ_r values are about 5 to 10%.

Table 4.1: Reorientation Times of 9-PA and R110 in [mmim⁺][Tf₂N⁻] as a Function of Temperature Along with Solvent Viscosity

T / K	$\eta / \text{mPa s}$	τ_r / ns	
		9-PA	R110
298	37.1	1.02	4.39
303	30.8	0.86	3.68
308	26.4	0.70	3.00
313	22.7	0.60	2.51
318	19.6	0.53	2.07
323	17.2	0.43	1.76
328	15.1	0.38	1.50
338	12.0	0.29	1.11
348	9.7	0.23	0.87

Table 4.2: Reorientation Times of 9-PA and R110 in [emim⁺][Tf₂N⁻] as a Function of Temperature Along with Solvent Viscosity

T / K	$\eta / \text{mPa s}$	τ_r / ns	
		9-PA	R110
298	32.4	0.96	4.11
303	27.4	0.83	3.27
308	23.4	0.63	2.82
313	20.2	0.56	2.36
318	17.6	0.49	2.04
323	15.4	0.45	1.71
328	13.7	0.37	1.51
338	10.9	0.30	1.13
348	8.8	0.21	0.87

Table 4.3: Reorientation Times of 9-PA and R110 in [mpim⁺][Tf₂N⁻] as a Function of Temperature Along with Solvent Viscosity

T / K	$\eta / \text{mPa s}$	τ_r / ns	
		9-PA	R110
298	45.2	1.22	5.59
303	36.9	1.01	4.52
308	30.9	0.82	3.72
313	26.1	0.68	3.12
318	22.1	0.55	2.57
323	19.1	0.48	2.17
328	16.7	0.40	1.83
338	12.9	0.31	1.41
348	10.2	0.25	1.04

Table 4.4: Reorientation Times of 9-PA and R110 in [bmim⁺][Tf₂N⁻] as a Function of Temperature Along with Solvent Viscosity

<i>T</i> / K	η / mPa s	τ_r / ns	
		9-PA	R110
298	50.2	1.40	6.79
303	41.1	1.16	5.48
308	33.8	0.97	4.65
313	28.5	0.82	3.68
318	24.1	0.68	2.95
323	20.7	0.58	2.40
328	17.9	0.49	2.02
338	13.7	0.37	1.47
348	10.9	0.28	1.09

Table 4.5: Reorientation Times of 9-PA and R110 in [hmim⁺][Tf₂N⁻] as a Function of Temperature Along with Solvent Viscosity

<i>T</i> / K	η / mPa s	τ_r / ns	
		9-PA	R110
298	68.8	1.67	7.43
303	55.8	1.34	6.32
308	45.9	0.99	5.38
313	37.8	0.90	4.59
318	31.5	0.71	3.85
323	26.5	0.61	3.22
328	22.7	0.52	2.83
338	16.9	0.39	2.03
348	13.1	0.27	1.47

Table 4.6: Reorientation Times of 9-PA and R110 in [moim⁺][Tf₂N⁻] as a Function of Temperature Along with Solvent Viscosity

T / K	$\eta / \text{mPa s}$	τ_r / ns	
		9-PA	R110
298	93.0	2.14	10.33
303	73.9	1.94	9.04
308	59.5	1.58	7.40
313	48.5	1.34	6.44
318	39.9	1.04	5.40
323	33.3	0.86	4.53
328	28.1	0.82	3.93
338	20.7	0.61	2.86
348	15.6	0.44	2.08

Table 4.7: Reorientation Times of 9-PA and R110 in [dmim⁺][Tf₂N⁻] as a Function of Temperature Along with Solvent Viscosity

T / K	$\eta / \text{mPa s}$	τ_r / ns	
		9-PA	R110
298	114	2.50	11.16
303	90.4	2.00	9.94
308	71.7	1.66	8.45
313	58.0	1.40	7.24
318	47.5	1.15	6.33
323	39.3	0.95	5.24
328	33.1	0.83	4.64
338	24.0	0.63	3.28
348	17.9	0.47	2.40

Table 4.8: Reorientation Times of 9-PA and R110 in [ddmim⁺][Tf₂N⁻] as a Function of Temperature Along with Solvent Viscosity

<i>T</i> / K	η / mPa s	τ_r / ns	
		9-PA	R110
298	155	2.76	12.61
303	120	2.16	10.74
308	91.9	1.73	9.76
313	75.8	1.39	8.43
318	61.2	1.04	7.48
323	50.1	0.86	6.23
328	41.5	0.73	5.35
338	29.6	0.53	3.88
348	21.8	0.38	2.94

Table 4.9: Reorientation Times of 9-PA and R110 in [mtdim⁺][Tf₂N⁻] as a Function of Temperature Along with Solvent Viscosity

<i>T</i> / K	η / mPa s	τ_r / ns	
		9-PA	R110
308	125	1.92	9.17
313	96.6	1.64	8.6
318	77.2	1.34	7.17
323	62.8	1.12	6.47
328	51.4	0.98	5.6
338	35.9	0.75	4.12
348	26.1	0.57	3.15

Table 4.10: Reorientation Times of 9-PA and R110 in [hdmim⁺][Tf₂N⁻] as a Function of Temperature Along with Solvent Viscosity

T / K	$\eta / \text{mPa s}$	τ_r / ns	
		9-PA	R110
323	82.1	1.20	6.38
328	66.7	0.98	5.78
338	45.5	0.78	4.55
348	32.4	0.59	3.56
358	23.9	0.46	2.68

Table 4.11: Reorientation Times of 9-PA and R110 in [modim⁺][Tf₂N⁻] as a Function of Temperature Along with Solvent Viscosity

T / K	$\eta / \text{mPa s}$	τ_r / ns	
		9-PA	R110
338	59.5	0.8	4.53
348	41.3	0.62	3.605
358	29.7	0.47	2.73

The experimentally measured reorientation times have been analyzed by means of SED hydrodynamic theory.^{14,203} According to this theory, the rotational diffusion of a solute molecule in a solvent continuum is assumed to occur by small-step diffusion and the reorientation time is related to the macroscopic viscosity of the solvent by the following relation.

$$\tau_r = A(\eta/T)^n \quad (4.1)$$

In the above equation, A is the ratio of hydrodynamic volume (V_h) of the solute to Boltzmann constant (k) and $n=1$ as predicted by the SED theory. The SED hydrodynamic theory has been discussed extensively in Chapter 3.

To find out if the SED hydrodynamic theory is able to explain the experimental data, reorientation times of 9-PA and R110 are plotted as a function of η/T in Figure 4.3.

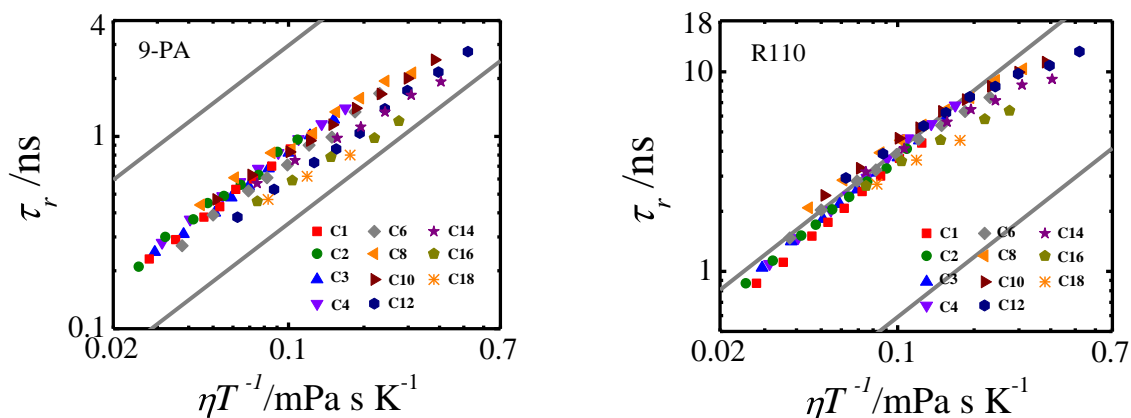


Figure 4.3 Plots of τ_r versus η/T for 9-PA and R110 in 1-alkyl-3-methylimidazolium bis(trifluoromethylsulfonyl)imides of varying alkyl chain lengths (C_1 to C_{18}). The SED slip and stick lines for the two solutes are also shown in the figure.

The SED slip and stick lines are also shown in the figures. Inspection of the figure indicates that the rotational diffusion of 9-PA is closer to the predictions of slip hydrodynamics, whereas reorientation times of R110 obey stick hydrodynamics due to specific interactions prevailing between R110 and the $[\text{Tf}_2\text{N}^-]$ anion of the ionic liquids. The parameters A and n (given in eq 4.1) have been obtained for both the solutes in $[\text{Rmim}^+][\text{Tf}_2\text{N}^-]$ from the linear least-squares fits of log-log plots (fitted lines not shown

in the plots). It has been observed that both A and n decrease with an increase in the length of the alkyl chain on the imidazolium cation and these trends have been depicted in Figure 4.4 for 9-PA and R110. It has been noticed that from methyl to octadecyl derivative, the parameter A decreases by a factor of 3 for both the solutes and n by a

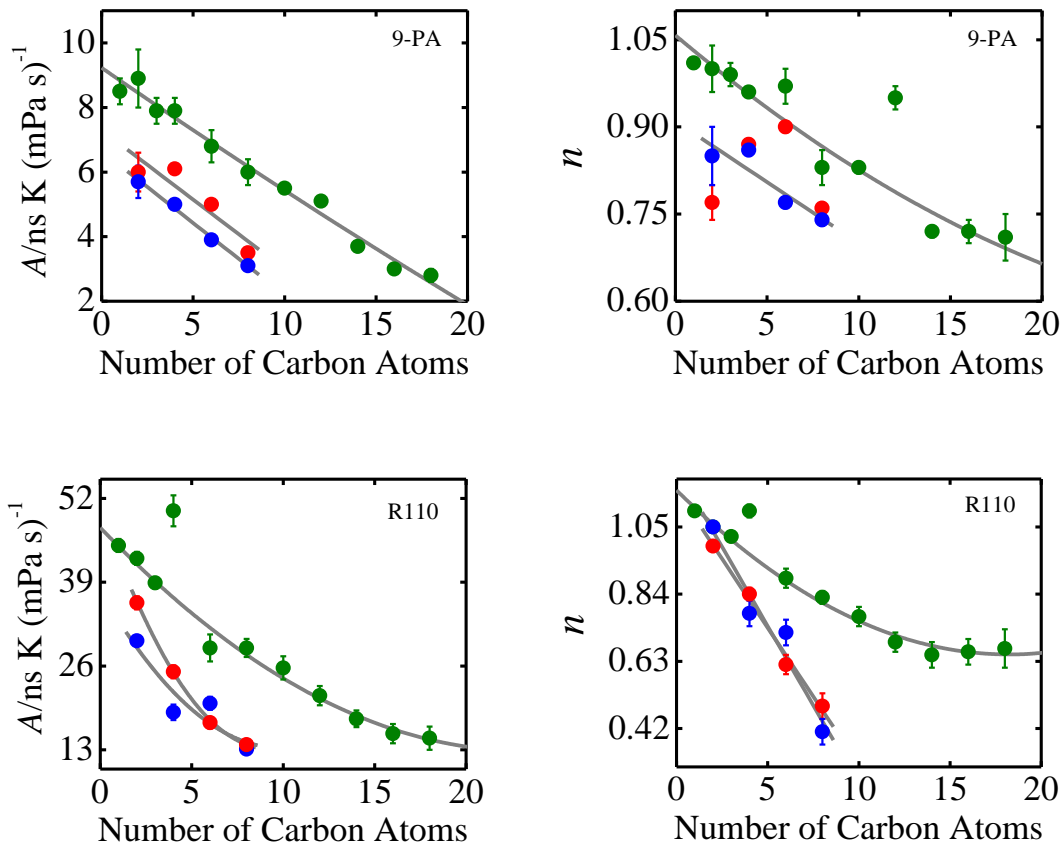


Figure 4.4 Plots of A and n versus number of carbon atoms present in the alkyl chain on the imidazolium cation with $[Tf_2N^-]$ (olive), $[BF_4^-]$ (red) and $[PF_6^-]$ (blue) anions for the solutes 9-PA and R110. The lines passing through the data points are drawn as visual aids and it can be noticed that barring a few exceptions. Data for 9-PA and R110 in $[Rmim^+][BF_4^-]$ and $[Rmim^+][PF_6^-]$ has been taken from Chapter 3.

factor of 1.4 and 1.6 for 9-PA and R110, respectively. However, it may be noted that in case of $[\text{ddmim}^+][\text{Tf}_2\text{N}^-]$ there is an increase in n for 9-PA, while for the cationic solute R110, there is an increase in both A and n in $[\text{bmim}^+][\text{Tf}_2\text{N}^-]$. To verify this anomaly, experiments have been repeated with fresh sets of samples for 9-PA in $[\text{ddmim}^+][\text{Tf}_2\text{N}^-]$ and R110 in $[\text{bmim}^+][\text{Tf}_2\text{N}^-]$. Such a repetition did not alter the earlier result and at this moment we do not have an explanation for this observation. Nevertheless, the results obtained from the analysis reveal that the value of the parameter A decreases with an increase in the length of the alkyl chain on the imidazolium cation, which is an indication that the boundary condition parameter C is not constant but varies in each member of the homologous series. Furthermore, the value of n deviates from the unity, notably from the octyl derivative onward and this observation suggests the failure of the SED hydrodynamic theory in explaining the experimental results especially in case of ionic liquids having longer alkyl chains on the imidazolium cation. It may be possible that the value of A decreases with an increase in the length of the alkyl chain because the volume of the solvent molecule increases, which in turn leads to a decrease in the boundary condition parameter. Quasihydrodynamic theory of Gierer-Wirtz (GW)²⁴⁹ has been considered to account for the changes associated with the A values and this model incorporates the size of the solute as well as the solvent (V_s) while calculating the boundary condition parameter. A detailed account of GW theory has been given in the Chapter 3.

The volumes of the ionic liquids used in this study have been calculated using Edward increment method²⁴⁵ and the limitations involved in this procedure have been discussed in the previous Chapter. It has been noticed that from [mmim⁺][Tf₂N⁻] to [modim⁺][Tf₂N⁻], V_s increases by a factor of 2, nevertheless, C_{GW} decreases by a mere 26% for both 9-PA and R110. Thus, the value of A calculated using C_{GW} for 9-PA in [mmim⁺][Tf₂N⁻] is 4.6 ns K (mPa s)⁻¹ and it decreases to 3.7 ns K (mPa s)⁻¹ in [modim⁺][Tf₂N⁻] and the corresponding decrease in case of R110 is from 6.6 to 5.3 ns K (mPa s)⁻¹. In other words, a factor of 3 decrease observed in the value of A from methyl to octadecyl derivatives of the ionic liquids could not be mimicked by the quasihydrodynamic theory of Gierer-Wirtz. Thus, the analyses carried out in this manner suggest that both hydrodynamic and quasihydrodynamic theories are unable to explain the observed trends.

The results presented here clearly indicate that the influence of the length of the alkyl chain on the rotational diffusion of both 9-PA and R110 in 1-alkyl-3-methylimidazolium bis(trifluoromethylsulfonyl)imides is similar although both the solutes are chemically distinct. The only difference is the significantly slower rotation of the ionic solute R110 as a consequence of its specific interactions with the [Tf₂N⁻] anion of the ionic liquids. Furthermore, the nonlinear dependence of τ_r on η/T could not be accounted by either hydrodynamic or quasihydrodynamic theories. Somewhat similar behavior has been noticed for the same solutes in 1-alkyl-3-methylimidazolium-based ionic liquids with [BF₄⁻] and [PF₆⁻] anions. It may be noted that in these studies,

significant deviations from the SED hydrodynamic theory have been noticed even though the length of the alkyl chain on the imidazolium cation was varied only from ethyl to octyl and these results have also been presented in Figure 4.4 for the sake of comparison. The observed results have been ascribed to the organized structure of the ionic liquids. The high charge to size ratio of $[\text{BF}_4^-]$ and $[\text{PF}_6^-]$ anions enables them to associate strongly with the imidazolium cation leading to the formation of organized structure even in the presence of shorter alkyl chains. Neutron diffraction studies carried out with $[\text{mmim}^+][\text{Tf}_2\text{N}^-]$ suggest that charge ordering is substantially less compared to $[\text{mmim}^+][\text{PF}_6^-]$ as result of delocalization of the charge over the anion and this has a major influence on the properties of $[\text{Tf}_2\text{N}^-]$ -based ionic liquids.⁴⁶ For example, viscosities of these ionic liquids are, in general, lower than those found for the corresponding ionic liquids with $[\text{BF}_4^-]$ and $[\text{PF}_6^-]$ anions due to the much softer ionic structure, which allows the ions to move more freely with respect to one another. Moreover, the weaker Coulombic interactions reduce the ability of long alkyl chain $[\text{Tf}_2\text{N}^-]$ -based ionic liquids to form liquid crystals.⁴⁷ Due to these reasons influence of the length of the alkyl chain on solute rotation has not been observed in the case of rotational diffusion of 9-PA and R110 in methyl to hexyl derivatives of 1-alkyl-3-methylimidazolium bis(trifluoromethylsulfonyl)imides, which is in contrast to the results observed in case of ionic liquids with $[\text{BF}_4^-]$ and $[\text{PF}_6^-]$ anions. This observation clearly indicates that the length of the alkyl chain has no bearing on solute rotation in ionic

liquids when a weakly coordinating anions such as $[\text{Tf}_2\text{N}^-]$ and $[\text{FAP}^-]$ are present in combination with the imidazolium cation having shorter alkyl chains.

However, when the length of the alkyl chain was varied from methyl to octadecyl in 1-alkyl-3-methylimidazolium ionic liquids with $[\text{Tf}_2\text{N}^-]$ anions, influence of solvent structure has been noticed on the rotational diffusion of 9-PA and R110, especially from the octyl derivative onward. This behavior can be ascribed to the organized structure of the ionic liquids. In other words, even $[\text{Tf}_2\text{N}^-]$ -based ionic liquids form organized structures in the presence of longer alkyl chains on the imidazolium cation, which influence solute rotation. Essentially, ionic liquids with $[\text{Tf}_2\text{N}^-]$ anions form softer ionic structure due to the less charge ordering, which is a result of delocalization of charge over the bulky anion.¹⁷ Therefore, in case of $[\text{Rmim}^+][\text{Tf}_2\text{N}^-]$ ionic liquids with shorter alkyl chains, the combination of ineffective Coulombic interactions and weaker van der Waals interactions cannot form the extensive organized structure. However, longer alkyl chains present on the imidazolium cation undergo aggregation due to the stronger van der Waals interactions prevailing between them, which results in organized domain structure of the ionic liquids even in the case of weakly associating anions.¹²² The size of the domain structure increases with an increase in the length of the alkyl chain on the imidazolium cation. Thus, solute rotation is significantly influenced by the length of the alkyl chain attached to the imidazolium cation in ionic liquids having longer alkyl chains.

At this juncture, it is pertinent to discuss somewhat similar alkyl chain length dependence observed on the rotational diffusion of 9-PA and R110 in 1-alkyl-3-

methylimidazolium bis(trifluoromethylsulfonyl)imides. Because of their distinct chemical nature, 9-PA and R110 are probably located in different regions of the ionic liquids. The nonpolar solute resides in the nonpolar domains, while the location of the charged solute is somewhat circumstantial. Considering the size and also the larger fraction being nonpolar, it is likely that R110 will be located at the boundary between the nonpolar domains and the ionic group region comprising $[\text{Tf}_2\text{N}^-]$ anions and imidazolium rings. Such a location would allow R110 to access $[\text{Tf}_2\text{N}^-]$ anions through its ionic groups, and the nonpolar domains of the ionic liquid via the nonpolar fraction. As the length of the alkyl chain increases on the imidazolium cation, the nonpolar domains become larger in size and therefore the nonpolar solute, 9-PA, which resides in these domains, experiences lower friction. In other words, at a particular η/T , the observed faster rotation of 9-PA upon increasing in the length of the alkyl chain is due to an increase in the size of the organized domains. In case of cationic solute, however, larger organized domain structures probably shield $[\text{Tf}_2\text{N}^-]$ anions from the solute and hence lead to weaker hydrogen bonding interactions between R110 and the anion of the ionic liquid. Thus, at a given η/T , rotation of the cationic solute becomes faster with an increase in the length of the alkyl chain on the imidazolium cation. In essence, an increase in the length of the alkyl chain on the imidazolium cation facilitates rotation of nonpolar as well as charged solutes via different mechanisms.

4.4. Conclusions

Rotational diffusion studies carried out with a pair of structurally similar nonpolar and charged solutes in 1-alkyl-3-methylimidazolium bis(trifluoromethylsulfonyl)imides indicate that the length of the alkyl chain on the imidazolium cation has a bearing on solute rotation only when the number of carbon atoms in the alkyl chain exceeds eight. Both hydrodynamic and quasihydrodynamic theories fail to rationalize the experimental results. Organized structure arising as a consequence of alkyl chain aggregation is responsible for the observed behavior. These results are somewhat different compared to the ones observed in case of 1-alkyl-3-methylimidazolium-based ionic liquids with tetrafluoroborate and hexafluorophosphate anions, where alkyl chain length dependence has been observed even from ethyl to octyl derivatives. Weakly associating nature of bis(trifluoromethylsulfonyl)imide, which results from the delocalization of charge over the bulky anion is responsible for the observed behavior. However, with an increase in the length of the alkyl chain on the imidazolium cation, stronger van der Waals interactions prevail between the alkyl chains leading to the formation of organized domains and ensuing faster rotation of the solutes.

Chapter 5

Photoisomerization Dynamics in Ionic Liquids

5.1. Introduction

Ionic liquids possess distinct physicochemical properties that enable them to function as favorable reaction media ensuing an increased reactivity, catalytic activity, selectivity and yield of reactions compared to conventional solvents.^{9,11,15,80,89} To get a better appreciation of chemical reactivity of various reactions in ionic liquids, a good number of studies have been carried out in literature, which include solvation dynamics,^{225,233,234,263,264} rotational diffusion,^{229,230,233-235} electron transfer,²⁶⁵ proton transfer,²⁶⁶ Diels-Alder,^{267,268} isomerization²⁶⁹⁻²⁷¹ and radical reactions.^{272,273} In a majority of the studies, the observed results have been assimilated in terms of physicochemical properties such as viscosity, polarity, solvation and specific interactions, of the ionic liquids.

Among the above-mentioned processes, photoisomerization studies dealing with olefins and polyenes have attracted considerable attention in the recent past since they serve as prototypical examples of unimolecular reactions in condensed phase.^{6,13,14} In view of the fact that large-amplitude conformational changes are involved in the photoisomerization process, the influence of solvent on reaction rates can be examined.

Since the rate of the reaction is governed by activated barrier crossing, Kramers theory²⁷⁴ has been widely used to understand the rate constants in terms of friction exerted by the solvent. Although Kramers theory has been quite successful, systematic deviations from Kramers model were observed, which have been rationalized on the basis of microscopic friction being different from the bulk viscosity of the solvent, frequency-dependent frictional effects and inadequacy of the one-dimensional model. Some of the systems investigated include stilbene and its analogs,^{6,275-280} diphenylbutadienes²⁸¹⁻²⁸⁶ and carbocyanines.²⁸⁷⁻²⁹³

Even though a large body of work exists in literature involving the photoisomerization of olefins and polyenes in conventional solvents, such studies are sparse in ionic liquids.^{269,270} Ozawa and Hamaguchi²⁶⁹ have shown that photoisomerization of *trans*-stilbene does take place in the ionic liquid 1-butyl-3-methylimidazolium hexafluorophosphate ([bmim⁺][PF₆⁻]) despite its high viscosity. Mali *et al.*²⁷⁰ have compared the photoisomerization of two carbocyanine derivatives, 3,3'-diethyloxadycarbocyanine iodide (DODCI) and merocyanine 540 (MC 540) in [bmim⁺][PF₆⁻] and aqueous glycerol of identical viscosity. It was found that the nonradiative rate constants of DODCI measured under isoviscous conditions are more or less identical in both the solvents indicating that viscosity alone controls the rate of photoisomerization. In contrast, the nonradiative rate constants of MC 540 were found to be a factor of two higher in aqueous glycerol compared to [bmim⁺][PF₆⁻]. This result has been rationalized on the basis of solute-solvent hydrogen bonding interactions between the hydroxyl groups of aqueous glycerol and the zwitterionic structures of MC 540, which

stabilize the twisted excited-state and thus lowering the barrier for isomerization. It must be noted that these studies have been carried out in a single ionic liquid therefore barrier height of the reaction could not be estimated. Moreover, stochastic theories such as Kramers model could not be employed to understand the role of viscosity on the rates of photoisomerization.

In view of the paucity of photoisomerization studies in ionic liquids, the present study has been undertaken. In this work, photoisomerization of a cationic solute DODCI (see Figure 5.1 for molecular structure) has been examined in a series of 1-alkyl-3-methylimidazolium (alkyl = methyl, ethyl, propyl, butyl and hexyl) bis(trifluoromethylsulfonyl)imides. DODCI has been chosen because its photoisomerization in alcohols has been investigated in the ground and excited states by

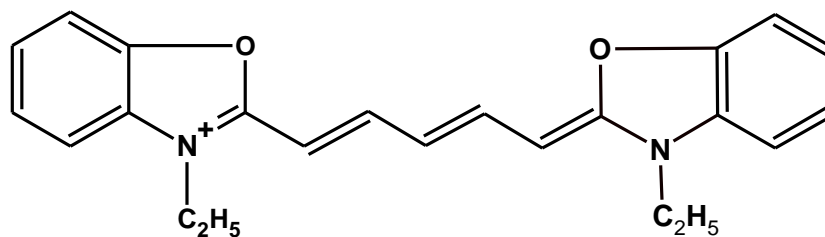


Figure 5.1 *Molecular Structure of DODCI.*

Fleming and coworkers.^{289,290} Furthermore, Hara and Akimoto²⁹¹ have examined its ground-state isomerization in alcohols at high pressure. The excited-state isomerization of DODCI essentially involves an activated twist motion about the double bonds to an intermediate geometry. Twisting motion or barrier crossing dominates the nonradiative process because internal conversion from the twisted excited state is very rapid as a

consequence of small energy difference between the two states. It must be noted that in case of DODCI, the nonradiative rate constant essentially represents the rate of photoisomerization since the contribution due to internal conversion from the normal excited state is negligible and also triplet yield is very low.²⁸⁹ The ionic liquid series comprising the cations 1,3-dimethylimidazolium ([mmim⁺]), 1-ethyl-3-methylimidazolium ([emim⁺]), 1-methyl-3-propylimidazolium ([mpim⁺]), 1-butyl-3-methylimidazolium ([bmim⁺]), 1-hexyl-3-methylimidazolium ([hmim⁺]) and the anion bis(trifluoromethylsulfonyl)imide ([Tf₂N⁻]) was chosen due to moderate viscosities. The moderate viscosities ensure that the measured nonradiative rate constants represent the rates of photoisomerization. It must be noted that for DODCI at very high viscosities the twisting motion gets inhibited and internal conversion from the normal excited state becomes the main nonradiative process.²⁸⁹ The objective of the present study is to find out how photoisomerization of DODCI transpires in these ionic liquids compared to alcohol series. In fact, it would also be interesting to make a comparison between the results obtained in ionic liquids and nonassociative polar solvents such as alkyl nitriles. Unfortunately, such a comparison is not feasible as DODCI, due to its ionic character, is insoluble in nitriles. In this study, nonradiative rate constants will be obtained from the measured fluorescence lifetimes and quantum yields and the activation energies will be estimated from the isoviscosity plots. Kramers theory will be applied to understand the reduced isomerization rate constants in terms of solvent friction.

5.2. Materials and Methods

The solute DODCI was purchased from Aldrich and all the ionic liquids employed in this study were purchased from io-li-tec. Both the DODCI and the ionic liquids are of the highest available purity and were used without further purification. Concentration of DODCI in ionic liquids was chosen such that the absorbance is in the range of 0.1–0.15 at the wavelength of excitation. For the purpose of quantum yield measurements, DODCI was excited at 540 nm and the corrected emission spectra were recorded from 550 nm to 720 nm. DODCI in ethanol with a reported quantum yield of 0.42 at 298 K was used as the standard.²⁹² Time-resolved fluorescence measurements were carried out with a setup that works on the principle of time-correlated single-photon counting.²¹⁰ The details of the setup, data acquisition procedure and analysis of the decay curves have been described in the Chapter 2. Samples containing the solute DODCI in ionic liquids were excited at 560 nm with a light emitting diode (LED) whose pulse width is about 1.3 ns and repetition rate is 1 MHz. The full-width at half-maximum of the instrument response function is same as the pulse width of the LED because a microchannel plate detector was used. The emission from the samples was monitored at 615 nm. Fluorescence decays were collected in the temperature range 280–370 K. The temperature of the sample was controlled with the aid of a thermoelectric controller (model DS) from IBH. Each measurement was repeated 2–3 times and the average values are reported. Refractive index measurements were carried out with the aid of ATAGO RX-5000 α refractometer and the detailed procedure has been given in the Chapter 2. The measured numbers are reproducible up to the third digit.

5.3. Results and Discussion

To find out if the length of the alkyl chain on the imidazolium cation influences the environment experienced by DODCI, its absorption and emission spectra have been recorded in $[\text{mmim}^+][\text{Tf}_2\text{N}^-]$ and $[\text{hmim}^+][\text{Tf}_2\text{N}^-]$. These spectra are displayed in Figure 5.2 and it can be noticed from the figure that there are no discernable changes in

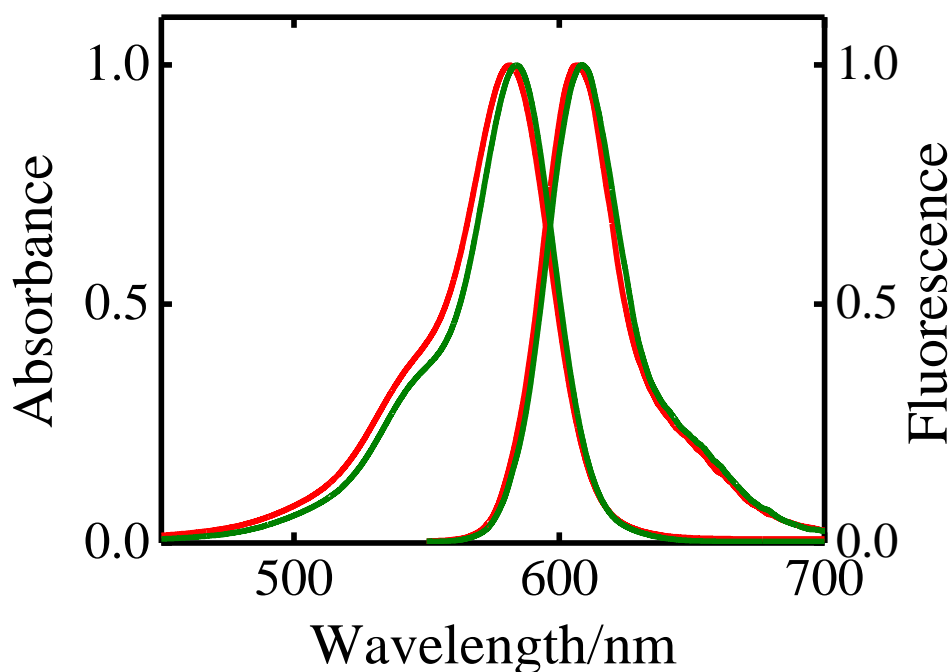


Figure 5.2 Normalized absorption and emission spectra of DODCI in $[\text{mmim}^+][\text{Tf}_2\text{N}^-]$ (red) and $[\text{hmim}^+][\text{Tf}_2\text{N}^-]$ (olive).

the peak positions of the spectra with an increase in the length of the alkyl chain on the imidazolium cation. It may be noted that dielectric relaxation studies carried out with 1-alkyl-3-methylimidazolium bis(trifluoromethylsulfonyl)imides indicate that there is a negligible variation in the dielectric constant from lower to the higher members of this

homologous series.²⁹⁴ Thus, it can be concluded that the environment experienced by DODCI is not altered significantly in bis(trifluoromethylsulfonyl)imides from methyl to hexyl derivative. Fluorescence decays of DODCI in each of the five ionic liquids used in the present study could be fitted with single exponential function. Typical fluorescence decays of DODCI in $[\text{mmim}^+][\text{Tf}_2\text{N}^-]$ as a function of temperature (T) are shown in Figure 5.3. It is worth mentioning that the presence of iodide in DODCI may quench its

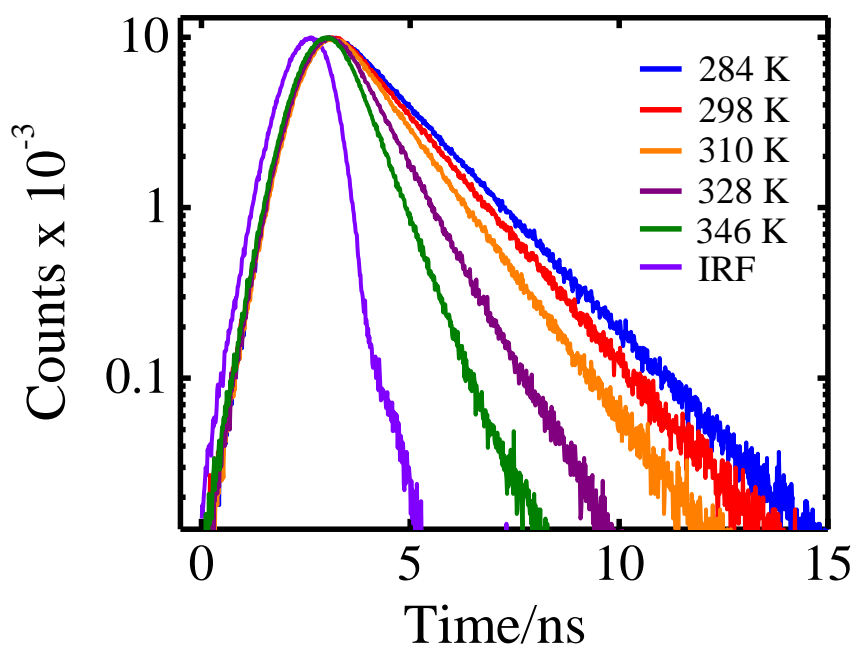


Figure 5.3 Fluorescence decays of DODCI in $[\text{mmim}^+][\text{Tf}_2\text{N}^-]$ at different temperatures along with the instrument response function. The fitted decay curves are not shown in the figure for the sake of clarity.

fluorescence due to the heavy-atom effect, which in turn can influence the measured lifetimes. Quenching due to heavy-atom effect usually occurs as a result of increased

intersystem crossing. However, Morrow and coworkers²⁹⁵ by means of flash photolysis experiments have shown that direct excitation of DODCI leads to photoisomerization without the formation of its triplet state. The quantum efficiency for intersystem crossing to the triplet state was observed to be < 0.01 for DODCI in ethanol. Thus, it is safe to conclude that the measured fluorescence lifetimes of DODCI are not influenced due to the presence of iodide. Variation of refractive index (n) of the five ionic liquids as a function of temperature is displayed in Figure 5.4. It can be noticed from figure that the

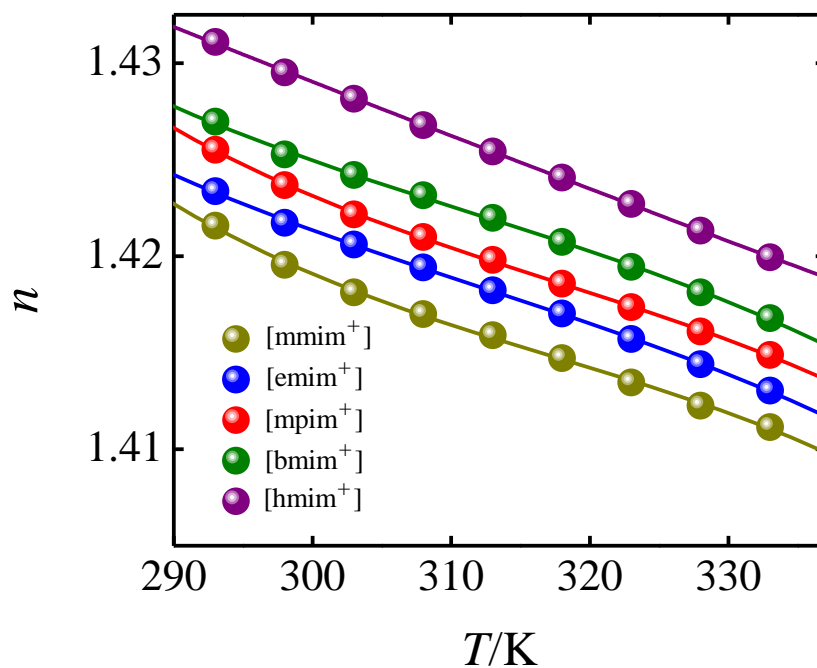


Figure 5.4 Plots of n versus T in the 1-alkyl-3-methylimidazolium bis(trifluoromethylsulfonyl)imides. The curves passing through the data points are drawn as a visual aid.

refractive index increases with an increase in the length of the alkyl chain on the imidazolium cation.

To comprehend the photoisomerization process of DODCI, nonradiative rate constants (k_{nr}) have been obtained from the measured fluorescence lifetimes (τ_f) using the following relation.²⁸⁹

$$k_{nr} = (1/\tau_f) - k_r \quad (5.1)$$

In the above equation, k_r is the radiative rate constant, which was obtained from the ratio of quantum yield (ϕ_f) and lifetime. Fluorescence quantum yields, lifetimes, radiative and nonradiative rate constants of DODCI measured at 298 K in the five 1-alkyl-3-methylimidazolium bis(trifluoromethylsulfonyl)imides are given Table 5.1 along with the

Table 5.1: Viscosities of 1-Alkyl-3-methylimidazolium bis(trifluoromethylsulfonyl) imides, Quantum Yields, Fluorescence Lifetimes, Radiative and Nonradiative Rate Constants of DODCI in 1-Alkyl-3-methylimidazolium bis(trifluoromethylsulfonyl) imides at 298 K.

Ionic Liquid	η / mPa s	ϕ_f	τ_f / ns	k_r / ns ⁻¹	k_{nr} / ns ⁻¹
[mmim ⁺][Tf ₂ N ⁻]	37.1	0.72	1.49	0.48	0.19
[emim ⁺][Tf ₂ N ⁻]	32.4	0.71	1.48	0.48	0.20
[mpim ⁺][Tf ₂ N ⁻]	45.2	0.71	1.48	0.48	0.20
[bmim ⁺][Tf ₂ N ⁻]	50.2	0.73	1.51	0.48	0.18
[hmim ⁺][Tf ₂ N ⁻]	68.8	0.76	1.63	0.47	0.14

solvent viscosities. Velsko and Fleming²⁸⁹ have shown that the radiative rate constant of DODCI in ethanol is almost independent of temperature and they obtained k_r values at different temperatures by n^2 correction. We have also adopted a similar method to obtain k_r values of DODCI as a function of temperature.

Activation energy of a reaction is usually obtained with the aid of Arrhenius law from the temperature dependent rate constants. In the present study, however, such a procedure was not employed because of the influence of temperature on solvent viscosity. Instead, nonradiative rate constants have been measured in a homologous series of 1-alkyl-3-methylimidazolium bis(trifluoromethylsulfonyl)imides under isoviscous conditions. In other words, by adjusting temperature in each solvent, Arrhenius plots have been constructed for the nonradiative rate in which solvent viscosity is kept constant while the temperature and member of the homologous series are varied. These plots are known as isoviscosity plots and such a procedure assumes that the differences involved in the solvation effects throughout the series are negligible. Two self-consistency checks for this method are that the Arrhenius plots have the same slope when performed at different viscosities and that different measures of the friction such as viscosity and collision frequency provide the same slope.⁶ Essentially, the procedure that has been adopted to separate the activation barrier from the solvent frictional effects is based on a general expression for the isomerization rate constant (k_{iso}), which has an Arrhenius type form and is given by the following relation.

$$k_{iso} = F(\zeta) \exp(-E_a/RT) \quad (5.2)$$

In the above equation, E_a is the intrinsic barrier height and R is the universal gas constant. The term $F(\zeta)$ is a dynamical quantity that depends on solute-solvent frictional coupling.

In the present work, nonradiative rate constants of DODCI in the five ionic liquids have been obtained at 12 different values of viscosity ranging from 8 to 63 mPa s by choosing appropriate temperatures. Typical isoviscosity plots are shown in Figure 5.5 and

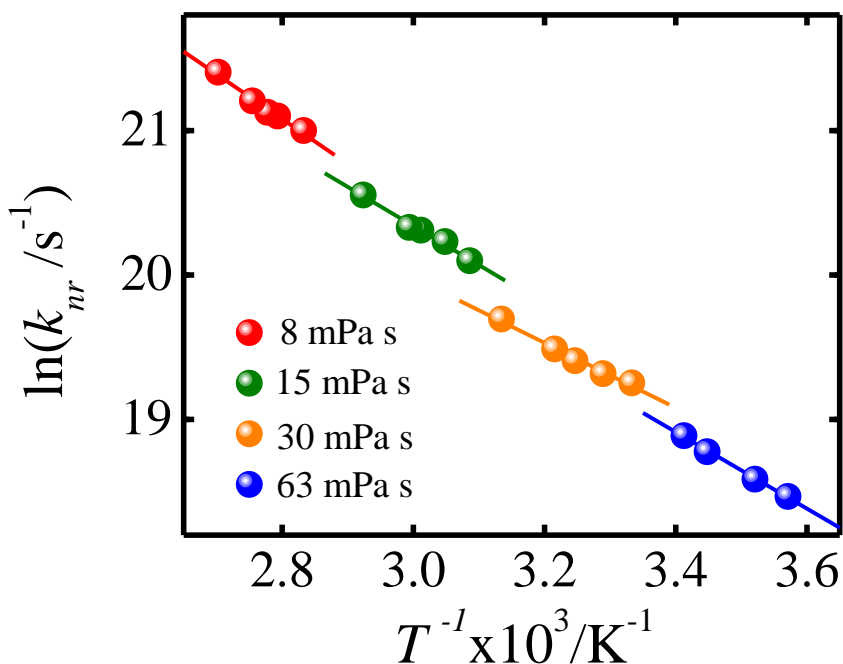


Figure 5.5 Isoviscosity plots for DODCI in the 1-alkyl-3-methylimidazolium bis(trifluoromethylsulfonyl)imides. The lines passing through the points are obtained by linear-least squares fit.

from the slopes of the plots activation energies and pre-exponential factors have been estimated, which are listed in Table 5.2. Inspection of the table reveals that although there is some random fluctuation in the data, the activation energies obtained in this manner are independent of viscosity and the average value has been found to be 22 ± 3 kJ mol⁻¹. To

Table 5.2: Pre-exponential Factors and Activation Energies for the Isomerization of DODCI obtained from Isoviscosity Plots.

$\eta / \text{mPa s}$	$\ln A$	$E_a / \text{kJ mol}^{-1}$
8.0	29.8±0.7	25.8±2.1
10.0	28.4±0.7	21.6±2.5
12.5	29.4±0.4	24.9±1.7
15.0	28.5±0.5	22.4±1.7
20.0	28.5±0.2	22.9±0.4
25.0	28.0±0.3	21.6±0.8
30.0	26.7±0.5	18.7±1.2
35.0	26.7±0.2	18.8±0.7
41.0	26.4±0.3	18.3±0.7
46.0	26.6±1.1	19.1±2.5
51.0	29.6±1.1	25.8±2.5
63.0	27.9±0.3	21.9±0.7

ensure that the nonradiative rate constants of DODCI measured throughout the temperature range represent the rate constants for twisting, $\ln(k_{nr})$ is plotted as a

function of $1/T$ for ionic liquids having lowest ($[\text{emim}^+][\text{Tf}_2\text{N}^-]$) and highest ($[\text{hmim}^+][\text{Tf}_2\text{N}^-]$) viscosities in Figure 5.6. It can be noticed from the figure that these

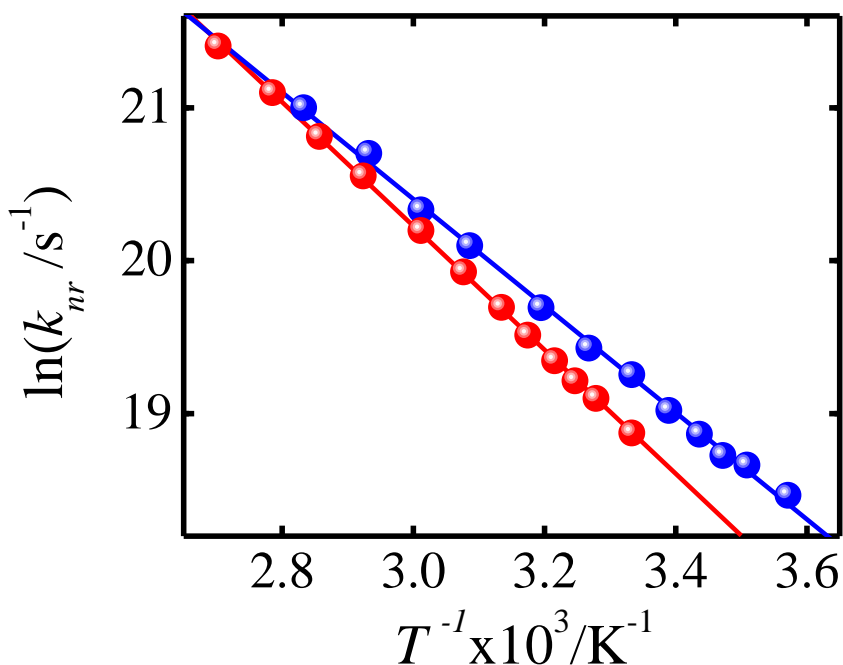


Figure 5.6 Plots of $\ln(k_{nr})$ versus $1/T$ in $[\text{emim}^+][\text{Tf}_2\text{N}^-]$ (blue) and $[\text{hmim}^+][\text{Tf}_2\text{N}^-]$ (red). The lines passing through the data points are obtained by linear-least squares fit.

plots are linear even at lower temperatures, which indicates that the important contribution to k_{nr} arises from the twisting process. Similar trends have been obtained for other ionic liquids used in this study (results not shown). These results are somewhat different compared to the ones obtained by Velsko and Fleming²⁸⁹ for DODCI in alcohols where they have noticed nonlinear behavior in $\ln(k_{nr})$ versus $1/T$ plots at lower temperatures. It may be noted that at low temperatures, internal conversion from the

normal excited state becomes a competing process along with twisting motion. Though not explicitly mentioned in the text, Velsko and Fleming²⁸⁹ have performed low temperature measurements in the range of 250–278 K and the onset of nonlinear behavior has been observed around 278 K. In contrast, the lowest temperature at which our measurements have been carried out is 280 K for DODCI in [emim⁺][Tf₂N⁻]. Thus, it is safe to assume that the contribution of internal conversion from the normal excited state to the nonradiative rate constant is negligible. For the sake of comparison activation energies obtained from $\ln(k_{nr})$ and $1/T$ plots in a single solvent (E_s) and activation energies for viscous flow (E_η) are given in Table 5.3. It is evident that activation energies obtained from single solvent are overestimated compared to those obtained from

Table 5.3: Activation Energies for the Isomerization of DODCI and for Viscous Flow obtained from Arrhenius Plots.

Ionic Liquid	$E_s / \text{kJ mol}^{-1}$	$E_\eta / \text{kJ mol}^{-1}$
[mmim ⁺][Tf ₂ N ⁻]	29.8±0.4	23.6±0.4
[emim ⁺][Tf ₂ N ⁻]	29.0±0.4	22.6±0.2
[mpim ⁺][Tf ₂ N ⁻]	29.6±0.5	25.9±0.4
[bmim ⁺][Tf ₂ N ⁻]	30.0±0.7	26.8±0.4
[hmim ⁺][Tf ₂ N ⁻]	33.7±0.2	29.0±0.4

isoviscosity plots. Having obtained the activation energy from isoviscosity plots, it is now possible to extract the preexponential factor $F(\zeta)$ using Eq. 5.2, which can be modeled using Kramers theory.

The most widely used model for the description of isomerization dynamics is that of Kramers, which treats the twisting motion as the escape of a particle over a potential barrier in one dimension. Under some assumptions the frequency factor for this process is given by²⁷⁴ equation 5.3.

$$F(\zeta) = k_{iso} \exp(E_a/RT) = \frac{\omega_0}{4\pi\omega'\tau_v} \left[1 + (2\omega'\tau_v)^2 \right]^{1/2} - 1 \quad (5.3)$$

In this equation, ω_0 is the frequency of the potential well of the initial minimum, ω' is the frequency of the barrier maximum and τ_v is the velocity relaxation time of the coordinate. The velocity relaxation time is related to the friction coefficient ζ by $\tau_v = \mu/\zeta$, where μ is the effective mass of the particle. In the limit of high friction, τ_v is short compared to the characteristic time scale of free motion on the potential surface such that $\omega'\tau_v \ll 1$ and $F(\zeta)$ becomes inversely proportional to friction. This high friction limit is also known as the Smoluchowski limit and under these conditions Eq. 5.3 reduces to equation 5.4.

$$F(\zeta) = \frac{\omega_0\omega'\mu}{2\pi\zeta} \quad (5.4)$$

Since ζ is not an experimentally observable quantity it becomes essential to model the friction experienced by the isomerizing moiety with an observable parameter. In the most

commonly used approach, it is assumed that the friction is proportional to viscosity, which results in the hydrodynamic form of the Kramers equation.²⁹⁰ Accordingly, $F(\zeta)$ is given by Eq. 5 with $A = \omega_0/2\pi$ and $B/\eta = 2\omega' \tau_v$.

$$F(\zeta) = \frac{A}{B/\eta} \left[1 + (B/\eta)^2 \right]^{1/2} - 1 \quad (5.5)$$

The reduced isomerization rate constant, k_{iso}^* , which is the same as $F(\zeta)$, of DODCI in 1-alkyl-3-methylimidazolium bis(trifluoromethylsulfonyl)imides as a function of viscosity has been calculated from the measured nonradiative rate constants with the aid of Eq. 5.2. A barrier height of 22 kJ mol⁻¹ that has been obtained from the isoviscosity plots was employed for this purpose. Figure 5.7 gives a plot of k_{iso}^* versus η and nonlinear least-squares method was employed to fit the data to Eq. 5.5 where A and B were treated as adjustable parameters. It is evident from the figure that the hydrodynamic Kramers expression does not have the curvature required to fit the entire data. To find out whether the Kramers model is able to explain the results in different friction regimes, separate fits were performed for low (8–20 mPa s) and high (25–63 mPa s) viscosity data and the resulting curves are also shown in the figure. It can be noticed from the figure that the fitted curve for the low viscosity data undershoots the high viscosity data points and vice-versa. Despite the failure, we would like to emphasize here that, to the best of our knowledge; this is the first instance where Kramers model has been applied to the photoisomerization studies in ionic liquids. It may be noted that hydrodynamic Kramers model also failed to mimic the observed trends for the isomerization of DODCI in

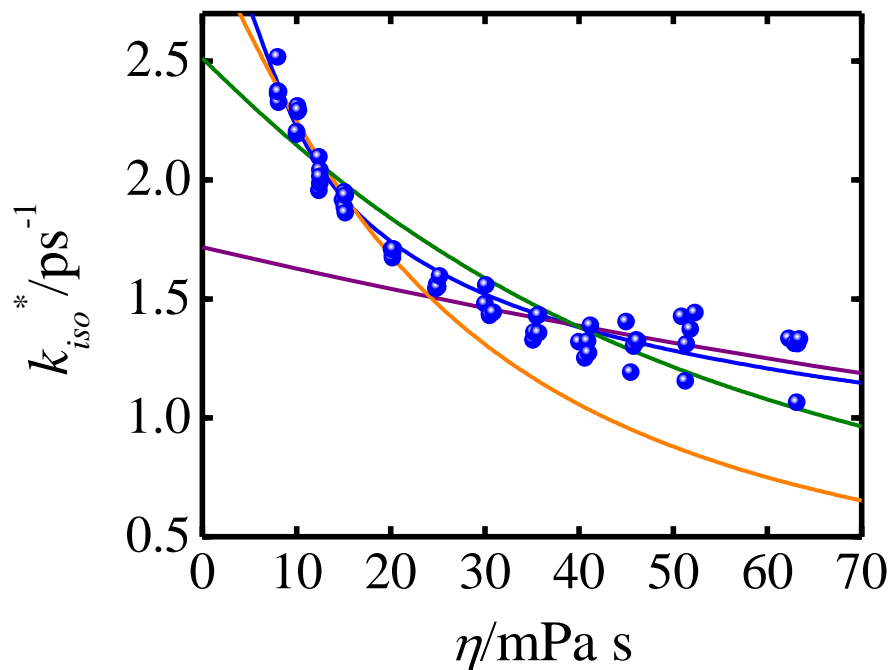


Figure 5.7 Plot of the reduced isomerization rate constant versus viscosity for DODCI in 1-alkyl-3-methylimidazolium bis(trifluoromethylsulfonyl)imides. The green, orange and purple colored curves represent fits to the Kramers model after considering the entire data, low viscosity data (8–20 mPa s) and high viscosity data (25–63 mPa s), respectively. The blue curve is a fit to the power law equation (see text for details).

alcohols in ground and excited states.^{289,290} Regardless of this, the parameters obtained from the fit are $\omega_0 = 15.8 \pm 0.4 \times 10^{12} \text{ s}^{-1}$ and $\omega' \tau_v = 32 \pm 2$ at unit viscosity. Since the condition, $\omega' \tau_v \ll 1$ is not fulfilled, it can be concluded that the isomerization process is not in the high friction limit (Smoluchowski limit). Although the k_{iso}^* does not follow $1/\eta$ dependence, it decreases upon increasing the viscosity, which indicates that the isomerization process is in the intermediate friction regime. A similar behavior has been

noticed for the ground and excited state isomerization of DODCI in alcohols.^{289,290} It has also been demonstrated that hydrodynamic Kramers model fails to fit the isomerization data of DODCI in alcohols even when rotational reorientation times of the solute were employed as a measure of solvent friction instead of bulk viscosity.²⁹⁰ However, such a procedure could not be performed in the present case as the anisotropy decays of DODCI in 1-alkyl-3-methylimidazolium bis(trifluoromethylsulfonyl)imides are significantly longer compared to the fluorescence decays. For the isomerization of DODCI in alcohols, the dependence of k_{iso}^* on η was explained by the one-dimensional Kramers model after taking into consideration frequency-dependence of the medium response.²⁹⁰

As an alternate method of analysis, a phenomenological functional form given by Eq. 5.6 has been considered, which resulted in an excellent fit of the DODCI isomerization data in 1-alkyl-3-methylimidazolium bis(trifluoromethylsulfonyl)imides.

$$k_{iso}^* = \frac{C}{\eta^a} \quad (5.6)$$

In this equation, a is a measure of dependence on solvent friction and C indicates the time scale of the isomerization motion.²⁹⁰ It must be noted that these parameters are not interpretable due to the lack of a physical model but provide a comparison between different systems for the purpose of identifying general trends.⁶ Despite this limitation, Eq. 5.6 has been employed in numerous isomerization studies^{276-280,282,290,291} involving different types of molecules that resulted in a power-law dependence on viscosity with $a < 1$. It has been observed that as barrier height increases the parameter a becomes

smaller. As the barrier becomes higher the frequency of the reactive motion increases and the zero-frequency shear viscosity turns out to be a worse measure of the friction experienced during isomerization. The values of C and a for DODCI in 1-alkyl-3-methylimidazolium bis(trifluoromethylsulfonyl)imides are $(4.7 \pm 0.2) \times 10^{12} \text{ s}^{-1}$ at unit viscosity and 0.33 ± 0.01 , respectively and the fitted curve is also shown in Figure 8. In case of alcohols, the ground state isomerization parameters, C and a are found to be $4 \times 10^{12} \text{ s}^{-1}$ at unit viscosity and 0.26, respectively and the corresponding numbers for the excited state isomerization are $0.8 \times 10^{12} \text{ s}^{-1}$ and 0.43. The barrier heights obtained from the isoviscosity plots are 57.3 and 11.3 kJ mol^{-1} , respectively, for the ground and excited state isomerization of DODCI in alcohols.²⁹⁰ The trends observed in these parameters for the isomerization of DODCI in 1-alkyl-3-methylimidazolium bis(trifluoromethylsulfonyl)imides are consistent with the above-mentioned arguments.

It has been suggested by Grote and Hynes²⁹⁷ that when the forces on the isomerization coordinate relax on a time scale comparable to the velocity relaxation time, the frequency dependent friction $\zeta(\omega)$ should be evaluated at the reactive frequency $\lambda_r = 2\pi k_{iso}^*$. If the well and the barrier frequencies are equal, then k_{iso}^* and $\zeta(\omega)$ can be related by the following equation.²⁹⁰

$$\frac{\zeta(2\pi k_{iso}^*)}{\mu} = \frac{\omega^2}{2\pi k_{iso}^*} - 2\pi k_{iso}^* \quad (5.7)$$

It must, however, be noted that the above equation cannot be applied to the experimental data in a simple way to yield the form of $\zeta(2\pi k_{iso}^*)$ since it is necessary to vary the viscosity for observing a change in k_{iso}^* , as a consequence use of Eq. 5.7 gives the form of $\zeta(\eta, 2\pi k_{iso}^*)$. In view of this difficulty, Eq. 5.7 was employed in conjunction with the experimental data to construct a plot of friction versus viscosity, which is displayed in

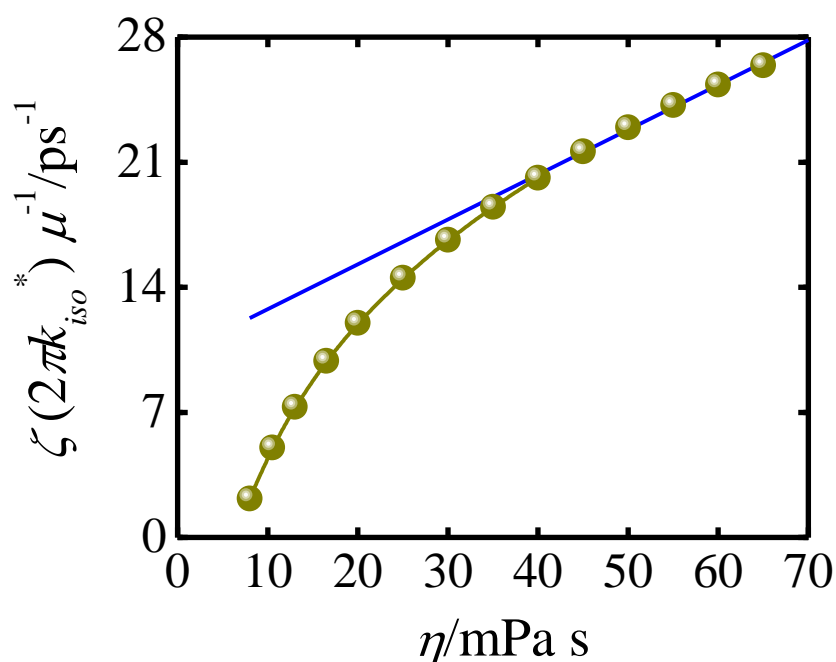


Figure 5.8 Plot of friction versus viscosity for DODCI isomerization in 1-alkyl-3-methylimidazolium bis(trifluoromethylsulfonyl)imides. The curve passing through the data points is drawn as a visual aid. The straight line is obtained from the linear least-squares fit of the data from 40 mPa s to show the transition from nonlinear to linear dependence of friction on η .

Figure 5.8 for the isomerization of DODCI in 1-alkyl-3-methylimidazolium bis(trifluoromethylsulfonyl)imides. For the purpose of obtaining the curve in Figure 5.8, a value of $1.58 \times 10^{13} \text{ s}^{-1}$ was used for ω' and k_{iso}^* as a function of viscosity was calculated with the aid of the relation, $k_{iso}^* = (4.7 \times 10^{12})/\eta^{0.33}$. It can be noticed from the figure that at high viscosities there is a linear dependence of friction on viscosity but as the viscosity decreases, the friction falls much more rapidly than linearly. From the figure it is evident that above 40 mPa s, the relation between friction and viscosity becomes linear. Whether such a transition is specific to the system of DODCI in 1-alkyl-3-methylimidazolium bis(trifluoromethylsulfonyl)imides or universal, remains to be seen, which can be tested by carrying out similar studies in different series of ionic liquids. Since a linear relation has been obtained between friction and viscosity from 40 mPas, it is tempting to find out whether k_{iso}^* varies linearly with $1/\eta$ instead of $1/\eta^a$ in the high viscosity regime, which can provide an experimental verification to Grote and Hynes theory. Unfortunately, such an attempt turned out to be futile as the scatter in the data is significant at higher viscosities.

Although the trends observed in the variation of k_{iso}^* with η for DODCI are similar in both 1-alkyl-3-methylimidazolium bis(trifluoromethylsulfonyl)imides and n-alcohols, the barrier heights are about a factor of two higher in ionic liquids (22 kJ mol^{-1}) compared to alcohols (11.3 kJ mol^{-1}). It is a well-known fact that barrier height for the isomerization process depends on the polarity of the solvent and also solute-solvent interactions. Even in a homologous series comprising n-alcohols, it has been observed

that isoviscosity plots for the isomerization of 4,4'-dimethoxystilbene lead to a series of lines with different slopes indicating that solvation effects are not uniform.²⁷⁷ However, for DODCI in alcohols it has been noticed that the barrier heights obtained at lower as well as higher viscosities are the same within the limits of experimental error^{289,290} and a similar trend has been observed in case of ionic liquids. These results suggest that solvent polarity is not the reason for the enhanced barrier heights obtained for the DODCI isomerization in 1-alkyl-3-methylimidazolium bis(trifluoromethylsulfonyl)imides. It has been established that ionic liquids can be viewed as three-dimensional networks of cations and anions held together by interactions such as hydrogen bonds, dispersive and Coulombic forces.^{11,89} In other words, the strong ion-ion interactions present in the ionic liquids lead to highly organized structures, which offer a completely different environment compared to conventional solvents. Thus, the organized structure of the ionic liquids could be responsible for impeding the twisting process ensuing higher activation energy. Somewhat similar explanation has been provided by Neta and Coworkers²⁷² while explaining the higher activation energies obtained for the radical reactions in the ionic liquids [bmim⁺][PF₆⁻] and [bmim⁺][BF₄⁻] compared to alcohols. Another possibility could be the ion pairing between DODCI cation and [Tf₂N⁻] anion, which is responsible for the observed higher activation energies. To verify this hypothesis, photoisomerization studies with DODCI need to be carried out in ionic liquids having different anions.

5.4. Conclusions

Barrier crossing reactions such as olefin and polyene photoisomerization have been extensively investigated in conventional solvents and the dependence of reaction rate on solvent friction has been rationalized using Kramers theory with a reasonable degree of success. However, to the best of our knowledge, such studies have not been performed in ionic liquids that are gaining prominence as alternative reaction media in numerous domains of Chemistry. Due to this reason, the present investigation has been undertaken wherein photoisomerization of a cationic solute DODCI has been examined in a series of 1-alkyl-3-methylimidazolium bis(trifluoromethylsulfonyl)imides and the important conclusions are summarized in this section. The variation of reduced isomerization rate constant of DODCI with the solvent viscosity could not be accounted by the hydrodynamic Kramers model and this result is similar to the one obtained in alcohols.^{41,42} Nevertheless, a power law relation, which is a phenomenological functional form, adequately describes the observed variation of k_{iso}^* with η . The nonlinear relation attained between friction and viscosity (Figure 5.8), especially at low values of η , is perhaps an indication that frequency dependence of the medium needs to be considered for improving the agreement between experiment and theory. The significantly higher activation energy obtained for DODCI isomerization in ionic liquids compared to alcohols is probably due to the organized structure of the medium, which inhibits the excited-state twisting.

Chapter 6

Photoisomerization Dynamics in AOT Reverse Micelles

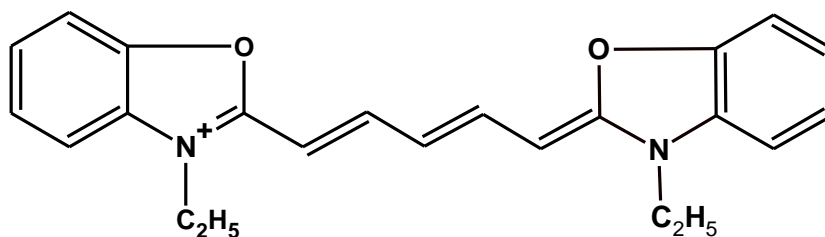
6.1. Introduction

Investigations dealing with photoisomerization of olefins and polyenes have attracted considerable attention in the recent past since they serve as prototypical examples of unimolecular reactions in condensed phase.^{6,14} The excited-state isomerization of these systems essentially involves an activated twist motion about the double bond/bonds to an intermediate geometry. Twisting motion or barrier crossing dominates the nonradiative process because internal conversion from the twisted excited state is very rapid due to the small energy difference between the two states. Since a large amplitude motion is involved in the barrier crossing, the nonradiative rate depends on the frictional coupling between the solute and its surroundings. In recent times, photoisomerization studies have been extended to complex systems such as organized assemblies,^{201,202,298,299,300} polymer systems³⁰¹⁻³⁰⁴ and ionic liquids.²⁷⁰ The consensus emerged from these studies in diverse environments is that the excited-state twisting motion of a solute molecule is essentially governed by the local friction. However, the parameter that is used to characterize friction depends on the medium in which the process of photoisomerization has been examined. In homogeneous media, bulk viscosity of the medium is usually employed to describe friction. In contrast, Young's modulus has been utilized to portray the friction experienced by the solute molecules undergoing

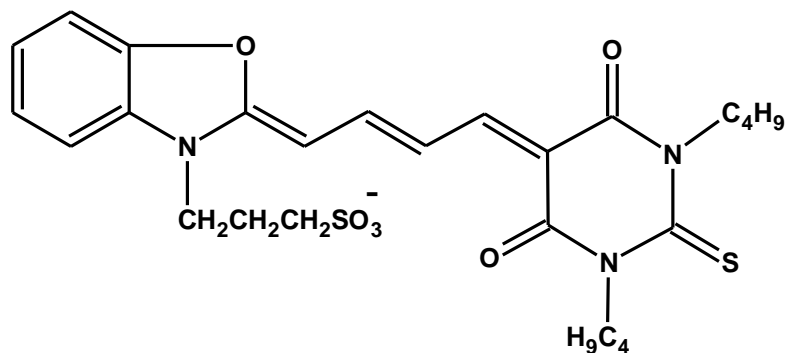
activated twist motion in polymer systems. Recently, it has been demonstrated³⁰¹⁻³⁰⁴ that the nonradiative rate constants and/or fluorescence lifetimes of various probe molecules in a range of polymer systems can be correlated with the Young's modulus of the polymers. Nonetheless, identification of the parameter that is associated with the local friction is not always straight forward. For example, in the reverse micellar system containing the surfactant bis(2-ethylhexyl) sodium sulfosuccinate (AOT), the variation in the photoisomerization rate constants of 3,3'-diethyloxadicyanine iodide (DODCI) and merocyanine 540 (MC 540) has been rationalized in terms of size of the water droplet in a qualitative manner.^{201,202} Furthermore, the friction experienced by the solute molecules in reverse micellar system of AOT could not be quantified. Hence, this premise forms the motive for undertaking the present study.

In this work, photoisomerization of a cationic solute DODCI and an anionic solute MC 540 has been examined in AOT/isooctane/water and AOT/cyclohexane/water reverse micellar systems as a function of mole ratio of water to the surfactant, W . The experiments were carried out over the W range of 4–30 and 1–15, respectively, in AOT/isooctane/water and AOT/cyclohexane/water systems. Figure 6.1 gives molecular structures of the two solutes used in the study. Since both DODCI and MC 540 are ionic they are expected to be located in the interfacial region of the reverse micelles. It is a well-known fact that the size and hydration of AOT reverse micelles increase with an increase in W .^{161,162} Thus, the purpose of this study is to find out how the variation in micellar properties influences the photoisomerization rates of DODCI and MC 540 and whether the observed changes in the rate constants can be correlated to a single micellar

parameter. In other words, the idea is to find out whether it is possible to identify a parameter that characterizes interfacial friction in reverse micelles.



DODCI



MC 540

Figure 6.1 *Molecular structures of the solutes.*

6.2. Materials and Methods

The solutes DODCI and MC 540 were obtained from Aldrich and Molecular Probes, respectively. The surfactant AOT was purchased from Aldrich, whereas the solvents isooctane and cyclohexane were from Spectrochem India Pvt. Ltd. and s. d. fine-chem Ltd, respectively. All these chemicals are of the highest available purity and were

used without further purification. Deionized water from Millipore A-10 was used in the preparation of AOT reverse micellar samples. Since the surfactant AOT is hygroscopic by nature, the amount of water present in it was estimated using Karl Fischer titration method. According to this estimate, the water that is inherently present in AOT gives rise to a W value of 0.6. Thus, appropriate amounts of water were taken in volumetric flasks and to these AOT stock solution was added such that the final concentration of the surfactant is 0.1 mol dm^{-3} . Concentrations of the probes in AOT reverse micelles were chosen such that the absorbance of both DODCI and MC 540 is in the range of 0.1–0.15 at the wavelength of excitation.

For the purpose of quantum yield measurements, the probes DODCI and MC 540 were excited at 540 nm and 525 nm, respectively. For both DODCI and MC 540, the respective quantum yields in ethanol were used as the standards. The reported quantum yield values of DODCI and MC 540 in ethanol are 0.42 and 0.20, respectively, at 298 K.^{15,16} Time-resolved fluorescence measurements were carried out with a setup that works on the principle of time-correlated single-photon counting.¹⁷ The details of the setup, data acquisition procedure and analysis of the decay curves have been described in Chapter 2. Samples containing the probes DODCI and MC 540 in AOT reverse micelles were excited at 560 nm with a light emitting diode (LED) whose pulse width is about 1.3 ns and repetition rate is 1 MHz. The full-width at half-maximum of the instrument response function is same as the pulse width of the LED because a microchannel plate detector was used. The emission from the samples was monitored at 615 nm. All the measurements were performed at 298 K.

6.3. Results and Discussion

Absorption and emission spectra of DODCI and MC 540 in AOT/isooctane/water and AOT/cyclohexane/water reverse micellar systems have been recorded to comprehend the microenvironment experienced by the solute molecules in these organized assemblies. Figure 6.2 displays normalized absorption and emission spectra of the two solutes in

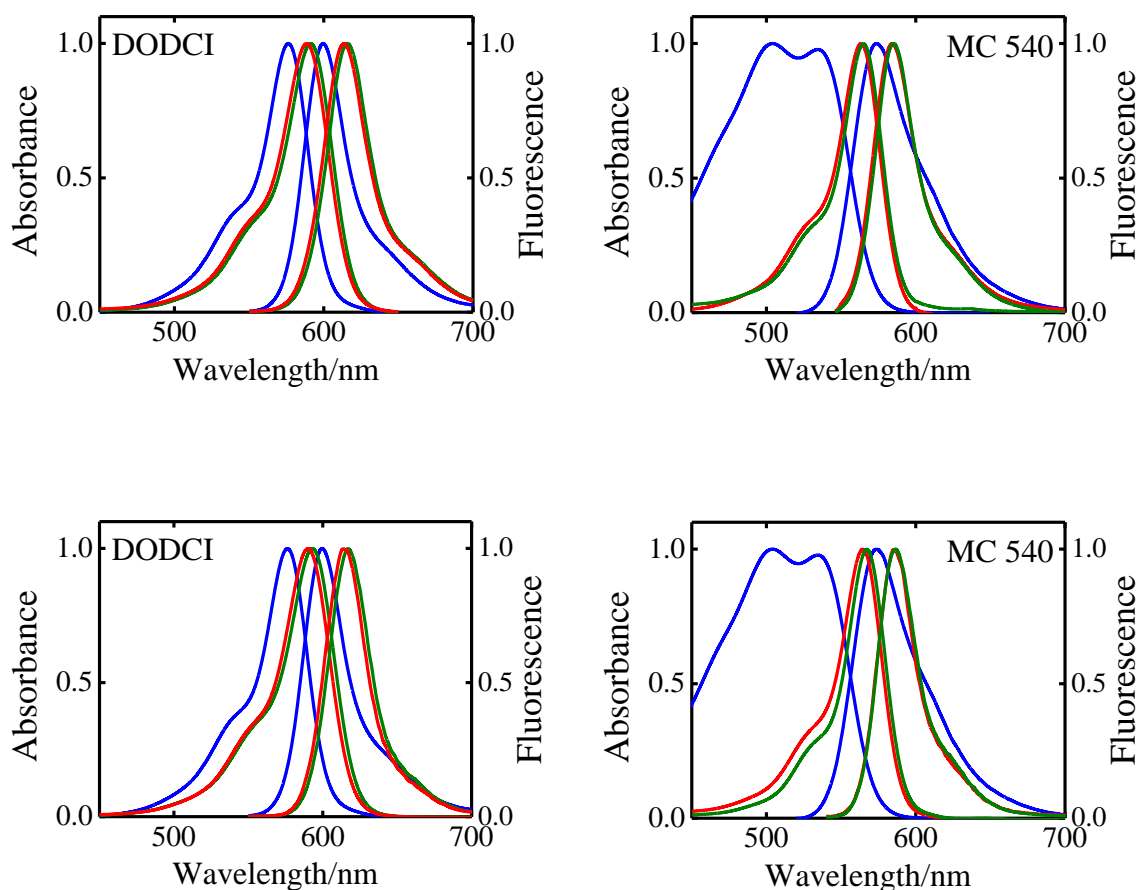


Figure 6.2 Normalized absorption and emission spectra of DODCI and MC 540 in AOT/isooctane/water reverse micelles at $W = 4$ (olive) and $W = 30$ (red) (top) and in AOT/cyclohexane/water reverse micelles at $W = 1$ (olive) and $W = 15$ (red) (bottom). The spectra of the solutes in water (blue) are also shown.

AOT/isooctane/water at $W = 4$ and 30 and in AOT/cyclohexane/water system at $W = 1$ and 15 . The spectra recorded in water are also presented in the figure for the sake of comparison. From the figure it can be noticed that, as W increases from 4 to 30 in the case of AOT/isooctane/water reverse micellar system, there is almost no change in the absorption and emission peak positions of DODCI as well as MC 540. The absorption and emission peak positions of both the solutes in water are blue-shifted by about 15 nm. A similar trend has been obtained in case of AOT/cyclohexane/water system. These results indicate that DODCI and MC 540 are not solubilized in the water pool of the AOT reverse micelles. Since there is no change in the peak positions of the two solutes upon increase in W , it can be concluded that the microenvironment experienced by the solute molecules is not altered. Essentially, both DODCI and MC 540 are located in the interfacial region of the AOT reverse micelles as they are not soluble in the bulk phases comprising isooctane and cyclohexane.

Fluorescence decays of DODCI and MC 540 in the two reverse micellar systems could be adequately fitted with a single exponential function over the entire range of W employed in this study. The lifetimes of DODCI and MC 540 in AOT/isooctane/water system decrease by 10 and 27% , respectively as W increases from 4 to 30 and the corresponding numbers in case of AOT/cyclohexane/water are 25 and 46% . Typical fluorescence decays of the two solutes in AOT/cyclohexane/water system at the two extreme values of W are displayed in Figure 6.3. The quantum yields of both the solutes in the two reverse micellar systems also follow similar trends. The uncertainties on the lifetimes are less than 5% and on quantum yields they are about 10% .

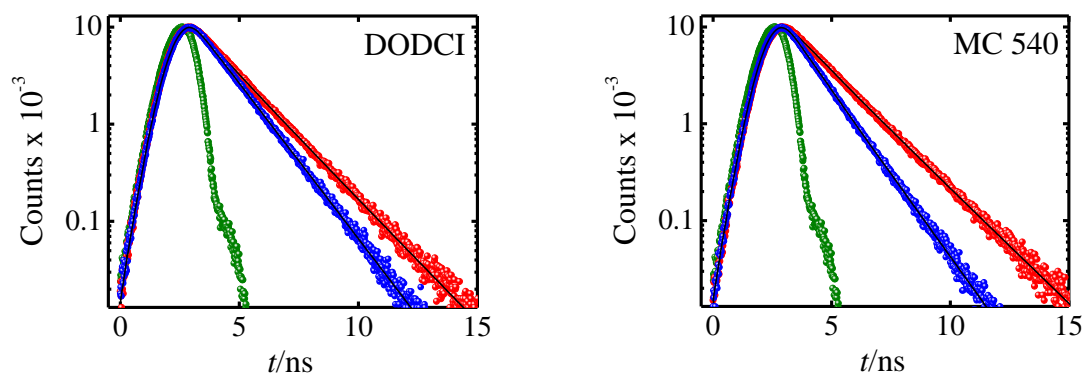


Figure 6.3 Fluorescence decays of DODCI and MC 540 in AOT/cyclohexane/water reverse micelles at $W = 1$ (red) and $W = 15$ (blue) along with the fitted curves (black lines). The instrument response function (olive) is also shown in the figure.

To comprehend the photoisomerization process of these solutes, the nonradiative rate constants (k_{nr}) were obtained from the measured fluorescence lifetimes and quantum yields and the procedure involved in obtaining the values of (k_{nr}) has been discussed in the Chapter 5. It has been observed that there is almost no variation in the radiative rate constants with an increase in W for a given probe in a particular reverse micellar system. The k_r values of DODCI and MC 540 in AOT/isooctane/water system are $0.40 \pm 0.01 \text{ ns}^{-1}$ and $0.36 \pm 0.02 \text{ ns}^{-1}$, respectively and the corresponding numbers in AOT/cyclohexane/water system are $0.36 \pm 0.02 \text{ ns}^{-1}$ and $0.46 \pm 0.01 \text{ ns}^{-1}$. Fluorescence lifetimes and nonradiative rate constants of DODCI and MC 540 in AOT/isooctane/water and AOT/cyclohexane/water reverse micellar systems are given in the Tables 6.1 and 6.2, respectively. It must be noted that in case of DODCI and MC 540, the nonradiative rate constant essentially represents the rate of photoisomerization, since the contribution due to internal conversion is negligible and triplet yields are very low.²⁰⁻²⁴ Figure 6.4 displays

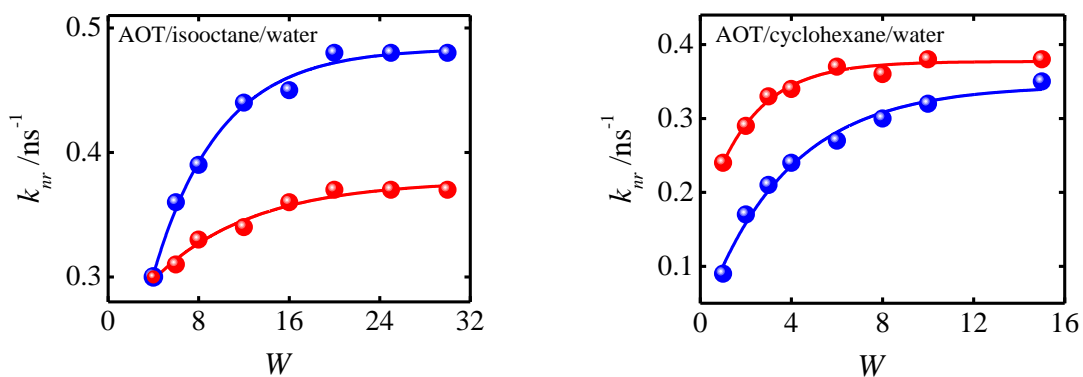


Figure 6.4 Plots of k_{nr} versus W for DODCI (red) and MC 540 (blue) in AOT/isooctane/water and AOT/cyclohexane/water reverse micelles. The curves passing through the data points are used to highlight the observed trends.

Table 6.1: Variation of Fluorescence Lifetimes and Nonradiative Rate Constants of DODCI and MC 540 in AOT/isooctane/water Reverse Micelles as a Function of W at 298 K.

W	DODCI		MC 540	
	τ_f / ns	k_{nr} / ns^{-1}	τ_f / ns	k_{nr} / ns^{-1}
4	1.42	0.30	1.51	0.30
6	1.41	0.31	1.38	0.36
8	1.37	0.33	1.33	0.39
12	1.35	0.34	1.26	0.44
16	1.31	0.36	1.23	0.45
20	1.30	0.37	1.19	0.48
25	1.29	0.37	1.19	0.48
30	1.30	0.37	1.19	0.48

Table 6.2: Variation of Fluorescence Lifetimes and Nonradiative Rate Constants of DODCI and MC 540 in AOT/cyclohexane/water Reverse Micelles as a Function of W at 298 K.

W	DODCI		MC 540	
	τ_f / ns	k_{nr} / ns^{-1}	τ_f / ns	k_{nr} / ns^{-1}
1	1.68	0.24	1.81	0.09
2	1.53	0.29	1.59	0.17
3	1.46	0.33	1.49	0.21
4	1.43	0.34	1.43	0.24
6	1.38	0.37	1.37	0.27
8	1.39	0.36	1.32	0.30
10	1.36	0.38	1.28	0.32
15	1.35	0.38	1.24	0.35

plots of k_{nr} versus W for DODCI and MC 540 in the two systems. It can be noticed from the figure that upon increasing W , the nonradiative rate constants of DODCI and MC 540 increase by a factor of 1.2 and 1.6, respectively in AOT/isooctane/water reverse micellar system and the corresponding numbers are 1.6 and 3.9 for AOT/cyclohexane/water system. However, the increase in the nonradiative rate constants is not uniform and reaches a saturation at $W = 20$ and 8 in AOT/isooctane/water and AOT/cyclohexane/water systems, respectively. Another interesting aspect that can be noticed from the figure is that k_{nr} values of MC 540 are higher compared to DODCI in AOT/isooctane/water system and the trend is reversed in AOT/cyclohexane/water system. Our results are

somewhat similar to the ones obtained by Bhattacharyya and co-workers for DODCI and MC 540 in AOT reverse micelles.^{201,202} As already mentioned in the Introduction, they have measured the nonradiative rate constants of these solutes at low and high values of W and rationalized the observed increase in k_{nr} on the basis of size of the water pool. It must be noted that the water pool radius R_w increases linearly with an increase in W for both the AOT reverse micellar systems employed in this study.¹⁶¹ In such a scenario, the nonradiative rate constants of DODCI and MC 540 should have increased linearly with an increase in W . However, a saturation of k_{nr} has been observed at higher values of W for the two solutes in both the reverse micellar systems (see Figure 6.4), which indicates that size of the water pool alone is not sufficient to explain these results. It is a well-known fact that an increase in W alters other structural parameters as well, including aggregation number N_a and hydrodynamic radius R_h of the reverse micelles. Thus, the main objective of this work is to find out whether the observed results can be described by a combination of these structural parameters of the reverse micelles.

To this effect, the structural parameters of AOT/isooctane/water and AOT/cyclohexane/water reverse micellar systems have been considered. According to the study of Maitra,¹⁶¹ the parameters N_a , R_w and R_h of AOT/isooctane/water system increase by a factor of 17.5, 5.1 and 2.5, respectively, upon increasing W from 4 to 30. In case of AOT/cyclohexane/water system they increase by a factor of 6.6, 4.5 and 2.2, respectively, with an increase in W from 1 to 15. Such an increase in the micellar structural parameters influences the critical packing parameter of the reverse micelles in a

significant manner. The critical packing parameter, which is defined as ν/a_0l_c , where ν , a_0 and l_c are, respectively, volume of the hydrophobic tail, effective head group area and effective chain length of the hydrophobic tail, has been calculated from the micellar structural parameters using the equations given below.¹⁷⁴

$$\nu = \frac{4\pi}{3N_a} [R_h^3 - R_w^3] \quad (6.1)$$

$$a_0 = \frac{4\pi R_w^2}{N_a} \quad (6.2)$$

$$l_c = [R_h - R_w] \quad (6.3)$$

The critical packing parameter for AOT/isooctane/water system decreases from 3.25 to 1.23 as W increases from 4 to 30 and for AOT/cyclohexane/water system it decreases from 3.97 to 1.46 upon enhancement in W from 1 to 15. However, the decrease in ν/a_0l_c for both the systems is not uniform and reaches saturation around $W = 20$ and 8, respectively, for AOT/isooctane/water and AOT/cyclohexane/water reverse micellar systems.¹⁶¹ It must be noted that the critical packing parameter should be greater than one for the formation of stable reverse micelles.¹⁷⁴ FT-IR studies carried out by Maitra and co-workers¹⁶² indicate that the maximum number of water molecules that can be bound to the surfactant head group in AOT/isooctane/water reverse micellar system is 12 and AOT molecules attain saturation hydration at $W = 18$. Essentially, binding of water molecules to AOT increases the effective head group area of the surfactant, which in turn leads to a

decrease in the critical packing parameter. Thus, upon complete hydration of AOT molecules there is no variation in the critical packing parameter.

In an attempt to find out how the nonradiative rate constants of DODCI and MC 540 in the two AOT reverse micellar systems vary with the critical packing parameter, k_{nr} values are plotted as a function of v/a_0l_c in Figure 6.5. It can be noticed from the figure that for DODCI and MC 540, k_{nr} decreases linearly with an increase in v/a_0l_c . In case of DODCI, the variation of nonradiative rate constant with critical packing parameter can be described by a single line in both the reverse micellar systems, whereas for MC 540 the rate constants in AOT/isooctane/water are significantly higher compared to those obtained in AOT/cyclohexane/water. The relationships between k_{nr} and v/a_0l_c for DODCI as well as MC 540 are given below with N and R being the number of data points and regression coefficient, respectively.

DODCI: AOT/isooctane/water & AOT/cyclohexane/water

$$k_{nr} = -0.047(v/a_0l_c) + 0.437 \quad (N = 16, R = -0.966)$$

MC 540: AOT/isooctane/water

$$k_{nr} = -0.087(v/a_0l_c) + 0.589 \quad (N = 8, R = -0.996)$$

MC 540: AOT/cyclohexane/water

$$k_{nr} = -0.096(v/a_0l_c) + 0.456 \quad (N = 8, R = -0.975)$$

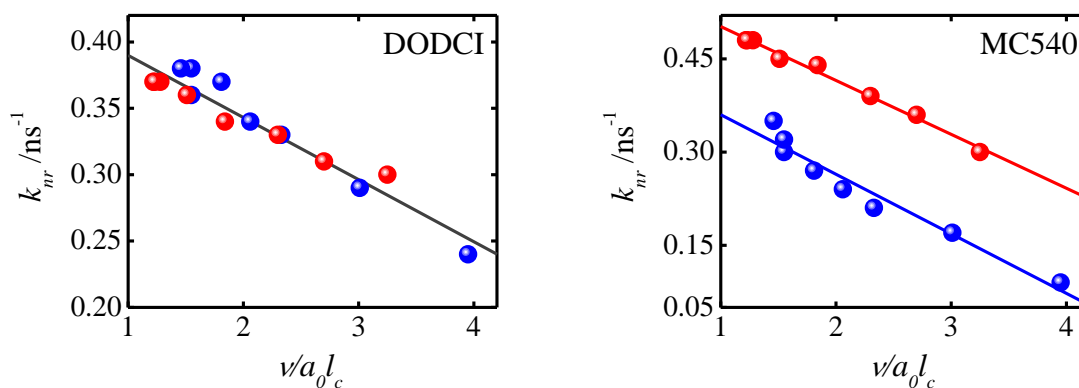


Figure 6.5 Plots of k_{nr} versus $v/a_0 l_c$ for DODCI and MC 540 in AOT/isooctane/water (red) and AOT/cyclohexane/water (blue) reverse micellar systems. The lines passing through the data points are obtained by linear least-squares fits.

To the best of our knowledge, this is the first instance where photoisomerization rate constants of solute molecules in reverse micellar systems have been quantitatively related to the critical packing parameter. As mentioned earlier, the variation of nonradiative rate constants of DODCI with $v/a_0 l_c$ in the two reverse micellar systems can be represented by a common line since its photoisomerization depends solely on the viscous friction.²⁸⁹ The interfacial region of both the AOT reverse micellar systems contains sulfonate head groups and water, and the critical packing parameter acts as a correction factor to account for the changes associated with the local viscosity. In contrast to DODCI, the nonradiative rate constants of MC 540 are significantly different in the two reverse micellar systems. It is tempting to rationalize these contrasting trends on the basis of the respective charges on DODCI and MC 540. In other words, the observed results are probably a consequence of attractive electrostatic interactions between positively charged DODCI and negatively charged headgroups of the AOT surfactant and

repulsive interactions between AOT headgroups and negatively charged MC 540. If electrostatic interactions are indeed responsible then the nonradiative rate constants of MC 540 should have been higher compared to DODCI in both the reverse micellar systems investigated. However, the trends in the nonradiative rate constants of DODCI and MC 540 are swapped in the two reverse micellar systems, which is an indication that electrostatic interactions are not responsible for the observed behavior. Thus, the results obtained can be understood in the following manner. It has been well-established that apart from viscosity, polarity of the medium also plays a significant role in the photoisomerization of MC 540.²⁹³ The interfacial region of AOT/isooctane/water system contains larger quantities of water ($W = 4-30$) compared to AOT/cyclohexane/water system ($W = 1-15$), which leads to higher interfacial polarity. Thus, this higher interfacial polarity is responsible for facilitating the isomerization of MC 540 more efficiently in the former system.

In a recent communication,²⁰⁰ somewhat similar correlation has been obtained between the average reorientation times of a cationic solute rhodamine 110 and critical packing parameter in the reverse micellar system of sodium dodecylsulfate/1-hexanol/water. However, it was observed that the reorientation times increase linearly with an increase in v/a_0l_c . It was also shown that the average reorientation times of rhodamine 110 and anionic solute fluorescein follow a similar pattern even in AOT/isooctane/water reverse micellar system. An attempt was made to find out whether the reorientation times of the solutes DODCI and MC 540 can be correlated to the respective packing parameters of the two AOT reverse micellar systems employed.

However, such an endeavor did not materialize because fluorescence lifetimes of both DODCI and MC 540 were found to be considerably shorter than their reorientation times. Nevertheless, the outcome of these studies essentially indicates that the rates of friction-dependent processes such as rotational diffusion and photoisomerization of solute molecules located at the micelle-water interface of reverse micelles are in effect governed by the critical packing parameter.

6.4. Conclusions

An attempt has been made to identify the parameter that describes interfacial friction in the reverse micellar systems of AOT/isooctane/water and AOT/cyclohexane/water. For this purpose photoisomerization of ionic solutes DODCI and MC 540 has been investigated by measuring their fluorescence lifetimes and quantum yields in these reverse micellar systems as a function of mole ratio of water to the surfactant. It has been noticed that the nonradiative rate constants increase upon increasing W . However, the increase in k_{nr} is not uniform and reaches a saturation at higher values of W . To rationalize this observed behavior, critical packing parameter of the reverse micellar systems has been considered, which depends on the micellar properties such as aggregation number, water pool radius and hydrodynamic radius of the reverse micelle. It has been observed that the nonradiative rate constants of both the solutes decrease linearly with an increase in the critical packing parameter in the two reverse micellar systems employed. This result affirms that critical packing parameter can be employed to depict interfacial friction in reverse micelles.

References

1. Dutt, G. B. *ChemPhysChem*. **2005**, *6*, 413 and references therein.
2. Horng, M. L.; Gardecki, J. A.; Papazyan, A.; Maroncelli. M. *J. Phys. Chem.* **1995**, *99*, 17311.
3. Weaver, M. J.; McManis, G. E. *Acc. Chem. Res.* **1990** *23*, 294.
4. Strandjord, A. J. G.; Barbara, P. F. *J. Phys. Chem.* **1985**, *89*, 2355.
5. Kurnikova, M. G.; Balbai, N.; Waldeck, D. H.; Coalson, R. D. *J. Am. Chem. Soc.* **1998**, *120*, 6121.
6. Walkdeck, D. H. *Chem. Rev.* **1991**, *91*, 415 and references therein.
7. Gelbart, W. M.; Ben-Shaul, A. *J. Phys. Chem.* **1996**, *100*, 13169.
8. Witten, T. A. *Phys. Today* **1990**, *43*, 21.
9. Weingärtner, H. *Angew. Chem., Int. Ed.* **2008**, *47*, 654.
10. Freemantle, M. *Chem. Eng. News* **2000**, *78*, 37.
11. Adams, D.; Dyson, P.; Tavener, S. *Chemistry in Alternative Reaction Media*, John Wiley & Sons: New York, 2004.
12. Fleming, G. R.; Joo, T. *Adv. Chem Phys.* **1997**, *101*, 141.
13. Fleming, G. R.; Wolynes, P. G. *Phys. Today* **1990**, *36*.
14. Waldeck, D. H. *Conformational Analysis of Molecules in Excited States*, Waluk, J., Ed.; Wiley-VCH: New York, 2000, pp. 113-176. and references therein.
15. Welton, T. *Chem. Rev.* **1999**, *99*, 2071.
16. Hallett, J. P.; Welton, T. *Chem. Rev.* **2011**, *111*, 3508.
17. Dupont, J. *Acc. Chem. Res.* **2011**, *44*, 1223.

18. Plechkova, N. V.; Seddon, K. R. *Chem. Soc. Rev.* **2008**, *37*, 123.
19. Luisi, P. L.; Giomini, M.; Pileni, M. P.; Robinson, B. H. *Biochim. Biophys. Acta* **1988**, *947*, 209.
20. Jones, M. N.; Chapman, D. *Micelles, Monolayers, and Biomembranes*; John Wiley and Sons: New York, 1995.
21. Armand, M.; Endres, F.; MacFarlane, D. R.; Ohno, H.; Scrosati, B. *Nat. Mater.* **2009**, *8*, 621.
22. Gabriel, S.; Weiner, J. *Bull. Acad. Imper. Berichte der deutschen chemischen Gesellschaft* **1888**, *21* 2669.
23. Walden, P. *Bull. Acad. Imper. Sci. (St. Petersburg)* **1914**, 1800.
24. Yoke, J. T.; Weiss, J.F.; Tollin, G. *Inorganic Chemistry* **1963**, *2*, 1210.
25. Nardi, J. C.; C. L. H. a. L. A. K. *US Patent*, **1978**, *4* 122 245.
26. Wilkers, J. S.; M. J. Z. *Chem. Soc. Chem. Commun* **1992**, 965.
27. Carlin, R. T.; Fuller, J.; Kuhn, W. K.; Lysaght, M. J.; Trulove, P. C. *Journal of applied Electrochemistry* **1996**, *26*, 147.
28. Zahn, S.; Uhlig, F.; Thar, J.; Spickermann, C.; Kirchner, C. *Angew. Chem. Int. Ed.* **2008**, *47*, 3639.
29. Gonfa, G.; Bustam, M. A.; Man, Z.; Mutalib, M. I. A. *Asian Transactions on Engineering* **2011**, *1*, 24.
30. Keskin, S.; Kayrak-Talay, D.; Akman, U.; Hortacsu, O. *J. Supercrit. Fluids.* **2007**, *43*, 150.
31. Fonseca, G.S.; Umpierre, A. P.; Fichtner, P. F. P.; Teixeira, S. R.; Dupont, J.

- Chem. Eur. J.* **2003**, *9*, 3263.
32. Cooper, E. I.; OJSullivan, E. J. M. *Proc. Electrochem. Soc.* **1992**, *16*, 386
(8th Int. Symp. Molten Salts, 1992).
33. Forsyth, S. A.; Pringle, J. M.; MacFarlane, D. R. *Aust. J.Chem.* **2004**, *57*, 113.
34. BonhRte, P.; Dias, A. P.; Papageorgiou, N.; Kalyanasundaram, K.; GrStzel, M.
Inorg. Chem. **1996**, *35*, 1168.
35. Holbrey, J. D.; Seddon, K.R. C. *Clean Products and Processes* **1999**, *1*, 223.
36. Chiappe, C.; Pieraccini, D. *J. Phys Org. Chem.* **2005**, *18*, 275.
37. Lopes, J. N. C.; Padua, A. A. H. *J. Phys. Chem. B* **2006**, *110*, 3330.
38. Lopes, J. N. C.; Padua, A. A. H. *J. Phys. Chem. B* **2006**, *110*, 19586.
39. Wang, Y.; Voth, G. A. *J. Am. Chem. Soc.* **2005**, *127*, 12192.
40. Bhargava, B. L.; Balasubramanian, S. *J. Chem. Phys.* **2007**, *127*, 114510.
41. Fumino, K.; Wulf, A.; Ludwig, R. *Phys. Chem. Chem. Phys.* **2009**, *11*, 8790.
42. Zahn, S.; Bruns, G.; Thar, J.; Kirchner, B. *Phys. Chem. Chem. Phys.*
2008, *10*, 6921.
43. Tokuda, H.; Tsuzuki, S.; Susan, Md. A. B. H.; Hayamizu, K.; Watanabe, M.
J. Phys. Chem. B **2006**, *110*, 19593.
44. Hunt, P. A. *J. Phys. Chem. B* **2007**, *111*, 4844.
45. Hardacre, C.; Holbrey, J. D.; McMath, S. E. J.; Bowron, D. T.; Soper, A. K.
J. Chem Phys. **2003**, *118*, 273.
46. Deetlefs, M.; Hardacre, C.; Nieuwenhuyzen, M.; Padua, A. A. H.; Sheppard, O.;
Soper, A. K. *J. Phys. Chem. B* **2006**, *110*, 12055.

47. Bradley, A. E.; Hardacre, C.; Holbrey, J. D.; Johnston, S.; McMath, S. E. J.; Nieuwenhuyzen, M. *Chem. Mater.* **2002**, *14*, 629.
48. Triolo, A.; Russina, O.; Fazio, B.; Triolo, R.; Cola, E. D. *Chem. Phys. Lett.* **2008**, *457*, 362.
49. Binetti, E.; Panniello, A.; Triggiani, L.; Tommasi, R.; Agostiano, A.; Curii, M. L.; Striccoli, M. *J. Phys. Chem. B.* **2012**, *116*, 3512.
50. Guo, J.; Baker, G. A.; Hillesheim, P. C.; Dai, S.; Shaw, R. W.; Mahurin, S. M. *Phys. Chem. Chem. Phys.* **2011**, *13*, 12395.
51. Lee, C. W. *Tetrahedron Lett.* **1999**, *40*, 2461.
52. West, A. *Chem. World* **2005**, 33.
53. Zhang, Q.; DeOliveiraVigier, K.; Royer, S.; Jorome, F. *Chem.Soc.Rev.* **2012**, *41*, 7108.
54. Ohno, H. *Electrochemical Aspects of Ionic Liquids* John Wiley & Sons. Hoboken, NJ, 2005.
55. Endres, F.; Zein, S.; Abedin, E. *Phys.Chem. Chem. Phys.* **2006**, *8*, 2101.
56. Silvester, D. S.; Compton, R. G. *International Journal of Research in Physical Chemistry and Chemical Physics* **2006**, *220*, 1247.
57. Chum, H. L.; V. R. Koch, V. R.; L. L. Miller, L. L.; R. A. Osteryoung, R. A. *J. Am. Chem. Soc.* **1975**, *97*, 3264.
58. J. S. Wilkes, J. S.; J. A. Levisky, J. A.; R. A. Wilson, R. A.; C. L. Hussey, C. L. *Inorg. Chem.* **1982**, *21*, 1263.
59. Nobuoka, K.; Kitaoka, S.; Iio, M.; Harran, J.; Ishikawa, Y. *Phys. Chem. Chem.*

- Phy.* **2007**, *9*, 5891.
60. Zhao, Y.; Noot, T. J. V. *Electrochimica Acta* **1997**, *42*, 3.
61. Mudring, A. V. *American Chemical society*, Washington D.C. **2009**, 177.
62. Liu, R.; Liu J. F.; Yin, Y. G.; Hu, X. L.; Jiang, G. B. *Analytical and Bioanalytical chemistry* **2009**, *393*, 871.
63. Yao, C.; Anderson, J. L. *J. Chromatography A*, **2009**, *1216*, 1658.
64. Berthod, A.; Angel, M. J. R.; Broch, S. C. *J. Chromatography A* **2008**, *1184*, 6.
65. Kamio, A.; Nagaosa, Y. *Anal, Sci.* **2008**, *24*, 1363.
66. Crank, J. A.; Armstrong, D. W.; *J. American Chemical Society Mass Spectrom* **2009**, *120*, 1790.
67. Soukup-hein, R. J.; Remsburg, J. W.; Dasguptha, P. K.; Armstrong, D. W. *Anal, chem.*, **2007**, *79*, 7346.
68. Mamantov, G.; Mamantov, C. Eds. *Advances in Molten Salt Chemistry* Elsevier: New York, 1983 Vol. 5 and 6.
69. Wilkes, J. S. *Green Chem.* **2002**, *4*, 73.
70. Earle, M. J.; Seddon, K. R. *Pure Appl. Chem.* **2000**, *72*, 1391.
71. Brennecke, J. F.; Maginn, E. J. *AIChE. J.* **2001**, *47*, 2384.
72. Olivier-Bourbigou, H.; Magna, L. *J. Mol. Cata A-Chem.* **2002**, *182*, 419.
73. Davis, J. H.; Fox, P. A. *Chem. Commun.* **2003**, 1209.
74. Welton, T. *Coord. Chem. Rev.* **2004**, *248*, 2459.
75. Forsyth, S. A.; Pringle, J. M.; MacFarlane, D. R. *Aust. J. Chem.* **2004**, *57*, 113.
76. Zhang, Z. C. *Adv. Catal.* **2006**, *49*, 153.

77. Dupont, J.; Suarez, P. A. Z. *Phys. Chem. Chem. Phys.* **2006**, *8*, 2441.
78. Chauvin, Y. *Act. Chim.* **1996**, *44*.
79. Seddon, K. R. *J. Chem. Technol. Biotechnol.* **1997**, *68*, 351.
80. Wasserscheid, W.; Keim, W. *Angew. Chem., Int. Ed.* **2000**, *39*, 3773.
81. Sheldon, R. *Chem. Commun.* **2001**, 2399.
82. Gordon, C. M. *Appl. Catal. A-Gen.* **2001**, *222*, 101.
83. Dyson, P. J. *Transition Met. Chem.* **2002**, *27*, 352.
84. Dupont, J.; de Souza, R. F.; Suarez, P. A. Z. *Chem. Rev.* **2002**, *102*, 3667.
85. Baudequin, C.; Baudoux, J.; Levillain, J.; Cahard, D.; Gaumont, A. C.;
Plaquevent, J. C. *Tetrahedron-Asymm.* **2003**, *14*, 3081.
86. Park, S.; Kazlauskas, R. *Curr. Opin. Biotech.* **2003**, *14*, 432.
87. Song, C. E. *Chem. Commun.* **2004**, 1033.
88. Poole, C. F. *J. Chromat. A* **2004**, *1037*, 49.
89. Wasserscheid, P.; Welton, T. Eds. *Ionic Liquids in Synthesis*, VCH-Wiley:
Weinheim, 2002.
90. Rogers, R. D.; Seddon, K. R. Eds. *Ionic Liquids as Green Solvents: Progress and
Prospects*, American Chemical Society: Washington DC, 2003.
91. Rogers, R. D.; Seddon, K. R. Eds. *Ionic Liquids: Industrial Applications to Green
Chemistry*, American Chemical Society: Washington DC, 2003.
92. Abraham, M. A.; Moens, L., Eds. *Clean Solvents: Alternative Media for Chemical
Reactions and Processing*, American Chemical Society: Washington DC, 2002.
93. Reichardt, C. *Solvents and Solvent Effects in Organic Chemistry*, 2nd ed.,

- VCH, Weinheim, **1990**.
94. Reichardt, C. *Solvents and Solvent Effects in Organic Chemistry*, 2nd ed.,
VCH, Weinheim, Germany, **2003**.
95. Muller, P. *Pure Appl. Chem.* **1994**, *66*, 1077.
96. Abraham, M. H. *Chem. Soc. Rev.* **1993**, *22*, 73.
97. Anderson, J. L.; Ding, J.; Welton, T.; Armstrong, D. W. *J. Am. Chem. Soc.*
2002, *124*, 14247.
98. Zhao, Q.; Eichhorn, J.; Pitner, W. R.; Anderson, J. L. *Anal. Bioanal. Chem.*
2009, *395*, 225.
99. Hunt, P. A.; Kirchner, B.; Welton, T. *Chem. Eur. J.* **2006**, *12*, 6762.
100. Ab Rani, M. A.; Brant, A.; Crowhurst, L.; Dolan, A.; Lui, M.; Hassan, N. H.;
Hallett, J. P.; Hunt, P. A.; Niedermeyer, H.; Perez- Arlandis, J. M.; Schrems,
M.; Welton, T.; Wilding, R. *Phys. Chem. Chem. Phys.* **2011**, *13*, 16831.
101. Karve, L.; Dutt, G. B. *J. Phys. Chem. B* **2012**, *116*, 1824.
102. Karve, L.; Dutt, G. B. *J. Phys. Chem. B* **2012**, *116*, 9107.
103. Seddon, K. R.; Stark, A.; Torres, M. J. *Pure. Appl. Chem.* **2000**, *72*, 2275.
104. Perry, R. L.; Jones, K. M.; Scott, W. D.; Liao, Q.; Hussey, C. L.
J. Chem. Eng. Data **2000**, *72*, 2275.
105. Paul, A.; Samanta, A. *J. Phys. Chem. B* **2008**, *112*, 947.
106. Chakrabarty, D.; Chakraborty, A.; Seth, D.; Hazra, P.; Sarkar, N. *Chem. Phys.*
Lett. **2004**, *397*, 469.
107. Chakrabarty, D.; Chakraborty, A.; Seth, D.; Sarkar, N. *J. Phys. Chem. A*

- 2005**, *109*, 1764.
108. Pramanik, R.; Rao, V. G.; Sarkar, S.; Ghatak, C.; Setua, P.; Sarkar, N. *J. Phys. Chem. B* **2009**, *113*, 8626.
109. Huddleston, J. G.; Visser, A. E.; Reichert, W. M.; Willauer, H. D.; Broker, G. A.; Rogers, R. D. *Green Chem.* **2001**, *3*, 156.
110. Carper, W.R.; Pflung, J. L.; Elias, A. M. E.; Wilkes, J. S. *J. Phys. Chem.* **1992**, *96*, 3828.
111. Avent, A. G.; Chaloner, P. A.; Day, M. P.; Seddon, K. R.; Welton, T. *J. Chem. Soc. Dalton Trans.* **1994**, 6405.
112. Huang, J. F.; Chen, P. Y.; Sun, I. W.; Wang, S. P. *Inorg. Chim. Acta* **2001**, *320*, 7.
113. Suarez, P. A. Z.; Einloft, S.; Dullius, J. E. L.; Souza, R. F.; Dupont, J. *J. Chim. Phys.* **1998**, *95*, 1626.
114. Lin, S. T.; Ding, M. F.; Chang, C. W.; Lue, S. S. *Tetrahedron* **2004**, *60*, 9441.
115. Fumino, K.; Wulf, A.; Ludwig, R. *Angew. Chem., Int. Ed.* **2008**, *47*, 8731.
116. Fumino, K.; Wulf, A.; Ludwig, R. *Angew. Chem., Int. Ed.* **2009**, *48*, 3184.
117. Wulf, A.; Fumino, K.; Ludwig, R. *Angew. Chem., Int. Ed.* **2010**, *49*, 449.
118. Thar, J.; Brehm, M.; Seitsonen, A. P.; Kirchner, B. *J. Phys. Chem. B* **2009**, *113*, 15129.
119. Pópolo, M. G. D.; Voth, G. A. *J. Phys. Chem. B* **2004**, *108*, 1744.
120. Hu, Z.; Margulis, C. J. *Proc. Natl. Acad. Sci. USA* **2006**, *103*, 831.
121. Wang, Y.; Jiang, W.; Yan, T.; Voth, G. A. *Acc. Chem. Res.* **2007**, *40*, 1193.

122. Iwata, K.; Okajima, H.; Saha, S.; Hamaguchi, H. *Acc. Chem. Res.* **2007**, *40*, 1174.
123. Hardacre, C.; Holbrey, J. D.; Mullan, C. L.; Youngs, T. G. A.; Bowron, D. T. *J. Chem. Phys.* **2010**, *133*, 074510.
124. Russina, O.; Triolo, A.; Gontrani, L.; Caminiti, R. *J. Phys. Chem. Lett.* **2012**, *3*, 27.
125. Li, S.; Bañuelos, J. L.; Guo, J.; Anovitz, L.; Rother, G.; Shaw, R. W.; Hillesheim, P.C.; Dai, S.; Baker, G. A.; Cummings, P. T. *J. Phys. Chem. Lett.* **2012**, *3*, 125.
126. Kashyap, H. K.; Hettige, J. J.; Annapureddy, H. V. R.; Margulis, C. J. *Chem. Commun.* **2012**, *48*, 5103.
127. Castner, E. W. Jr.; Margulis, C. J.; Maroncelli, M.; Wishart, J. F. *Annu. Rev. Phys. Chem.* **2011**, *62*, 85.
128. Wang, Y.; Voth, G. *J. Phys. Chem. B* **2006**, *110*, 18601.
129. Dupont, J. *J. Braz. Chem. Soc.* **2004**, *15*, 341.
130. Triolo, A.; Russina, O.; Bleif, H.J.; Di Cola, E. *J. Phys. Chem. B* **2007**, *111*, 4641.
131. Schröder, U.; Wadhawan, J. D.; Compton, R. G.; Marken, F.; Suarez, P. A. Z.; Consorti, C. S.; de Souza, R. F.; Dupont, J. *New J. Chem.* **2000**, *24*, 1009.
132. Tokuda, H.; Hayamizu, K.; Ishii, K.; Susan, M. A. B. H.; Watanabe, M. *J. Phys. Chem. B* **2004**, *108*, 16593.
133. Gordon, C. M.; McLean, A. J. *Chem. Commun.* **2000**, 1395.
134. Ozawa, R.; Hamaguchi, H. *Chem. Lett.* **2001**, 736.
135. Skrzypczak, A.; Neta, P. *J. Phys. Chem. A* **2003**, *107*, 7800.

136. Mandal, P. K.; Sarkar, M.; Samanta, A. *J. Phys. Chem. A* **2004**, *108*, 9048.
137. Iwata, K.; Kakita, M.; Hamaguchi, H. *J. Phys. Chem. B* **2007**, *111*, 4914.
138. Russina, O.; Triolo, A. *Faraday Discuss.* **2012**, *154*, 97 and references therein.
139. Hartley, G.S. *Aqueous Solutions of Paraffinic-Chain Salts. A Study of Micelle Formation*, Herman, Paris, 1936.
140. Mittal K., Ed., *Micellization, Solubilization and Microemulsions*, Plenum Press, New York, vol. 1, p. 23.
141. Myers, D. *Surfactant Science and Technology*, VCH Publ. Inc., Weinheim, Germany, 1988.
142. Moroi, Y. *Micelles: Theoretical and Applied Aspects*, Plenum Press, New York, 1992.
143. Mukerjee, P. *Adv. Colloid Interface Sci.* **1967**, *1*, 241.
144. Israelachvili, J. N.; Mitchell, D. J., Ninham, B.W. *J. Chem. Soc., Faraday Trans.* **1976**, *72*, 1525.
145. Mitchell, D. J.; Ninham, B. W. *J. Chem. Soc. Faraday Trans. 2* **1981**, *77*, 601.
146. Israelachvili, J. N.; *Intermolecular and Surface Forces*, 2nd ed., Academic Press London, 1992.
147. Moulik, S. P. *Curr. Sci.*, **1996**, *71* 368.
148. Moulik, S. P.; Paul, B. K. *Adv. Colloid Interface Sci.* **1998**, *78*, 99.
149. Uskokovic', V.; Drogenik, M. *Adv. Colloid Interface Sci.* **2007**, *133*, 23.
150. Silber, J. J.; Biasutti, M. A.; Abuin, E.; Lissi, E. *Adv. Colloid Interface Sci.* **1999**, *82*, 189.

151. De, T. K.; Maitra, A. *Adv. Colloid Interface Sci.* **1995**, *59*, 95.
152. Moulik, S. P.; Paul, B. K. *Adv. Colloid Interface Sci.* **1998**, *78*, 99.
153. Fogler, H. S.; Chang, C.L. *Langmuir* **1997**, *13*, 3295.
154. Zulauf, M.; Eicke, H. F. *J. Phys. Chem.* **1979**, *83*, 480.
155. Keh, E.; Valeur, B. *J. Colloid Interface Sci.* **1981**, *79*, 465.
156. Robinson, B. H.; Steytler, D. C.; Tack, R. D. *J. Chem. Soc., Faraday I*
1984, *80*, 3307.
157. Day, R. A.; Robinson, B. H.; Clark, J. H. R.; Doherty, J. V. *J. Chem. Soc.,
Faraday I* **1979**, *75*, 132.
158. Cazabet, A. M.; Langevin, D. *J. Chem. Phys.* **1981**, *74*, 3148.
159. Robinson, B. H.; Toprakcioglu, C.; Dore, J. C.; Chieux, P. *J. Chem. Soc.,
Faraday I* **1984**, *80*, 13.
160. Toprakcioglu, C.; Dore, J. C.; Robinson, B. H.; Howe, A.; Chieux, P. *J. Chem.
Soc., Faraday I* **1984**, *80*, 413.
161. Maitra, A. *J. Phys. Chem.* **1984**, *88*, 5122 and references therein.
162. Jain, T. K.; Varshney, M.; Maitra, A. *J. Phys. Chem.* **1989**, *93*, 7409.
163. Nave, S.; Eastoe, J.; Heenan, R. K.; Steytler, D.; Grillo, I. *Langmuir*
2000, *16*, 8741.
164. Goto, A.; Yoshioka, H.; Kishimoto, H.; Fujita, T. *Langmuir* **1992**, *8*, 441.
165. Goto, A.; Harada, S.; Fujita, T.; Miwa, Y.; Yoshioka, H.; Kishimoto, H.
Langmuir **1993**, *9*, 86.
166. Goto, A.; Yoshioka, H.; Manabe, M.; Goto, R. *Langmuir* **1995**, *11*, 4873.

167. Zhou, N.; Li, Q.; Wu, J.; Chen, J.; Weng, S.; Xu, G. *Langmuir* **2001**, *17*, 4505.
168. Sando, G. M.; Dahl, K.; Owrutsky, J. C. *J. Phys. Chem. A* **2004**, *108*, 11209.
169. Sando, G. M.; Dahl, K.; Owrutsky, J. C. *J. Phys. Chem. B* **2005**, *109*, 4084.
170. Sando, G. M.; Dahl, K.; Owrutsky, J. C. *Chem. Phys. Lett.* **2006**, *418*, 402.
171. Cringus, D.; Bakulin, A.; Lindner, J.; Vohringer, P.; Pshenichnikov, M. S.;
Wiersma, D. A. *J. Phys. Chem. B* **2007**, *111*, 14193.
172. Cringus, D.; Lindner, J.; Milder, M. T. W.; Pshenichnikov, M. S.; Vohringer, P.;
Wiersma, D. A. *Chem. Phys. Lett.* **2005**, *408*, 162.
173. Penwell, S. B.; Wright, J. C. *J. Phys. Chem. B* **2011**, *115*, 5564.
174. Mitchell, D. J.; Nimham, B. W. *J. Chem. Soc. Faraday Trans. 2* **1981**, *77*, 601.
175. Corbeil, E. M.; Levinger, N. E. *Langmuir* **2003**, *19*, 7264.
176. Rodenas, E.; Perez-Benito, E. *J. Phys. Chem.* **1991**, *95*, 4552.
177. Atik, S. S.; Thomas, J. K. *J. Am. Chem. Soc.* **1981**, *103*, 4367.
178. Giustini, M.; Palazzo, G.; Colafemmina, G.; Monica, M. D.; Giomini, M.;
Ceglie, A. *J. Phys. Chem.* **1996**, *100*, 3190.
179. Das, P. K.; Chaudhuri, A.; Saha, S.; Samanta, A. *Langmuir* **1999**, *15*, 4765.
180. Levinger, N. E. *Curr. Opin. Colloid Interface Sci.* **2000**, *5*, 118.
181. Nandi, N.; Bhattacharyya, K.; Bagchi, B. *Chem. Rev.* **2000**, *100*, 2013.
182. Willard, D. M.; Riter, R. E.; Levinger, N. E. *J. Am. Chem. Soc.*
1998, *120*, 4151.
183. Riter, R. E.; Undiks, E. P.; Levinger, N. E. *J. Am. Chem. Soc.*
1998, *120*, 6062.

184. Moilanen, D. E.; Levinger, N. E.; Spry, D. B.; Fayer, M. D. *J. Am. Chem. Soc.* **2007**, *129*, 14311.
185. Wittouck, N.; Negri, R. M.; Ameloot, M.; De Schryver, F. C. *J. Am. Chem. Soc.* **1994**, *116*, 10601.
186. Dutt, G. B. *J. Phys. Chem. B* **2004**, *108*, 805.
187. Dutt, G. B. *J. Phys. Chem. B* **2004**, *108*, 7944.
188. Riter, R. E.; Willard, D. M.; Levinger, N. E. *J. Phys. Chem. B* **1998**, *102*, 2705.
189. Shirota, H.; Horie, K. *J. Phys. Chem. B* **1999**, *103*, 1437.
190. Spry, D. B.; Goun, A.; Glusac, K.; Moilanen, D. E.; Fayer, M. D. *J. Am. Chem. Soc.* **2007**, *129*, 8122.
191. Bhattacharyya, K. *Acc. Chem. Res.* **2003**, *36*, 95.
192. Pal, S. K.; Zewail, A. H. *Chem. Rev.* **2004**, *104*, 2099.
193. Biasutti, M. A.; Correa, N. M.; Silber, J. J. *Curr. Top. Colloid Interface Sci.* **1999**, *3*, 35.
194. Yehta, A.; Aikawa, M.; Turro, N. *J. Chem. Phys. Lett.* **1979**, *63*, 543.
195. Grand, D.; Dokutchaev, A. *J. Phys. Chem. B* **1997**, *101*, 3181.
196. Mitra, R. K.; Sinha, S. S.; Pal, S. K. *Langmuir* **2008**, *24*, 49.
197. Dutt, G. B. *J. Phys. Chem. B* **2008**, *112*, 7220.
198. Dutt, G. B. *J. Chem. Phys.* **2008**, *129*, 014501.
199. Mali, K. S.; Dutt, G. B. *J. Chem. Phys.* **2009**, *131*, 174708.
200. Dutt, G. B. *ChemPhysChem.* **2010**, *11*, 1646.
201. Datta, A.; D. Mandal, D.; S. K. Pal, S. K.; Battacharyya, K. *Chem. Phys. Lett.*

- 1997**, 278, 77.
202. Mandal, D.; S. K. Pal, S. K.; D. Sukul, D.; Battacharyya, K. *J. Phys. Chem. A*
1999, 103, 8156.
203. Fleming, G. R. *Chemical Applications of Ultrafast Spectroscopy*, Oxford
University Press: New York, 1986.
204. Birks, J. B. *Photophysics of Aromatic Molecules*, Wiley Interscience:
New York, 1970.
205. Rohatgi-Mukherjee, K. K. *Fundamentals of Photochemistry*, Wiley Eastern Ltd.:
India, 1986.
206. Lackowicz, J. R. *Principles of fluorescence spectroscopy*, 3rd ed.; Springer:
New York, 2006.
207. Michael Hollas, J. *Modern Spectroscopy*, J., 1996, 3rd Ed., John Wiley and Sons.
208. Smith, B. C. *Quantitative Spectroscopy: Theory and Practice*, 2002,
Academic Press.
209. Bernath, P. F. *Spectra of atoms and molecules*, 1995, Oxford University Press.
210. O'Connor, D. V.; Phillips, D. *Time-Correlated Single-Photon Counting*,
Academic Press: London, 1984.
211. Fleming, G. R. *Adv. Chem. Phys.* **1982**, 49, 1.
212. Shapiro, S. L. *Ultrashort light pulses*, Springer: Berlin, 1984.
213. Murao, T.; Yamazaki, I.; Yoshihara, K. *Appl. Opt.* **1982**, 21, 2297.
214. Yamazaki, I.; Murao, T.; Yoshihara, K. *Chem. Phys. Lett.* **1982**, 87, 384.
215. Wijnaedts van Resandt, R. W.; Vogel, R. H.; Provencher, S. W. *Rev. Sci.*

- Instrum.* **1982**, *53*, 1392.
216. Yamazaki, I.; Tamai, N.; Kume, H.; Tsuchiya, H.; Oba, K. *Rev. Sci. Instrum.* **1985**, *56*, 1187.
217. Ito, M.; Kume, H.; Oba, K. *IEEE Trans. Nucl. Sci.* **1984**, *NS-31*, 408.
218. Cross, A. J.; Fleming, G. R. *Biophys. J.* **1984**, *46*, 45.
219. Knutson, J. R.; Beechem, J. M.; Brand, L. *Chem. Phys. Lett.* **1983**, *102*, 501.
220. O'Connor, D. V.; Ware, W. R.; Andre, J. C. *J. Phys. Chem.* **1979**, *83*, 1333.
221. Good, H. P.; Kallir, A. J.; Wild, U. P. *J. Phys. Chem.* **1985**, *88*, 5435.
222. Grinvald, A.; Steinberg, I. Z. *Anal. Biochem.* **1974**, *59*, 583.
223. Bevington, P. R. *Data Reduction and Error Analysis for the Physical Sciences*, McGraw-Hill: New York, 1969.
224. Barnes, H. A.; Hutton, J. F.; Walters, K. *An Introduction to Rheology* Elsevier, Amsterdam, 1989.
225. Samanta, A. *J. Phys. Chem. B* **2006**, *110*, 13704.
226. Jin, H.; Xiang Li, X.; Maroncelli, M. *J. Phys. Chem. B* **2007**, *111*, 13473.
227. Mali, K. S.; Dutt, G. B.; Mukherjee, T. *J. Chem. Phys.* **2005**, *123*, 174504
228. Mali, K. S.; Dutt, G. B.; Mukherjee, T. *J. Chem. Phys.* **2008**, *128*, 054504
229. Dutt, G. B. *J. Phys. Chem. B* **2010**, *114*, 8971.
230. Karve, L.; Dutt, G. B. *J. Phys. Chem. B* **2011**, *115*, 725.
231. Ingram, J. A.; Moog, R. S.; Ito, N.; Biswas, R.; Maroncelli, M. *J. Phys. Chem. B* **2003**, *107*, 5926.
232. Ito, N.; Arzhantsev, S.; Heitz, M.; Maroncelli, M. *J. Phys. Chem. B*

- 2004**, *108*, 5771.
233. Jin, H.; Baker, G. A.; Arzhantsev, S.; Dong, J.; Maroncelli, M. *J. Phys. Chem. B* **2007**, *111*, 7291.
234. Funston, A. M.; Fadeeva, T. A.; Wishart, J. F.; Castner, E. W.; *J. Phys. Chem. B* **2007**, *111*, 4963.
235. Fruchey, K.; Fayer, M. D. *J. Phys. Chem. B* **2010**, *114*, 2840.
236. Paul, A.; Samanta, A.; *J. Phys. Chem. B* **2007**, *111*, 4724.
237. Khara, D. C.; Samanta, A. *Phys. Chem. Chem. Phys.* **2010**, *12*, 7671.
238. Khara, D. C.; Samanta, A. *J. Phys. Chem. B* **2012**, *116*, 13430.
239. Das, S. K.; Sarkar, M. *J. Phys. Chem. B* **2012**, *116*, 194.
240. Das, S. K.; sahu, P. K.; Sarkar, M. *ChemPhysChem.* **2012**, *113*, 2761.
241. Das, S. K.; Sarkar, M. *Chem. Phys. Lett.* **2011**, *515*, 23.
242. Das, S. K.; Sahu, P. K.; Sarkar, M. *J. Phys. Chem. B* **2013**, *117*, 636.
243. Perrin, F. *J. Phys. Radium* **1934**, *5*, 497.
244. Hu, C. M.; Zwanzig, R. *J. Chem. Phys.* **1974**, *60*, 4354.
245. Edward, J. T. *J. Chem. Educ.* **1970**, *47*, 261.
246. Small, E. W.; Isenberg, I. *Biopolymers* **1977**, *16*, 1907.
247. Sension, R. J.; Hochstrasser, R. M. *J. Chem. Phys.* **1993**, *98*, 2490.
248. Hartman, R. S.; Alavi, D. S.; Waldeck, D. H. *J. Phys. Chem.* **1991**, *95*, 7872.
249. Gierer, A.; Wirtz, K. *Z. Naturforsch. A*, **1953**, *8*, 532.
250. Dote, J. L.; Kivelson, D.; Schwartz, R. N. *J. Phys. Chem.* **1981**, *85*, 2169.
251. Ben-Amotz, D.; Drake, J. M. *J. Chem. Phys.* **1988**, *89*, 1019.

252. Roy, M.; Doraiswamy, S. *J. Chem. Phys.* **1993**, *98*, 3213.
253. Anderton, R. M.; Kauffman, J. F. *J. Phys. Chem.* **1994**, *98*, 12117.
254. Horng, M. L.; Gardecki, J. A.; Maroncelli, M. *J. Phys. Chem. A* **1997**, *101*, 1030.
255. Dutt, G. B.; Krishna, G. R. *J. Chem. Phys.* **2000**, *112*, 4676.
256. Dutt, G. B. *J. Chem. Phys.* **2000**, *113*, 11154.
257. Znamenskiy, V.; Kobrak, M. N. *J. Phys. Chem. B* **2004**, *108*, 1072.
258. Anderton, R. M.; Kauffman, J. F. *J. Phys. Chem.* **1994**, *98*, 12117.
259. Andreozzi, L.; Faetti, M.; Giordano, M.; Leporini, D. *J. Phys. Chem. B.* **1999**, *103*, 4097.
260. Faetti, M.; Giordano, M.; Leporini, D.; Pardi, L. *Macromolecules* **1999**, *32*, 1876.
261. Ueno, K.; Angell, C. A. *J. Phys. Chem. B* **2011**, *115*, 13994.
262. Karve, L.; Dutt, G. B. *J. Phys. Chem. B* **2011**, *115*, 725.
263. Samanta, A. *J. Phys. Chem. Lett.* **2010**, *1*, 1557.
264. Chowdhury, P. K.; Halder, M.; Sanders, L.; Calhoun, T.; Anderson, J. L.;
Armstrong, D W.; Song, X.; Petrich, J. W. *J. Phys. Chem. B* **2004**, *108*, 10245.
265. Santhosh, K.; Samanta, A. *J. Phys. Chem. B* **2010**, *114*, 9195.
266. Bhattacharya, B.; Samanta, A. *J. Phys. Chem. B* **2008**, *112*, 10101.
267. Tiwari, S.; Kumar, A. *Angew. Chem., Int. Ed.* **2006**, *45*, 4824.
268. Tiwari, S.; Khupse, N.; Kumar, A. *J. Org. Chem.* **2008**, *73*, 9075.
269. Ozawa, R.; Hamaguchi, H. *Chem. Lett.* **2001**, *30*, 736.
270. Mali, K. S.; Dutt, G. B.; Mukherjee, T. *J. Chem. Phys.* **2008**, *128*, 124515.
271. Baba, K.; Ono, H.; Itoh, E.; Itoh, S.; Noda, K.; Usui, T.; Ishihara, K.; Inamo, M.;

- Takagi, H. D.; Asano, T. *Chem. Eur. J.* **2006**, *12*, 5328.
272. Behar, D.; Gonzalez, C.; Neta, P. *J. Phys. Chem. A* **2001**, *105*, 7607.
273. Grodkowski, J.; Neta, P. *J. Phys. Chem. A* **2002**, *104*, 5468.
274. Kramers, H. A. *Physica* **1940**, *7*, 284.
275. Rothenberger, G.; Negus, D. K.; Hochstrasser, R. M. *J. Chem. Phys.* **1983**, *79*, 5360.
276. Courtney, S. H.; Fleming, G. R. *J. Chem. Phys.* **1985**, *83*, 215.
277. Zeglinski, D. M.; Waldeck, D. H. *J. Phys. Chem.* **1988**, *92*, 692.
278. Sivakumar, N.; Hoburg, E. A.; Waldeck, D. H. *J. Chem. Phys.* **1989**, *90*, 2305
279. Park, N. S.; Waldeck, D. H. *J. Chem. Phys.* **1989**, *91*, 943.
280. Park, N. S.; Waldeck, D. H. *J. Phys. Chem.* **1990**, *94*, 662.
281. Velsko, S. P.; Fleming, G. R. *J. Chem. Phys.* **1982**, *76*, 3553.
282. Keery, K. R.; Fleming, G. R. *Chem. Phys. Lett.* **1982**, *93*, 322.
283. Lee, M.; Bain, A. J.; McCarthy, P. J.; Han, C. H.; Haseltine, J. N.; Smith III, A. B.; Hochstrasser, R. M. *J. Chem. Phys.* **1986**, *85*, 4341.
284. Lee, M.; Haseltine, J.N.; Smith, A. B.; Hochstrasser, R. M.; *J. Am. Chem.Soc.* **1989**, *111*, 5044.
285. Anderton, R. M.; Kauffman, J. F. *J. Phys. Chem.* **1994**, *98*, 12125.
286. Anderton, R. M.; Kauffman, J. F. *J. Phys. Chem.* **1995**, *99*, 14628.
287. Rullière, C.; *Chem. Phys. Lett.* **1976**, *43*, 303.
288. Sundström, V.; Gillbro, T. *J. Phys. Chem.* **1982**, *86*, 1788.
289. Velsko, S. P.; Fleming, G. R. *Chem. Phys.* **1982**, *65*, 59.

290. Velsko, S. P.; Waldeck, D. H.; Fleming, G. R. *J. Chem. Phys.* **1983**, *78*, 249.
291. Hara, K.; Akimoto, S. *J. Phys. Chem.* **1991**, *95*, 5811.
292. Aramendía, P. F.; Negri, R. M.; Román, E. S. *J. Phys. Chem.* **1994**, *98*, 3165.
293. Onganer, Y.; Yin, M.; Bessire, D. R.; Quitevis, E. L. *J. Phys. Chem.* **1993**, *97*, 2344.
294. Dagenet, C.; Dyson, P. J.; Krossing, I.; Oleinikova, A.; Slattery, J.; Wakai, C.; Weingärtner, H. *J. Phys. Chem. B* **2006**, *110*, 12682.
295. Dempster, D. N.; Morrow, T.; Kankin, R.; Thompson, G. F. *J. Chem. Soc., Faraday Trans.2* **1972**, *68*, 1479.
296. Tokuda, H.; Hayamizu, K.; Ishii, K.; Susan, M. A. B. H.; Watanabe, M. *J. Phys. Chem. B* **2005**, *109*, 6103.
297. Grote, R. F.; Hynes, J. T. *J. Chem. Phys.* **1981**, *74*, 4465.
298. Grieser, F.; M. Lay, M.; Thistlethwaite, P.J. *J. Phys. Chem.* **1985**, *89*, 2065.
299. Mali, K. S.; Dutt, G. B.; Mukherjee, T. *J. Chem. Phys.* **2006**, *124*, 054904.
300. Mali, K. S.; Dutt, G. B.; Mukherjee, T. *Langmuir* **2006**, *22*, 6837.
301. Jee, A. Y.; Kwon, H.; Lee, M. *J. Chem. Phys.* **2009**, *131*, 171104.
302. Jee, A. Y.; Bae, E.; Lee, M. *J. Phys. Chem. B* **2009**, *113*, 16508.
303. Jee, A. Y.; Lee, M. *Chem. Phys. Chem* **2010**, *11*, 793.
304. Jee, A. Y.; Bae, E.; Lee, M. *J. Chem. Phys.* **2010**, *133*, 014507.
305. Lakowicz, J. R. *Principles of Fluorescence Spectroscopy*, 2nd ed. (Plenum Press, New York, 1999).
306. Hoebeke, M.; Piette, J.; Vorst, A.V. *J. Photochem. Photobiol. B*.

1990, 4, 273.

307. Aramendía, P. F.; Kreig, M.; Nitsch, C.; Bittersmann, E.; Braslavsky, S. E.

Photochem. Photobiol. **1988, 48, 187.**

308. Aramendía, P. F.; Duchowicz, R.; Scaffardi, L.; Tocho, J.O. *J. Phys. Chem.*

1990, 94, 1389.

List of Publications Included in the Present Thesis

1. Characterizing interfacial friction in AOT reverse micelles from photoisomerization studies of carbocyanine derivatives
Gangamallaiiah, V.; Dutt, G. B. *J. Chem. Phys.* **2011**, *134*, 024706.
2. Photoisomerization dynamics of 3,3'-diethyloxadecarborocyanine iodide in ionic liquids: Breakdown of hydrodynamic Kramers model
Gangamallaiiah, V.; Dutt, G. B. *J. Chem. Phys.* **2011**, *135*, 174505.
3. Rotational diffusion of nonpolar and ionic solutes in 1-alkyl-3-methylimidazolium bis(trifluoromethylsulfonyl)imides: Is solute rotation always influenced by the length of the alkyl chain on the imidazolium cation?
Gangamallaiiah, V.; Dutt, G. B. *J. Phys. Chem. B* **2012**, *116*, 12819.
4. Fluorescence anisotropy of a nonpolar solute in 1-alkyl-3-methylimidazolium-based ionic liquids: Does the organized structure of the ionic liquid influence solute rotation?
Gangamallaiiah, V.; Dutt, G. B. *J. Phys. Chem. B* **2013**, *117*, 5050.
5. Influence of the organized structure of 1-alkyl-3-methylimidazolium-based ionic liquids on the rotational diffusion of an ionic solute
Gangamallaiiah, V.; Dutt, G. B. *J. Phys. Chem. B* **2013**, *117*, 9973.
6. Effect of alkyl chain length on the rotational diffusion of nonpolar and ionic solutes in 1-alkyl-3-methylimidazolium bis(trifluoromethylsulfonyl)imides
Gangamallaiiah, V.; Dutt, G. B. *J. Phys. Chem. B* **2013**, *117*, 12261.